# The growth of InGaN/GaN scintillation heterostructures

## Doctoral thesis

| | |
|---|---|
| *Study program:* | P3901 – Applied Sciences in Engineering |
| *Study branch:* | 3901V055 – Applied Sciences in Engineering |



| | |
|---|---|
| *Author:* | **Ing. Tomáš Hubáček** |
| *Supervisor:* | prof. Ing. Eduard Hulicius, CSc. |
| *Co-advisor:* | prof. Ing. Pavel Mokrý, Ph.D. |
| | Ing. Alice Hospodková, Ph.D. |
| | RNDr. Jan Touš, Ph.D. |

Liberec 2020

# Růst InGaN/GaN scintilačních heterostruktur

## Disertační práce

| | |
|---|---|
| *Studijní program:* | P3901 – Aplikované vědy v inženýrství |
| *Studijní obor:* | 3901V055 – Aplikované vědy v inženýrství |


| | |
|---|---|
| *Autor práce:* | **Ing. Tomáš Hubáček** |
| *Vedoucí práce:* | prof. Ing. Eduard Hulicius, CSc. |
| *Konzultanti:* | prof. Ing. Pavel Mokrý, Ph.D. |
| | Ing. Alice Hospodková, Ph.D. |
| | RNDr. Jan Touš, Ph.D. |

Liberec 2020

# Declaration

I hereby certify that I have been informed that Act 121/2000, the Copyright Act of the Czech Republic, namely Section 60, School-work, applies to my doctoral thesis in full scope. I acknowledge that the Technical University of Liberec (TUL) does not infringe my copyrights by using my doctoral thesis for TUL's internal purposes.

I am aware of my obligation to inform TUL on having used or licensed to use my doctoral thesis in which event TUL may require compensation of costs incurred in creating the work at up to their actual amount.

I have written my doctoral thesis myself using literature listed therein and consulting it with my supervisor and my tutor.

I hereby also declare that the hard copy of my doctoral thesis is identical with its electronic form as saved at the IS STAG portal.

Date:

Signature:

# Preface

This doctoral thesis is a summary of my PhD study at the Faculty of Mechatronics, Informatics and Interdisciplinary Studies at the Technical University of Liberec. Most of the research work has been done in the Institute of Physics of the Czech Academy of Sciences at the Department of Semiconductors under the supervision of Prof. Hulicius and Dr. Hospodková. The doctoral thesis is written as a collection of published papers in impacted journals including a brief introduction to nitride semiconductor materials and Metal Organic Vapour Phase Epitaxy.

# Abstract

Devices based on nitride semiconductors are nowadays a part of our daily life. They are for example widely spread in blue light emitting diodes. This thesis is focused on a new application of nitride semiconductors which is a scintillation detector. This detector is based on InGaN/GaN multiple quantum well heterostructures and requires very efficient and fast luminescence response without any slow defect bands in luminescence spectra. In this thesis we have used Metal Organic Vapour Phase Epitaxy for the growth of these structures. We have improved a luminescence quality of GaN buffer layers by using different growth parameters and significantly suppressed slow yellow luminescence. By increasing QW number we have increased the thickness of InGaN/GaN heterostructures up to 1 μm which is necessary for more efficient scintillation detectors. With such thick structures come a lot of problems, such as increase of the strain in the structure or too big surface defects (called V-pits). These problems are discussed in this work as well. This thesis puts emphasis on the epitaxial growth of these structures. Based on the results obtained during this work, it seems that our proposed structure is suitable for scintillation detectors and it could be used in some commercial applications in the future.

**Key words:** MOVPE, InGaN/GaN heterostructure, scintillator, fast decay

# Abstrakt

Zařízení na bázi nitridových polovodičů jsou součástí našeho každodenního života. Rozšířená a používaná jsou například v modrých světlo emitujících diodách. Tato práce zkoumá novou možnost využití nitridových polovodičů, kterou je scintilační detektor. Detektor je tvořen heterostrukturami na bázi InGaN/GaN mnohonásobných kvantových jam a vyžaduje velice účinnou a rychlou luminiscenční odezvu bez pomalých defektních pásů v luminiscenčních spektrech. Pro růst těchto struktur jsme použili organokovovou epitaxi z plynné fáze. Pomocí různých růstových parametrů jsme zlepšili luminiscenční vlastnosti GaN podkladových vrstev, kde jsme potlačili pomalou defektní žlutou luminiscenci. Zvýšením počtu kvantových jam bylo dosaženo tloušťky InGaN/GaN heterostruktury téměř 1 μm. Takto tlustá struktura je nezbytná pro účinný scintilační detektor, avšak vzhledem k této tloušťce jsme narazili na mnoho problémů, jakými jsou například zvýšení napětí ve struktuře nebo příliš velké povrchové defekty (nazývané V-pity). Diskuze těchto problémů je také součástí práce. Disertační práce klade důraz na epitaxní růst scintilačních struktur. Na základě poznatků získaných v průběhu zkoumání nitridových scintilačních heterostruktur se zdá, že naše navrhovaná struktura je vhodná jako scintilační detektor a mohla by být v blízké budoucnosti použita v některých komerčních aplikacích.



**Klíčová slova:** MOVPE, InGaN/GaN heterostruktury, scintilátor, rychlý dosvit

# Acknowledgements

At first, I would like to acknowledge Prof. Eduard Hulicius and Dr. Alice Hospodková for supervising my scientific work during my PhD study. Their fruitful advice and comments helped me every time I had problems during my work. I would like to thank all my colleagues from the Department of Semiconductors from the Institute of Physics of the Czech Academy of Sciences. Namely, Dr. Jiří Pangrác and Dr. Markéta Slavická Zíková for their help with MOVPE apparatus and growths, Dr. Jiří Oswald, Dr. Karla Kuldová, Dr. Filip Dominec, Tomáš Vaněk, František Hájek, Tereza Košutová and Radek Novotný for measurements of photo- and cathodo-luminescence, Dr. Pavel Hubík for Hall measurements and Prof. Jiří J. Mareš for allowing me to work at the Department of Semiconductors. Further thank belongs to colleagues from other departments of the Institute of Physics, such as Dr. Pavel Machek and Dr. Oliva Pacherová for X-ray diffraction measurements, Dr. Alexej Vetushka for AFM measurements, Dr. Vítězslav Jarý for luminescence and kinetic measurements and Dr. Martin Nikl for financial support during my stays in CERN and Claude Bernard University Lyon 1.

Another acknowledgement belongs to Prof. Pavel Mokrý from the Technical University of Liberec for his critical view on my doctoral thesis and valuable feedback.

During my PhD study I had six-month internship at the Institute of Functional Nanosystems (Optoelectronics Division) of the Ulm University. This internship improved my scientific skills very significantly in the field of nitrides and many thanks belong to Prof. Ferdinand Scholz and Oliver Rettig for their amazing support and help during my work there.

Finally, and most importantly, I would like to thank my whole family for their lifelong love and moral and material support during my studies. They helped me to achieve my dreams and stayed with me whenever I had problems.

This doctoral thesis would not be done without support of different projects. Namely, GAČR project no. 16-11769S, MŠMT project no. NPUI-LO1603 - ASTRANIT, TAČR project no. TH02010580, MŠMT project LM201587 - LNSM and EC project H2020-TWINN-2015 no. 690599 (ASCIMAT). Moreover, my conference contributions would not be able to realize without TUL Mobility Fund support as well.

# Content


Declaration ... iii

Preface ... iv

Abstract ... v

Abstrakt ... vi

Acknowledgements ... vii

List of Acronyms ... x

Introduction ... 1

1 Thesis Outline ... 3

1.1 Aims ... 3

1.2 Connection of thesis papers ... 4

2 III-Nitride Semiconductors ... 5

2.1 Brief history of III-nitrides ... 5

2.2 Crystal structure ... 6

2.3 Chemical, mechanical and thermal properties ... 6

2.4 Optical properties of GaN ... 7

2.5 InGaN/GaN MQW heterostructure ... 8

2.6 Polarization field ... 8

2.7 Carrier localization ... 10

2.8 V-shape defects ... 10

2.9 MQW structure design ... 11

3 Epitaxial Growth and Experimental Techniques ... 12

3.1 Introduction ... 12

3.2 MOVPE technology ... 13

3.3 Design of the reactor ... 16

3.4 Growth process of scintillation structure ... 18

3.5 Wafer and structure in situ measurement ... 21

3.6 Structure ex situ measurement ........ 21

4 Collection of Papers ........ 26

4.1 Improvement of luminescence properties of GaN buffer layer for fast nitride scintillator structures [i] ........ 27

4.2 Improvement of luminescence properties of n-GaN using TEGa precursor [ii] ........ 33

4.3 Influence of Si doping of GaN layers surrounding InGaN quantum wells on structure photoluminescence properties [iii] ........ 41

4.4 Influence of GaN buffer layer under InGaN/GaN MQWs on luminescent properties [iv] ........ 48

4.5 InGaN/GaN Structures: Effect of the Quantum Well Number on the Cathodoluminescent Properties [v] ........ 54

4.6 Advancement toward ultra-thick and bright InGaN/GaN structures with a high number of QWs [vi] ........ 60

4.7 Strong suppression of In desorption from InGaN QW by improved technology of upper InGaN/GaN QW interface [vii] ........ 68

5 Conclusions ........ 75

References ........ 77

List of Publications ........ 82

Author's articles related to thesis (in impact journals) ........ 82

Author's articles out of thesis scope (in impact journals) ........ 84

Patent application related to thesis ........ 84

Author's selected conference contributions related to thesis ........ 84

Author's selected conference contributions out of thesis scope ........ 85

# List of Acronyms

| | |
|---|---|
| AFM | Atomic Force Microscopy |
| BB | Blue Band |
| CCS | Close Coupled Showerhead |
| CL | Cathodoluminescence |
| DAP | Donor-Acceptor Pair |
| HRTEM | High-Resolution Transmission Electron Microscopy |
| HRXRD | High-Resolution X-ray Diffraction |
| HVPE | Hydride Vapour Phase Epitaxy |
| LED | Light Emitting Diode |
| LPE | Liquid Phase Epitaxy |
| MBE | Molecular Beam Epitaxy |
| MOVPE | Metal Organic Vapour Phase Epitaxy |
| MQW | Multiple Quantum Well |
| PAS | Positron Annihilation Spectroscopy |
| PL | Photoluminescence |
| QW | Quantum Well |
| TCSPC | Time-Correlated Single Photon Counting |
| TEM | Transmission Electron Microscopy |
| VPE | Vapour Phase Epitaxy |
| YB | Yellow Band |

# Introduction

It is more than one hundred years when William Crookes used the first scintillation counter (called spinthariscope) in practice. In that time, scintillation process was visualised on the ZnS screen. Since that time, a lot of scintillation materials were discovered and used in scintillation detectors. However, the research in the field of scintillation materials (especially inorganic materials) is still very active nowadays and new materials need to be developed for many different applications, such as medical imaging, electron detection, high-energy physics calorimetry, homeland security or industrial control.

The requirements for new scintillation materials are very demanding and depend on the application. For example, for Time-of-flight applications sub-100 ps time resolution is necessary or energy resolution down to 2 – 3 % for large crystals is necessary for homeland security [1]. These very high demands cannot meet common scintillation materials (bismuth germanate, garnets, perovskites, ortho-silicates, etc.) and new materials have to be found. Especially performance of radiation detectors used in X-ray and nuclear medicine imaging [2], high-energy physics [3] or scanning electron microscopes needs to be improved. For example, Time-of-flight applications (positron emission tomographs) need to speed up the rise time to get sub-100ps resolution. Scanning electron microscopes need faster scintillator to increase scanning rate with the same quality of images.

In last two decades, nanomaterials gained considerable attention in the scintillation community for their suitable properties. Due to the quantum confinement effect, they can offer a very high quantum efficiency and ultrafast decay time [1]. For example, ZnO nanoparticles co-doped with $Ga^{3+}$ or $La^{3+}$ showed decay time around 250 ps [4] and they are promising in ultrafast X-ray imaging [5]. CdSe nanoplatelets have been also proposed as a fast emitter with sub-100 ps decay time [6]. Finally, CdSe/CdS core shell quantum dots were also investigated and showed decay time around 850 ps [6]. These two CdSe based nanocrystals are promising for fast timing applications. All of these new nanomaterials have also disadvantages, such as necessity of some matrix where these nanoparticles have to be embedded. For example, ZnO nanoparticles co-doped with $Ga^{3+}$ were embedded in polystyrene matrix, which is not sufficiently resistant against high energy irradiation. CdSe nanocrystals are unstable in colloidal solution and appropriate matrix has to be found. Moreover, density of these materials embedded in matrix is not so high. Finally, stopping power and energy transfer efficiency can be a limitation as well.

Another nanomaterial, which was proposed for fast timing applications, is InGaN/GaN multiple quantum well (MQW) heterostructure. It was shown in our publication [7], that luminescence spectrum of this heterostructure contains fast quantum well excitonic band with the decay time of a few nanoseconds and slow defect band (called yellow band - YB), which have decay time in the range of microsecond scale. Ratio of the intensity of these two bands depends strongly on the type and density of excitation. Suppression of the YB intensity is necessary for the scintillation applications. With a proper design of the heterostructure can be reached excitonic decay time below 1 nanosecond, which is a good precondition for fast

timing applications. Moreover, InGaN/GaN MQW heterostructures have high efficiency (light yield) and good radiation resistance compared to mentioned scintillating nanomaterials. They are also mechanical robust. The rise time of these structures is very fast, which is another good precondition for fast timing applications.

At the beginning of the 21$^{st}$ century GaN has been considered as a suitable material for scintillation detection. GaN layers were studied as a promising detector in harsh radiation environment [8] or detector for X-ray detection [9]. GaN layers grown on sapphire substrate were used and investigated for neutron detection when suitable neutron conversion layers were used [10]. Moreover, implantable dosimetric system based on GaN was proposed for real-time measurements of dose and dose rate [11,12]. Luminescence properties of epitaxially grown GaN layers were studied and compared with ZnO epitaxial layers (widely used scintillation material) by Schenk *et al.* [13]. They have shown that GaN layers doped with silicon have decay time below 1 ns and external photon yield $1.4 \pm 0.2$ photons per 1 keV incident electrons. Despite low planar light extraction coefficient, the external photon yield was low compared to classical single crystalline and powder scintillators (YAG:Ce, YSO:Ce, etc.).

The work contained in this doctoral thesis is concentrated on the growth of InGaN/GaN MQW heterostructures with Metal Organic Vapour Phase Epitaxy (MOVPE). These heterostructures are nowadays commercially used in blue light emitting diodes (LED) but for scintillation detectors, there are different requirements for the structure, such as very thick active region, suppression of defect bands as much as possible and others. All these growth challenges are subject of this doctoral thesis. It is written as a collection of published papers in impacted journals related to this topic. At first, a brief introduction to III-nitride properties will be given. Afterwards, aspects of MOVPE technology with in situ and ex situ measuring techniques are described and finally, collection of seven papers with a brief description of each paper and connection of these papers are shown.

# 1 Thesis Outline

## 1.1 Aims

Based on the previous works on the GaN epitaxial layers it seemed that GaN is promising material for scintillation application. Drawbacks of this material was low external photon yield due to the small thickness of epitaxial layer structure in comparison to bulk scintillators and slow luminescence defect components which are presented in GaN layers.

We have proposed an idea, that external photon yield could be enhanced by using InGaN/GaN MQW heterostructure instead of using only GaN layers doped with silicon. Thanks to the quantum confined effect the luminescence efficiency should be much higher and the external photon yield should be enhanced as well.

Undoped GaN layers are always unintentionally n-type due to the residual impurities. Creation of acceptor levels is much probable than donor levels in these n-type layers. Deep or shallow acceptor levels are the source of various defect bands, which have slow decay time, and they are detrimental for fast scintillation applications. One of this defect band is called yellow band (YB) with the maximum around 2.2 eV. The decay time of this band is in microsecond range and needs to be suppressed as much as possible. The luminescence intensity of the YB can be reduced with proper growth parameters.

Aims of my doctoral thesis can be summarized in following steps:

- Proposal of InGaN/GaN heterostructure in order to get fast excitonic decay time (around 1 ns)
- Suppression of defect luminescence
- Growth of these structures by the MOVPE technology
- Adjustment of the structure according to the results obtained by different measurement techniques

The main and the most time consuming task of my thesis was the growth of the structure by MOVPE technology. The structure is very similar to blue LED structure, which is commercially used, but there are a few important differences, which are discussed in my doctoral thesis. The advantage of our structure is the fact that we do not need p-type GaN layers (only n-type GaN layer is grown below MQW structure). On the other hand, any kind of defect bands in the luminescence spectrum is undesirable in our structure, which means having very precisely adjusted growth parameters and controlling level of impurities. Another difference is the number of quantum wells (QWs). MQW structure in LEDs contains few QWs, usually less than five. In scintillator structures, much thicker MQW region with higher QW number is necessary, to increase detected part of high energy deeply penetrating irradiation. Our structure usually contains more than 30 QWs with total MQW thickness up to 1 μm. The growth of such thick MQW region is very challenging due to increasing strain in the structure (coming from the different lattice parameters of InGaN and GaN layers) and enlarging of V-pits (surface defects with V-shape character).

## 1.2 Connection of thesis papers

During our project, we have focused on the growth of different parts of the structure separately. Simplified scheme of the whole structure is shown in Fig. 1.1.

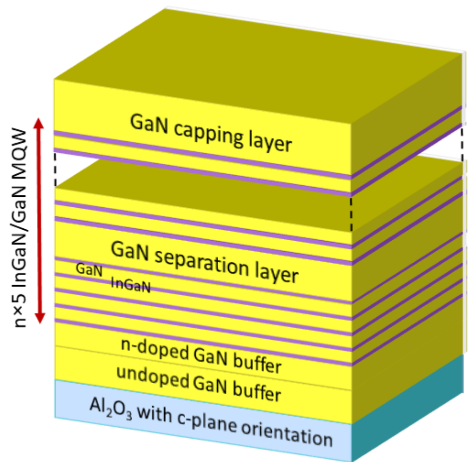


*Fig. 1.1. Simplified scheme of the scintillation structure based on InGaN/GaN multiple quantum well heterostructure.*

As a substrate, we have used sapphire with c-plane orientation. The growth on this substrate is well described in the literature and it is cheaper compared to GaN or SiC substrates. The initial growth of GaN on sapphire substrate is very important for the quality of the whole structure.

We have studied the first phases (nucleation and coalescence layer) of the growth in the article [i].

Very good quality of n-doped GaN buffer layer is necessary for scintillation purpose as well. That is why we have studied growth parameters of n-doped GaN layers as well (article [ii]).

Level of dopants in the layer beneath the MQW structure influences internal electric field inside the MQW structure and its luminescence properties. It has been studied in the article [iii].

Level of impurities and defects penetrating from GaN buffer layer into MQW region can be supressed by different techniques. One of them was studied in the article [iv].

MQW structure is the most important part of the whole structure. Depending on the application (different kinds of irradiation), the structure has to be optimized with respect to QW number and thickness of MQW region. Structures with different number of QWs have been studied in the articles [v] (focused on the excitation with electrons) and [vi] (focused on the X-ray excitation).

Finally, we have found the way how to supress indium desorption from InGaN QWs during the growth of the MQW structure (article [vii]).

# 2 III-Nitride Semiconductors

This chapter contains basic information about III-nitride semiconductors. After the historical overview of material development, the crystal structure and other fundamental optical and material properties of GaN will be described. Next part will be devoted to properties of InGaN/GaN MQW structure which converts high energy irradiation into the visible light.

## 2.1 Brief history of III-nitrides

Most of the research involving III-nitride technology is dated to late 1960s, however the first synthesis of GaN occurred in 1928 by Johnson *et al.* [14]. In 1938, Juza and Hahn synthesized the first GaN by passing ammonia through hot gallium [15]. Afterwards, in 1969 Maruska and Tietjen grew epitaxially GaN layer on sapphire substrate using halide vapour phase epitaxy [16]. Two years later, Pankove *et al.* [17] fabricated the first blue GaN based LED. Violet LED was fabricated by the same group in 1972 [18]. Despite these achievements, quality of GaN epitaxial layers were not sufficient for future devices.

The growth of III-nitrides was accomplished in Czechoslovakia Academy of Sciences during 1960s as well. Pastrňák *et al.* [19,20] grew mainly AlN crystals and studied their optical properties.

In 1980s, the quality of GaN layers grown on sapphire substrate was improved by using modern growth techniques, such as Molecular Beam Epitaxy (MBE) or MOVPE. In 1983 Yoshida *et al.* [21] grew AlN layer between sapphire substrate and GaN layer for improvement of the electrical and luminescence properties of GaN (using MBE technique). Amano *et al.* [22] later improved this two-step growth technique using MOVPE technique. They grew amorphous AlN layer on the sapphire substrate and then GaN epitaxial layer at higher temperature which resulted in smooth surface with high crystallographic quality and high room temperature photoluminescence intensity. GaN layers were typically unintentionally n-type. Akasaki and Amano used zinc as an acceptor dopant for p-type GaN, but they did not succeed. They tried magnesium as a dopant with no success as well. In 1988, Amano found out that after electron beam irradiation cathodoluminescence intensity of Mg-doped GaN layer increases. One year later, Amano *et al.* [23] made first p-n junction with Mg dopant activated by electron beam irradiation. After that, Nakamura *et al.* [24] found out that acceptor activation also occurs after thermal annealing in hydrogen-free atmosphere. Also by introduction of indium into GaN matrix and formation of InGaN QWs the emission was shifted from UV to blue spectral region. Since that time, there was no obstacle to grow blue LED with sufficient quality [25]. Later on LED became commercially available from Nichia Laboratories. For these achievements the scientists (I. Akasaki, H. Amano and S. Nakamura) were awarded the Nobel Prize in Physics in 2014. In electronic devices found GaN material utilization as well due to high breakdown voltage, high saturation velocity of electrons and high density of electrons in 2D electron gas which can be obtained on heterostructure interfaces due to the polarization field. These properties are necessary for implementation in high power transistors for electrical vehicles and high frequency applications in next

generation communication systems. Due to their advantageous properties nitrides became the second most important semiconductor after Si. However, Si remains unbeatable in general electronics due to the low production price, well established technology and availability of large wafers.

## 2.2 Crystal structure

Gallium nitride's most stable crystal structure is wurtzite, which is stable under ambient conditions. Another two structures, zincblende and rocksalt, are stable at specific conditions, such as a high pressure or growth on specific crystal planes. The wurtzite structure is in fact two interpenetrating hexagonal close packed sub-lattices, each with one type of atoms, offset along the c axis by 5/8 of the cell height. GaN hexagonal unit cell is shown in Fig. 2.1. Each gallium atom is surrounded by four nitrogen atoms and vice versa.

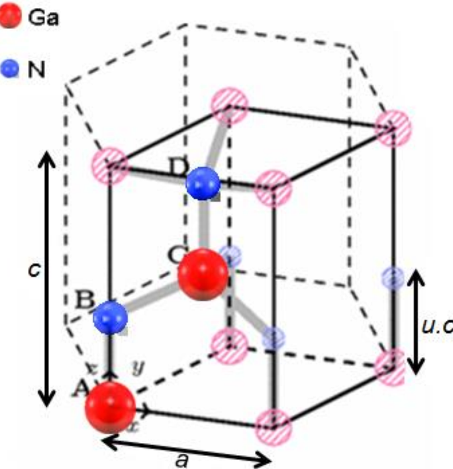


*Fig. 2.1. Unit cell of the wurtzite GaN with lattice parameters* a *(3.189 Å) and* c *(5.185 Å). Unit cell consists two atoms of gallium and two atoms of nitrogen. Taken from [26].*

## 2.3 Chemical, mechanical and thermal properties

GaN is exceedingly stable compound and exhibits significant hardness. It is chemically stable even at elevated temperatures. It was found that GaN is insoluble in water, acids or bases at room temperature, but dissolves in hot alkali solutions at a very slow rate [16]. Low quality layers can be etched at reasonably high rates in NaOH, $H_2SO_4$ or $H_3PO_4$ [27]. Especially, material around dislocations is well etched (smooth surface is much difficult to etch), so this technique can be used for estimating density of defects in GaN. This technique is destructive but gives reasonable information about the dislocation density.

Wurtzite structure is mechanically stable up to 50 GPa when changes to rocksalt phase [28]. Mean thermal expansion coefficient of GaN is in the *c* plane $\Delta a/a = 5.59\ 10^{-6}\ K^{-1}$ (300 – 900 K), $\Delta c/c = 3.17\ 10^{-6}\ K^{-1}$ (300 – 700 K) and $\Delta c/c = 7.75\ 10^{-6}\ K^{-1}$ (700 – 900 K) [16]. During epitaxial growth of GaN on sapphire substrate, slightly different thermal expansion

coefficient of sapphire and GaN causes bending of the sample during cool down process. This phenomenon has to be taken into account during fabrication of devices by opposite pre-bending during the growth.

Radiation resistance of GaN layers was studied as well. Look *et al.* [29] studied formation of point defects under 1 – 2 MeV electron irradiation. They showed that GaN is quite resistant to displacement changes and the most dominant formed defect is nitrogen vacancy. Good radiation resistance predestines GaN to be used as a good scintillation material.

## 2.4 Optical properties of GaN

GaN is a direct semiconductor with the bandgap energy of $E_g$ = 3.42 at 300 K [27]. It is suitable material for optoelectronic devices, such as LEDs or laser diodes. Luminescence characteristic of GaN layers is very important for optoelectronic devices and even for scintillation devices. Typical luminescence spectrum of undoped GaN layer is shown in Fig. 2.2.

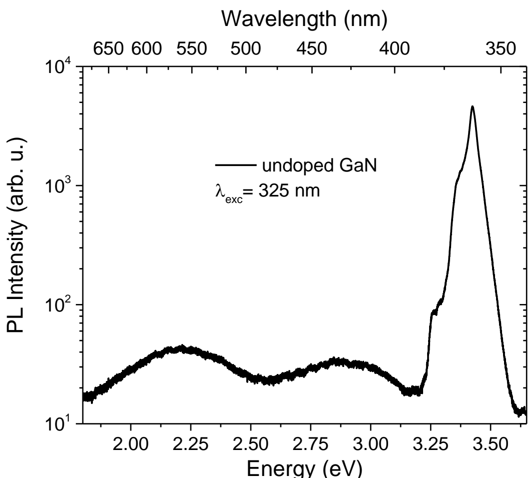


*Fig. 2.2. Room temperature photoluminescence spectrum of undoped GaN layer grown on sapphire substrate by MOVPE technology at standard conditions, and pumped by 325 nm laser with 50 W/cm².*

This spectrum consists of four recombination parts, excitonic emission, donor-acceptor pair (DAP) emission, blue luminescence and yellow luminescence bands (BB and YB respectively). The emission around 3.42 eV is attributed to bound exciton to neutral donors [30]. In some cases, free excitons associated with the A, B and C valence bands can be measured, but due to unintentionally n-type GaN layers, bound excitons are measured in most cases. Emission around 3.28 eV comes from DAP recombination, where electrons are bound to donors and holes are bound to acceptors. Broad band centred at about 2.9 eV is BB, which comes from some shallow acceptor level. The BB is observed usually in undoped, Zn-doped [31], Mg-doped [32] or C-doped [33] layers. The decay time of this band is in the range of hundreds of nanoseconds (around 400 ns) and it is unwanted for the scintillation applications. The second broad band centred at about 2.2 eV is YB. The YB is usually observed in

undoped, C-doped, Si-doped or Fe-doped layers. The source of the YB is deep acceptor level but after more than 20 years of research, there is still controversy in the literature about the origin of this acceptor level. The acceptor level was attributed to $V_{Ga}$-related complexes [34,35] or $C_N$-related complexes [36,37]. Nevertheless, the decay time of the YB is very slow (in the range of microseconds) and suppression of this band is essential for fast scintillation applications.

## 2.5 InGaN/GaN MQW heterostructure

InGaN/GaN MQW heterostructure is in fact a stack of $In_xGa_{1-x}N$ and GaN layers with varying composition of indium. InN has larger lattice parameter *a* than GaN, which means that InGaN layers are compressively strained in the heterostructure. Moreover, InN has smaller bandgap, so InGaN layers, surrounded by GaN barriers with higher bandgap, act as QWs. Bandgap energy versus lattice parameter of III-nitrides is shown in Fig. 2.3.

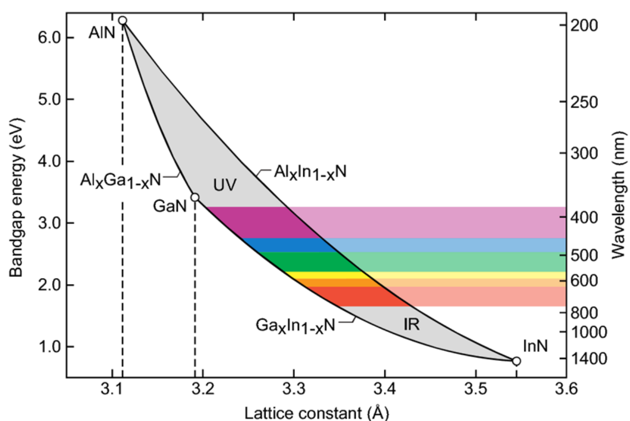


*Fig. 2.3. Bandgap energy vs lattice parameter* a *of III-nitrides. Taken from [38].*

## 2.6 Polarization field

In nitride heterostructures we are dealing with a quite huge macroscopic polarization. This polarization has two components: spontaneous ($P_{SP}$) and piezoelectric polarization ($P_{PZ}$). The reason of the spontaneous polarization is an intrinsic asymmetry of the bonding in the wurtzite crystal structure. It increases from GaN (-0.034 C/m$^2$) over InN (-0.042 C/m$^2$) to AlN (-0.090 C/m$^2$) and it has a negative sign [39]. Bernardini and Fiorentini [40] showed nonlinear behaviour of polarization for ternary III-nitride alloys. Spontaneous polarization follows Vegards-like relationship with a bowing parameter *b* describing nonlinear relationship between InN and GaN. For InGaN alloy we can describe spontaneous polarization as:

$$P_{InGaN}^{SP}(x) = -0.042\,x - 0.034\,(1-x) + 0.037x(1-x)$$

where 0.037 C/m$^2$ is bowing parameter value for this case [41].

Knowledge of the spontaneous polarization is not sufficient for the description of the MQW heterostructure. As was already mentioned, InGaN QWs are compressively strained to match GaN lattice parameter. It leads to creation of piezoelectric polarization. In the growth along c-axis ([0001]) the strain in epitaxial layers is directed along the plane parallel to the substrate surface and crystal can relax freely in the growth direction. Assuming biaxial stress and negligible shear stresses, the piezoelectric polarization has only one non-vanishing component, which is directed along the growth direction and can be expressed as:

$$P_3^{PZ} = 2\frac{a_{InGaN} - a_{GaN}}{a_{GaN}}\left(e_{31} - e_{33}\frac{C_{13}}{C_{33}}\right)$$

where $a$ is the lattice parameter, $e_{31}$ and $e_{33}$ are piezoelectric constants of InGaN and $C_{13}$ and $C_{33}$ are the elastic constants of InGaN [41]. $P_3^{PZ}$ is always negative for layers under tensile strain and positive for layers under compressive strain. InGaN layers grown on GaN are compressively strained and the $P^{PZ}$ is anti-parallel to the $P^{SP}$. Piezoelectric polarization is nonlinear in terms of the alloy compositions (same as $P^{SP}$) and can be expressed as:

$$P_{InGaN/GaN}^{PZ}(x) = 0.148\,x - 0.0424\,x\,(1-x)$$

where -0.0424 C/m$^2$ is the bowing parameter value for InGaN/GaN structure [41]. This equation is true when the piezoelectric polarization depends linearly on the strain. If high forces or pressures are applied to the crystal, this relation becomes nonlinear. It is the case of high indium content heterostructures, which are hard to prepare in practice.

The piezoelectric polarization has a strong contribution to the overall polarization in the structure. The piezoelectricity gives rise to an electric field pointing from the substrate side (N face) to the surface side (Ga face), which leads to a corresponding inclination of the conduction and valence band edges in QWs and barriers, see Fig. 2.4. It directly leads to a redistribution of the electrons and holes to the upper and lower surface, respectively. Decreasing of the wave function overlap can be observed, resulting in the lower recombination probability. Moreover, the effective band gap shrinks. This effect is called quantum confined Stark effect. The reduction of the overlap leads to the longer decay time and less effective recombination process, which is detrimental for the scintillators.

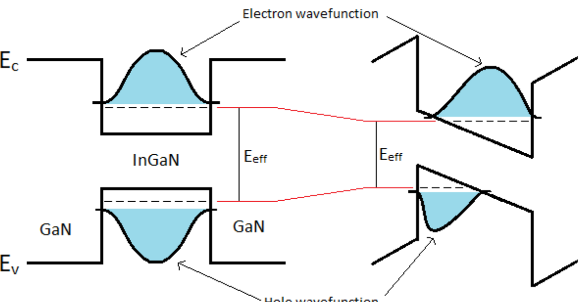


*Fig. 2.4. Illustration of the band structure of InGaN/GaN heterostructure without electric field (left) and with electric field (right). Effective bandgap shrinks and the overlap of wave function decreases.*

## 2.7 Carrier localization

MQW structures grown on sapphire substrate have dislocation density in the order of $10^8 – 10^9$ cm$^{-2}$. Despite of such high dislocation density, the light emission is not quenched and the room temperature photoluminescence efficiency can be very high. In InGaN/GaN heterostructures are created localization centres which confine carriers and prohibit non-radiative recombination. Localization centres are generally attributed to the fluctuation of indium concentration [42], indium clustering [43] or fluctuation in quantum well width [44]. The precise nature of the localization centres is still unknown because it is hard to directly measure them and moreover some of the measurement techniques can give rise to false localization centres (for example indium clustering in InGaN QWs caused by electron beam damage in transmission electron microscope (TEM) images [45]).

## 2.8 V-shape defects

Threading dislocations, which penetrate through the whole structure, are created during the initial growth of GaN on the sapphire substrate (due to 16 % lattice mismatch between sapphire and GaN). Dislocation density is typically between $10^8 – 10^9$ cm$^{-2}$ and screw, edge and mixed type dislocations can be distinguished. During the growth of MQW structure (low temperature growth), V-shape defects (called V-pits) start to open on the dislocations with screw component. Cross sectional TEM images of such V-pits in the real structure are shown in Fig. 2.5.

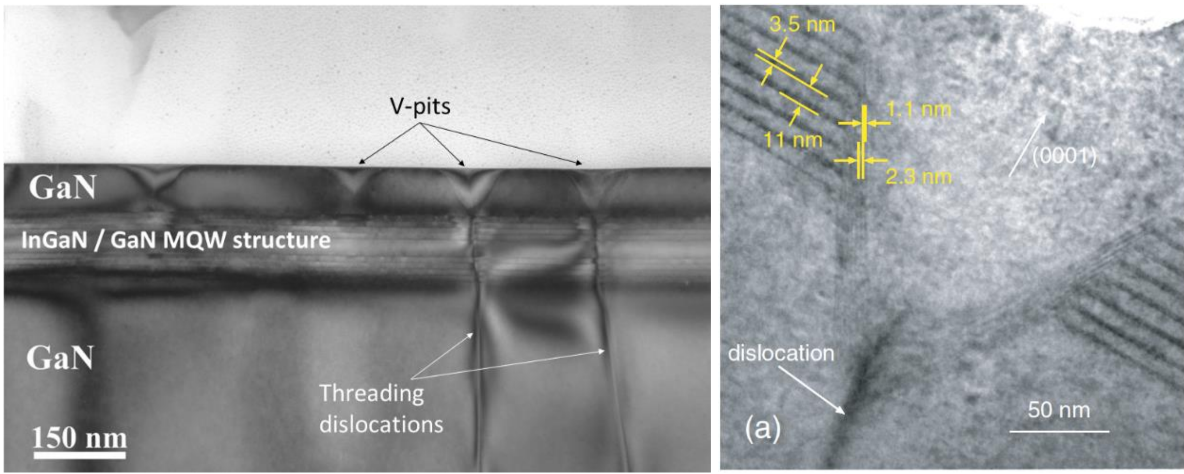


*Fig. 2.5. Bright field XTEM image (g = 0002) of the InGaN/GaN MQW structure grown in our laboratory (left image) and TEM image of InGaN/GaN MQW structure (right image) with QWs thickness marked on the c-plane (3.5 nm) and sidewall of V-pit (1.1 nm). Right image was taken from [46].*

Most of the surface defects are detrimental for the luminescence efficiency of the structures but it was found that role of the V-pits is different. The growth rate significantly depends on the different crystallographic planes. Sidewalls of the V-pits have {1-101} or {11-22} planes and the growth rate is much slower compared to (0001) plane. Therefore, QWs and barriers have much lower thickness, as you can see in Fig. 2.5, and with increasing

layer thickness V-pits tend to be larger. Such thinner QWs act as barriers for excitons generated in c-plane QWs. Thus, excitons are screened from the non-radiative centres located around the threading dislocation by the thinner QWs in the V-pit sidewall, which act as a potential barrier [46].

## 2.9 MQW structure design

As explained before, quantum confined Stark effect in InGaN/GaN MQW heterostructures causes separation of electron and hole wave functions and worse recombination efficiency. To minimize this phenomenon, it is necessary to have a very thin InGaN QWs to get fast response and good recombination efficiency. Most of our structures had QW thickness between 1 and 2 nm. Higher indium composition decreases luminescence efficiency as well as higher thickness. Therefore, low indium concentration of InGaN layers was necessary for our purpose. Our scintillation structures with the fastest decay time had InGaN layers with indium concentration below 10 %. Different decay profile of samples with different QW thickness is shown in Fig. 2.6. Measurements were done with the same time window and we can see that thicker QW sample has longer components and stronger background (decay components longer than time window).

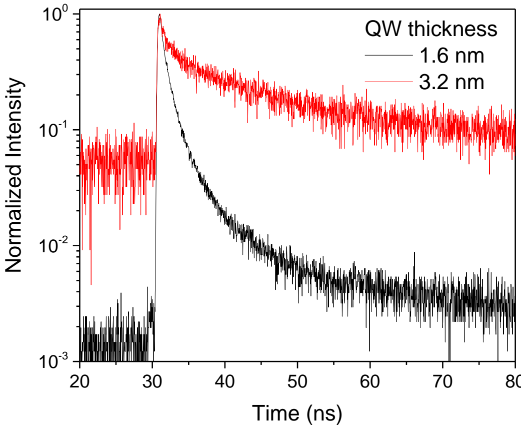


*Fig. 2.6. Time-resolved radioluminescence decay measurement of samples with 1.6 and 3.2 nm thick InGaN QWs. Measurement was done with 10 nm bandpass filter to get response only from the fast excitonic band.*

We have also added GaN separation layers after each stack of five QWs (see Fig. 1.1). Increase of QW number (MQW thickness) causes higher strain in the structure and GaN separation layer should decrease it a little bit, so we are able to grow thicker MQW structure (higher QW number) without any cracking. GaN separation layer itself increases MQW thickness and if we choose a proper thickness (below diffusion length of excitons), we will increase detection efficiency for high energy irradiation. For example, Hocker *et al.* [47] found diffusion length of excitons in undoped GaN around (150 ± 25) nm. Our GaN separation layer had usually thickness around 30 nm.

# 3 Epitaxial Growth and Experimental Techniques

## 3.1 Introduction

Epitaxy can be described as a growth of monocrystalline layers on a monocrystalline substrate. The term “epitaxy” was established by L. Royer in 1936. The word comes from Greek words *epi* (upon) and *taxis* (ordered) meaning together “arranging upon”. Epitaxial process is carried on the temperatures below melting point of the material, which means better crystallographic perfection and purity of the layers compared to the monocrystals grown from melt by Czochralski or Bridgman growth techniques (due to role of entropy – disorder at higher temperatures) [48].

The principle of the epitaxial growth is following. Atoms or molecules of the compound, which we would like to deposit on suitable substrate, are transported to epitaxial surface, which has to be atomically clean (cleaned from oxides and sorbants) and atomically smooth (only with atomic steps due to disorientation of the monocrystalline substrate). On the surface, the atoms will be physisorbed, and after that, chemisorbed to the crystal structure. By this way epitaxial atomic layers and all structures are grown.

Family of epitaxial techniques can be divided to the three techniques: solid, liquid and vapour phase epitaxy. From the beginning, compound semiconductors were mainly grown either by liquid phase epitaxy (LPE) or vapour phase epitaxy (VPE). LPE was used for the growth of II-VI and III-V compound semiconductors since the early 1960s. This technique produced high-purity semiconductors from a very simple apparatus designed for production of thick layers (up to 100 μm). The limitation of this technique was a growth of multiple layers with different composition, which are needed in today’s complex and advanced devices. Hydride vapour phase epitaxy (HVPE) was also used since 1960s for the growth of high-quality thick epitaxial layers. Limitation of this technique is the same as for LPE, difficulty in the growth of thin layers and superlattices with different composition. Unlike LPE, it is still nowadays used thanks to very high growth rate >100 μm/h with dislocation density $<10^6$ $cm^{-2}$. Such grown crystals are especially used in the growth of GaN due to the lack of native GaN substrates [49].

Limits of both LPE and HVPE techniques in growing complex devices and nanostructures led to development of new techniques, such as MBE or MOVPE. Both techniques can grow nearly atomically abrupt interfaces and high quality superlattices. MBE technique was still not widely adopted for the industrial production of compound semiconductor devices due to the ultrahigh vacuum system requirements, very complex maintenance procedures and wafer size limits. On the other hand, MOVPE became the primary production technique used in the semiconductor industry. Despite the fact that the equipment and procedure is quite expensive, MOVPE was adopted worldwide for the production of most of the III-V and II-VI devices due to its versatility, simplicity, large wafer area and fast turnover of growth process [49]. Both MBE and MOVPE techniques are able to growth semiconductor heterostructures with sharp interfaces and precise composition of each layers. The MBE is a physical process while the MOVPE is a chemical one.

## 3.2 MOVPE technology

MOVPE technology is an epitaxial process for the deposition of very thin layers of atoms onto a (usually semiconductor) monocrystalline wafer. In principle, source materials are delivered onto the heated monocrystalline substrate which becomes atomically clean and flat by this heating. Substrate is placed in the cold-wall reactor chamber. Molecules, close to the heated substrate, are decomposed to radicals which react on the epitaxial surface and create monocrystalline layer. The epitaxial temperature must be high enough to decompose metalorganic and ammonia molecules and low enough to prevent the thermal desorption of atoms from the surface and to prevent pre-reactions of source molecules in the gas phase. The growth is done by chemical reaction (not only a physical deposition as in MBE process). The growth on the same material is called homo-epitaxy, but the growth can be done on different substrates (hetero-epitaxy). Variety of compound semiconductors for many device applications can be prepared by MOVPE technology, see summarizing table in Fig. 3.1.

| Semiconductor Material | Device Application |
|---|---|
| GaAs | Solar cells, transistors, lasers |
| AlGaAs | Solar cells, lasers, VCSEL, HBTs, HEMTs |
| InGaAs and InGaAsN | Solar cells, HBT |
| InGaAsP | Lasers, PICs |
| InGaP and InGaAs | IMM solar cells, multi-junction solar cells, HBT |
| InAsSb | IR detectors, lasers |
| InGaAsSb, GaAsSb | Thermophotovoltaics |
| HgCdTe | IR detectors |
| CdZnTe | Radiation detectors |
| InGaN | Visible LEDs and lasers, solar cells |
| AlGaN | UV LEDs, HEMTs and lasers |

*Fig. 3.1. Summary of many kinds of semiconductor materials grown by MOVPE with different application utilization (VCSEL = vertical cavity surface emitting laser, HBT = heterojunction bipolar transistor, HEMT = high electron mobility transistor, PIC = photonic integrated circuit, IMM = inverted metamorphic multi-junction). Taken and modified from [49].*

Source materials (named precursors) used for the growth of monocrystalline thin layers by MOVPE technology are hydrides and metalorganics (chemical compound containing metal atom and organic ligands). In case of III-nitrides, trimethylgallium (TMGa), triethylgallium (TEGa), trimethylindium (TMIn), trimethylaluminium (TMAl) and ammonia ($NH_3$) are usually used for the growth. Metalorganic precursors are placed in the stainless steel bubblers (solid form – TMIn, liquid form – TMGa, TEGa, TMAl). High purity carrier gasses (hydrogen or nitrogen at the purity level of ppb or better) go through the bubbler and take metalorganic molecules into the chamber on the heated substrate, where the layer deposition takes place. Silane ($SiH_4$) is usually used as n-type dopant and biscyclopentadienyl magnesium ($Cp_2Mg$) as p-type dopant.

The chemical reaction of precursors can occur either in the hot vapour above the surface or on the hot substrate. In case of GaN growth, summary stoichiometric reaction can be written as:

$$Ga(CH_3)_3 + NH_3 \rightarrow GaN + 3\ CH_4$$

The reaction mentioned above is a just simplified chemical reaction. During the GaN growth, complex gas-phase and surface reactions occur. Gas reactions have been extensively studied by many research groups and it was found that there are two competing paths in the gas reactions during MOVPE growth of GaN, the adduct/amide reaction formation path and the TMGa pyrolysis path [50]. Schematic diagram of these two formation paths is shown in Fig. 3.2.

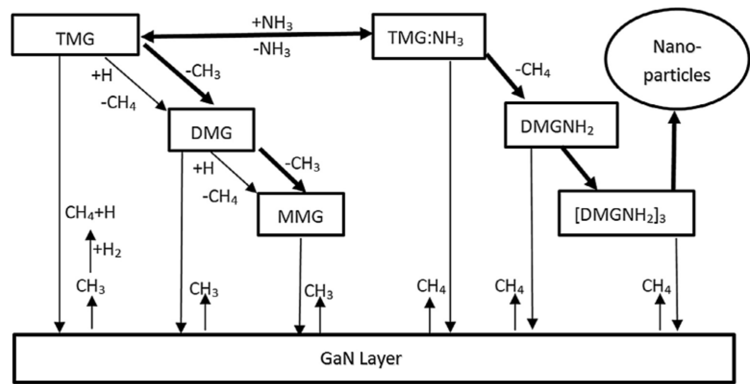


*Fig. 3.2. Schematic diagram of the gas reactions paths during MOVPE growth of GaN. The pyrolysis path (the left one) and the adduct/amide path (the right one). Taken from [50]. (TMG = $(CH_3)_3Ga$, DMG = $(CH_3)_2Ga$, MMG = $(CH_3)Ga$)*

TMGa and $NH_3$ make adduct at room temperature and at elevated temperature this adduct (TMGa:$NH_3$) can decompose into the amides DMGa$NH_2$. The amides are highly reactive and they can create oligomers $[DMGaNH_2]_x$, where x can be 2 or 3. This process is known as an adduct path. During the pyrolysis path are TMGa:$NH_3$ adducts dissociated back to TMGa and $NH_3$. At sufficiently high temperature TMGa decomposes to DMGa ($Ga(CH_3)_2$) and MMGa ($GaCH_3$). For this pyrolysis path is needed higher temperature and higher activation energy compared to the adduct path. Which gas reaction path dominates during the growth depends on the value of the reaction kinetics parameters[1] (activation energy and pre-exponential factor) [50]. For the modelling of GaN MOVPE growth are usually used these gas reactions (or part of them) [50]:

| | | |
|---|---|---|
| G1: | $(CH_3)_3Ga \rightarrow (CH_3)_2Ga + CH_3$ | pyrolysis reaction of TMGa |
| G2: | $(CH_3)_2Ga \rightarrow (CH_3)Ga + CH_3$ | pyrolysis reaction of DMGa |
| G3: | $(CH_3)_3Ga + NH_3 \rightarrow (CH_3)_3Ga{:}NH_3$ | adduct formation |
| G4: | $(CH_3)_3Ga{:}NH_3 \rightarrow (CH_3)_3Ga + NH_3$ | adduct decomposition |
| G5: | $(CH_3)_3Ga{:}NH_3 \rightarrow (CH_3)_2GaNH_2 + CH_4$ | adduct decomposition |
| G6: | $3(CH_3)_2GaNH_2 \rightarrow [(CH_3)_2GaNH_2]_3$ | formation of cyclic trimer |

[1] Reaction kinetic parameters, activation energy E [kcal/mol] and pre-exponential factor $k_0$ $[(cm^3/mol)^{\alpha-1}s^{-1}]$ are part of the equation $k = k_0\, T^n \exp(-E/RT)$. This equation calculates rate constant of the chemical reaction. Values of calculated or experimentally observed kinetic parameters differ in the literature. See for example [50-52].

G7: $CH_3 + H_2 \rightarrow CH_4 + H$ — $CH_3$ radical reaction

G8: $NH_3 + H \rightarrow NH_2 + H_2$ — H radical reaction

G9: $NH_3 \rightarrow H + NH_2$ — ammonia pyrolysis

G10: $(CH_3)_3Ga + H \rightarrow (CH_3)_2Ga + CH_4$ — H radical reaction

G11: $(CH_3)_2Ga + H \rightarrow (CH_3)Ga + CH_4$ — H radical reaction

The kinetics parameters of the reactions listed above are important for the basic idea of the GaN MOVPE growth process. For example, incorporation of hydrogen into GaN layers is very important for the layer quality. When we look at the H radical in the mentioned reactions, we can see that H formation is done by reaction G7 and G9 and depletion of H radical is done by reaction G8, G10 and G11. From the activation energies, we can conclude that G7 is the main reaction of the generation of H radical (lower activation energy compared to G9). On the other hand, G8 is the main reaction for depletion of H radical because much more $NH_3$ molecules are in the reactor (compared to TMGa or DMGa molecules) and the probability of the collision is higher [50].

GaN MOVPE growth contains surface reactions as well. Surface reactions usually considered in the simulations are listed below [50]:

S1: $(CH_3)_3Ga \rightarrow Ga(s) + 3CH_3$

S2: $(CH_3)_2Ga \rightarrow Ga(s) + 2CH_3$

S3: $(CH_3)Ga \rightarrow Ga(s) + CH_3$

S4: $(CH_3)_3Ga{:}NH_3 \rightarrow GaN(s) + 3CH_4$

S5: $(CH_3)_2Ga{:}NH_2 \rightarrow GaN(s) + 2CH_4$

S6: $[(CH_3)_2GaNH_2]_3 \rightarrow 3GaN(s) + 6CH_4$

S1 – S3 describe decomposition of TMGa, DMGa and MMGa. These reactions provide Ga atoms to the layer. Reactions S4 – S6 describe decomposition of adducts, amides and trimers. These reactions provide stoichiometric amounts of Ga and N atoms into the layer. Very high V/III ratio is commonly used during the GaN growth, which means that surface reactions of $NH_3$ are not considered in the simulations [50].

The growth temperature is usually high enough to have the growth transport-limited. The growth rate is almost independent on the growth temperature during this regime. When the temperature is low, the growth regime is kinetic-limited. Molecules and radicals have not enough energy to be sufficiently decomposed and transported to the surface. On the other hand, desorption occurs at very high temperatures and the growth rate decreases. This growth regime is called evaporation-limited [53]. Typical dependence of the growth rate on the growth temperature is shown in Fig. 3.3.

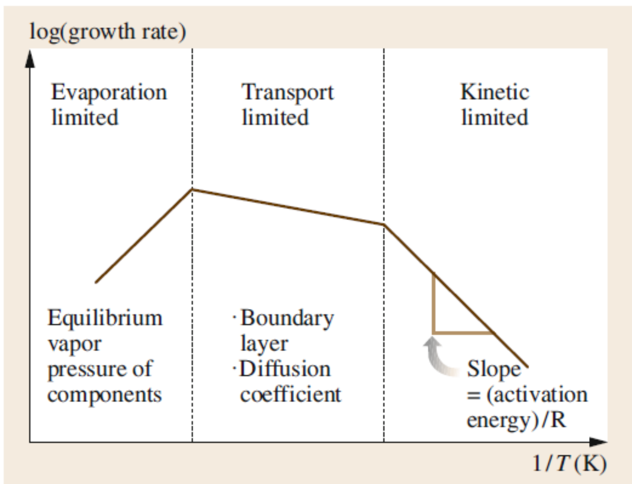


*Fig. 3.3. Schematic diagram of the three different regimes during the MOVPE growth. Taken from [53].*

Although the GaN MOVPE growth is much more complex, gas and surface reactions listed above can give us basic information about the growth and the processes which occur during the growth. However, details of processes during the GaN growth are still not well described and much more investigations and simulations need to be done.

The process of III-nitrides growth is significantly more complex than that of the other III-V or II-VI compounds. There are three main reasons. At first, the growth is mostly done on the lattice-mismatched substrates (sapphire, silicon, SiC, etc.) and various nucleation layers have to be implemented into the process. The second reason is a formation of adducts in the vapour phase which inhibits the mass transport of the elements to the surface. Finally, no p-type dopants with low ionization energy are available. The best choice is Mg with ionization energy around 200 meV in GaN (for AlGaN or AlN is the ionization energy much higher) resulting in only few percent of Mg atoms producing holes at room temperature [49].

## 3.3 Design of the reactor

There are two common types of MOVPE reactors according to the design of gas transport channel inputs, horizontal and vertical reactors. In horizontal reactors, gas flow is approximately parallel to the wafer surface. These reactors suffer from a decrease of the growth rate along the path of gas flow. Wall or wafer inclination, wafer rotation or optimized inlet flow rate were implemented to increase the homogeneity of the growth rate along the wafer. In vertical reactors, gases flow perpendicular to the wafer surface. In past two decades, different designs of the reactors were invented, for example close coupled showerhead (CCS) reactors, planetary reactors or high-speed rotating disk reactors. They are designed and used for the mass production of III-nitride devices with excellent growth homogeneity uniformity and reproducibility.

Our laboratory is equipped by Aixtron 3x2 CCS MOVPE reactor for III-nitride growth with LayTec EpiCurveTT system for in situ measurement of reflectivity, curvature and

temperature. Schematic diagram of our MOVPE system is shown in Fig. 3.4. Scheme of the reactor is shown in Fig. 3.5.

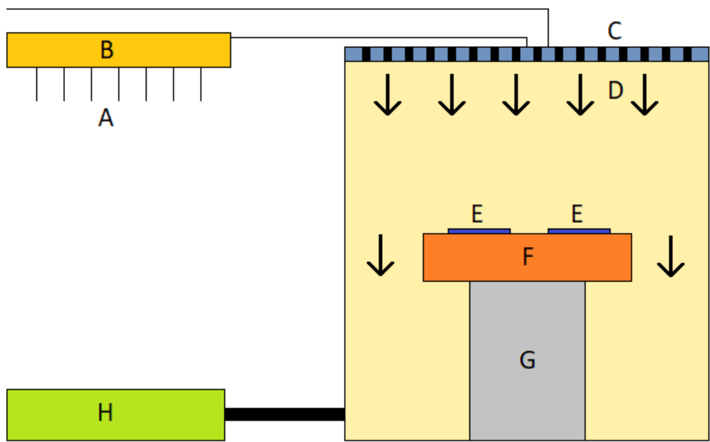


*Fig. 3.4. Schematic diagram of the CCS MOVPE reactor (A – process gas supply, B – gas mixing system, C – showerhead, D – reactor chamber, E – substrates, F – susceptor, G – heater, H – pump system).*

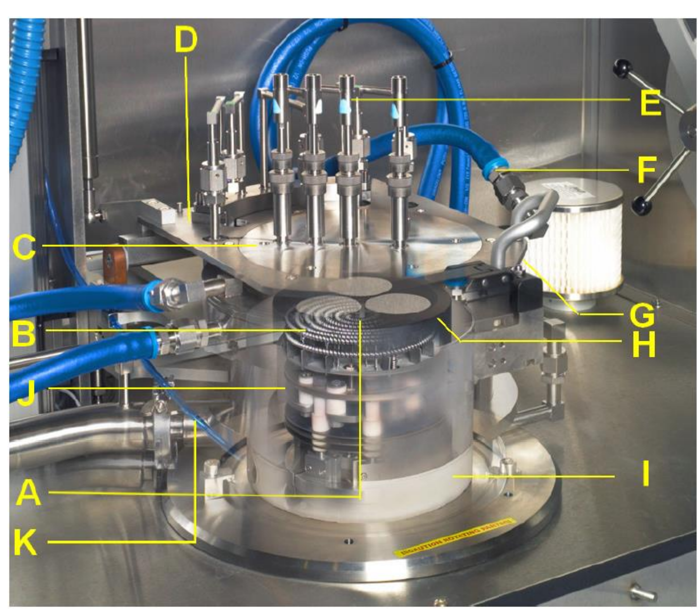


*Fig. 3.5. Scheme of the 3x2 CCS MOVPE reactor (A – thermocouple, B – tungsten heater, C – showerhead, D – reactor lid, E – optical probe, F – showerhead water cooling, G – double O-ring seal, H – susceptor, I – quartz liner, J – susceptor support, K – exhaust). Taken from the Aixtron manual.*

Our reactor has 3 pockets for two-inch wafers. This kind of reactor is designed for scientific research. For the mass production of epitaxial III-nitrides films in the industry are used much bigger reactors (for example 124 four-inch wafers in one run).

Wafers are located on the susceptor, which is generally a graphite disk with approximately 100 μm SiC coating. Susceptor rotates in a clockwise direction during the growth for better temperature homogeneity. Heater coils are located inside of the susceptor support and below the susceptor (see Fig. 3.5). The system is heated by a three-zone heater, see schematic diagram in Fig. 3.6(a).

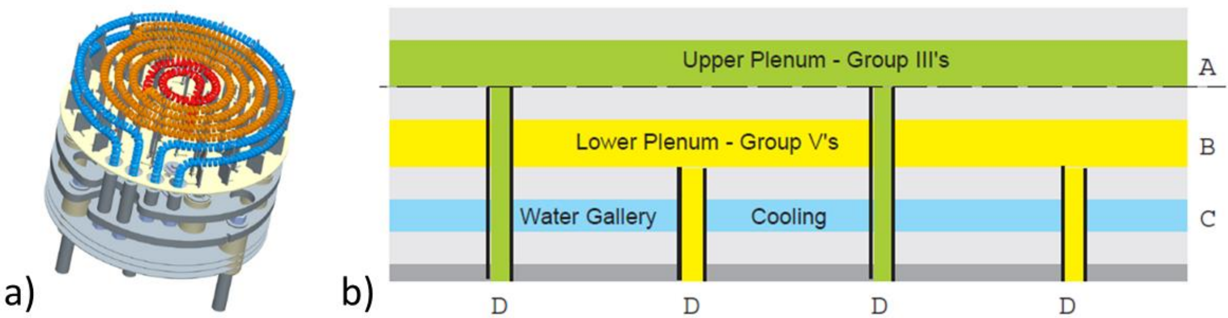


*Fig. 3.6. a) Schematic diagram of the three zone heaters (red – centre, orange – middle, blue – outside) and b) cross section of the showerhead (A – upper plenum, B – lower plenum, C- water cooling, D – tubes). Taken from the Aixtron manual.*

Cross section of the showerhead is shown in Fig. 3.6(b). Showerhead has normally two plenums, upper plenum for metalorganics (group III's) and lower one for ammonia (group V's). Both precursors come to the reactor from tubes with diameter 0.6 mm. Distance between showerhead and susceptor influences the growth (growth rate, amount of the pre-reactions in the gas phase, etc.) The distance can be adjusted, but it is typically around 11 mm.

## 3.4 Growth process of scintillation structure

The typical growth process of InGaN/GaN scintillation structure on sapphire substrate, which is the subject of this work, is performed in following technological steps:

- Substrate annealing at high temperature (1100°C) in $H_2$ ambient (desorption of contaminants from the surface and smoothing the surface)
- Nitridation of the sapphire substrate with ammonia flow to terminate the dangling bonds with N
- Nucleation layer deposition at low temperature (500 – 600°C)
- Annealing of the nucleation layer during the temperature ramp up to 1000°C to create monocrystalline islands
- Slow coalescence of the islands
- Growth of undoped GaN buffer layer
- Growth of n-doped GaN layer
- Growth of the InGaN/GaN heterostructure
- Cool down process in $NH_3$ ambient

The first steps of the growth are important when the growth is performed on the foreign mismatched substrate. In case of sapphire, the lattice mismatch is 16%, which is quite a lot and many dislocations are formed at the interface between sapphire and GaN layer. Two-step model growth (nucleation layer growth, annealing and coalescence of monocrystalline islands) helps to decrease the amount of threading dislocations and capability of the 2D growth (to get smooth surface).

At first, sapphire substrate is annealed at 1100°C in $H_2$ ambient for desorption of any contaminants from the surface. Afterwards, the temperature is reduced down to 550°C and surface is nitrified with ammonia flow. GaN layer with very poor crystallographic quality (called nucleation layer) is grown at the same temperature. This layer with typical thickness around 60 nm acts as a wetting layer for the next growth. During the temperature ramp up to 1000°C the nucleation layer is annealed and monocrystalline islands are created. The size and amount of these islands can be controlled by different growth parameters. It influences the quality of GaN layer. At defined point, annealing is stopped and gallium precursor is introduced into the chamber. Islands grow in all directions and the growth switches from 3D to 2D growth in the point when islands coalesce and create smooth surface. During this process, a lot of threading dislocations are bended and they annihilate with one another. The reduction of density is very significant (from almost $10^{10}$ $cm^{-2}$ down to $10^{8}$ $cm^{-2}$). The growth continues with n-doped layer when $SiH_4$ is introduced into the chamber. MQW structure can be grown on the top of these layers.

InGaN quantum wells are grown at lower temperature (650 – 800°C) compared to the GaN barriers (higher than 800°C) because indium incorporation is very sensitive on the temperature and at lower temperature more indium is incorporated into QWs. Therefore, temperature has to be cycled during the MQW structure growth. Record of the surface temperature for the whole growth is shown in Fig. 3.7 (red curve). Reflectance record (black curve) is shown in the same figure. It gives us useful information about the growth and capability to control the growth in the real time.

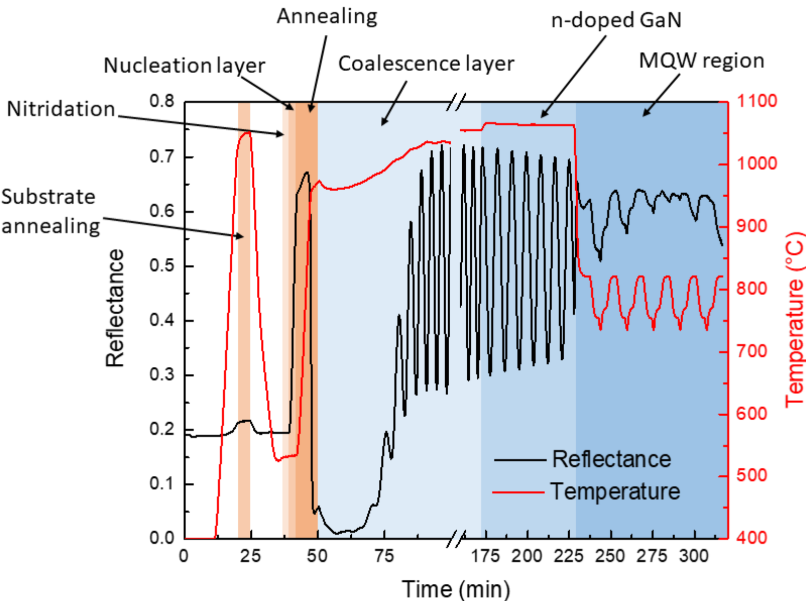


*Fig. 3.7. Reflectance (black curve) and surface temperature (red curve) record during the growth of scintillation structure with each growth step marked with different background colour.*

MQW structure growth is the most important part which influences significantly scintillation properties. Especially InGaN growth is very sensitive to the growth conditions and just a slight adjustment of the growth parameters can dramatically change the InGaN quality (optical, structural and electrical properties). There are a few problems with growing

high-quality InGaN layers. InN has a relative high vapour pressure compared to GaN, which leads to low indium incorporation into InGaN layer. Moreover, the difference in formation enthalpies for InN and GaN leads to a strong indium surface segregation. Appropriate growth parameters (low growth temperature, high V/III ratio or slow growth rate) can minimize these problems [54]. Reduction of the growth temperature reduces desorption of indium atoms from the surface. On the other hand, cracking of the ammonia is reduced significantly at lower temperature (the percentage of decomposed ammonia varies from only a few percent at 900 °C up to 40 – 50 % at 1050 °C). It leads to lower growth rate and lower indium incorporation into InGaN layer. A compromise has to be found between these two phenomena.

Since InGaN QWs need lower growth temperature, it is necessary to use different gallium precursor. TMGa precursor is usually used during the high temperature growth of undoped and n-doped GaN layers. At lower temperatures (below 1000°C), this precursor would be inefficiently decomposed and layers would contain many carbon impurities. TEGa precursor is decomposed at lower temperatures thanks to the bigger organic ligands with weaker bond to Ga atoms and additional way of decomposition (β-hydrogen elimination process) further lower the carbon contamination in layers. That is the reason why TEGa precursor is used during the growth of InGaN QWs and GaN barriers.

Another very important difference of MQW and buffer growth is in a carrier gas. During the high temperature GaN growth, hydrogen is normally used as a carrier gas. On the other hand, during the MQW growth nitrogen has to be used, because hydrogen used during the growth of InGaN reduces significantly indium incorporation [55] and thickness [56]. Understanding of the effect of the hydrogen during InGaN growth is still not well described. Recently, increased coverage of surface with H adatoms and easy desorption of In-H species from the surface was suggested as a reason of a bad indium incorporation in InGaN layers [57].

To get good crystallographic GaN barriers, it is necessary to grow them at higher temperature than InGaN QWs. It brings problems during the growth because temperature ramp is necessary to introduce and indium can easily desorb from InGaN QWs during temperature ramp to GaN barrier growth temperature. Moreover, many defects are concentrated at this upper interface between InGaN QW and GaN barrier. A lot of growth approaches were used, such as thin low temperature GaN cap layer, GaN growth during temperature ramp or many others. Each approach brings different problems and to find a proper way how to grow the upper interface for different nitride application is quite challenging.

As a summary, MQW growth is much more complex than growth of high temperature GaN buffer layers and different growth conditions are necessary, such as nitrogen carrier gas, TEGa precursor, lower growth temperature, higher pressure, slower growth rate and higher V/III ratio (higher amount of $NH_3$ flow).

## 3.5 Wafer and structure in situ measurement

Precise measurement of wafer temperature during epitaxial growth is one of the most important thing. It influences most of the parameters, such as growth rate, composition of ternary/quaternary compounds, roughness or doping level. Temperature is measured during the process by a thermocouple, which is mounted on the backside of a susceptor. It does not tell us the true information about wafer surface temperature due to limited thermal contact between the wafer and susceptor and due to cooling the wafer surface by gas flow and surface emanation (radiation emission). Data of true wafer temperature are obtained by emissivity corrected pyrometry measured at 950 nm wavelength.

Reflectance measurement at 405 nm or 633 nm wavelength tell us information about the growth rate, thickness and roughness of the grown layers. Incoming light is partly reflected at the surface and at the interface between layer and substrate. The overall intensity of the reflected light is given by the superposition of all reflected beams. Constructive or destructive interference will happen, leading to an intensity modulation of the reflected light (Fabry-Pérot oscillations). Moreover, from the evolution of intensity of these oscillations during the growth time we can get information about optical waviness and roughness of the surface.

A curvature of the wafer is also important parameter which changes during the epitaxial growth. Large curvature can lead to non-uniformities of wafer temperature and hence different layer composition and or thickness. Measurement is done by two parallel laser beams. If the wafer is curved, the reflected laser beams are not parallel any more. These two reflected laser beams are detected by Charge-coupled device camera and the curvature is determined from the distance between these spots. Curvature is influenced by different temperature at lower and upper face of the wafer, lattice mismatch between two different layers and different thermal expansion of the substrate and epitaxially grown GaN layer. All these three features contribute to the total curvature.

## 3.6 Structure ex situ measurement

For a description of specific sample properties, we have examined samples by several ex-situ measuring techniques. The structure quality was examined by high-resolution X-ray diffraction (HRXRD). More detailed pictures of structure quality were obtained on several samples by high-resolution transmission electron microscopy (HRTEM). Positron annihilation spectroscopy (PAS) was used for investigation of negative and neutral point defects in the structures (mainly gallium vacancies). For the visualization of the surface morphology, atomic force microscopy (AFM) was usually used. Electrical properties were examined by Hall measurement. Luminescence properties were examined by photo- and cathodo-luminescence (PL and CL). Finally, scintillation decay time was measured by time-resolved radioluminescence.

The HRXRD measurement give us information about the threading dislocation density of the GaN layers beneath the MQW region and information about the periodicity and mean

indium composition in the MQW region. The principle of this method is based on the Bragg's law which describes the diffraction of incoming waves on the periodic crystal structure. More details about the measurement of X-ray diffraction especially on nitrides can be found in Moram's overview paper [58]. Typical record of HRXRD measurement of MQW region is shown in Fig. 3.8.

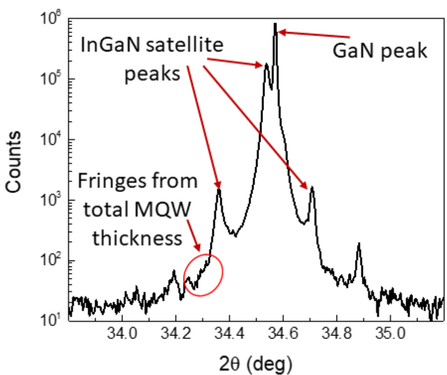


*Fig. 3.8. 2Theta-omega scan of a sample with 70 QWs. Main substrate GaN peak visible at 34.57° as well as satellite peaks from InGaN/GaN superlattice. Periodicity of $t_{InGaN} + t_{GaN}$ was estimated from the simulation to be 6.6 nm. Fringes from the total MQW thickness were not clearly visible due to bad interfaces (typical for structure with high number of QWs).*

The HRTEM measurement is very precise technique to distinguish monoatomic layers in the structure. We can resolve (In)GaN layer thickness in the MQW region and the InGaN composition for example. Together with HRXRD measurement, it can tell us complex information about the properties of MQW region and GaN buffer layers. The HRTEM measurement tell us more accurate information about the TDD but this technique is destructive and the preparation of the samples is very complicated. HRTEM image of InGaN QWs and GaN barriers with atomic resolution is shown in Fig. 3.9(a). Cross-section TEM image of the whole structure is shown in Fig. 3.9(b), where threading dislocations can be visible (see yellow arrow).

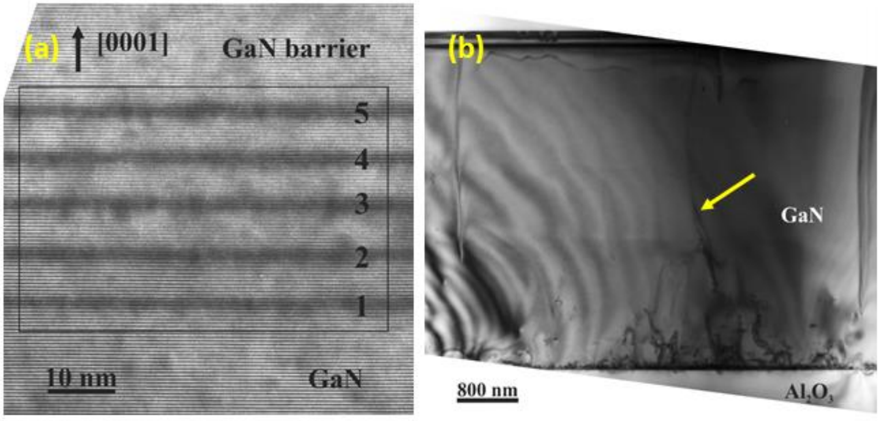


*Fig. 3.9. (a) HRTEM image of the 5x InGaN QWs (dark contrast) with GaN barriers (bright contrast) viewed along the [11-20] zone axis, (b) Bright Field Cross-section TEM image viewed using g = 0002. Measurement were done in the Aristotle University of Thessaloniki in Greece in the laboratory of Professor Philomela Komninou.*

PAS is non-destructive method for detection of negatively charged or neutral vacancies in semiconductors. Measurements were done by professor Jakub Čížek from the Charles University in Prague. The principle of this technique is based on the measurement of positron lifetime in structures which varies due to different number or type of vacancies. The lifetime of positron annihilated in the free state is significantly shorter than that for a positron trapped in vacancy because electron density in vacancy is reduced. Consequently, positron lifetime increases with increasing open volume of vacancy. That is why PAS can give us not only the estimation of vacancy concentration but also the information about the vacancy size or type.

For an investigation of a surface quality, AFM is usually used. The principle of this method is to scan the surface by a tip and measure the response of the surface. The tip holder bends due to the van der Waals forces between the tip and surface atoms. Bending of the tip holder is recorded by a reflection of the laser beam which is detected by photodiode. As an example, two AFM images of our GaN layer and whole scintillation structure with 20 QW InGaN/GaN region are shown in Fig. 3.10(a) and (b) respectively.

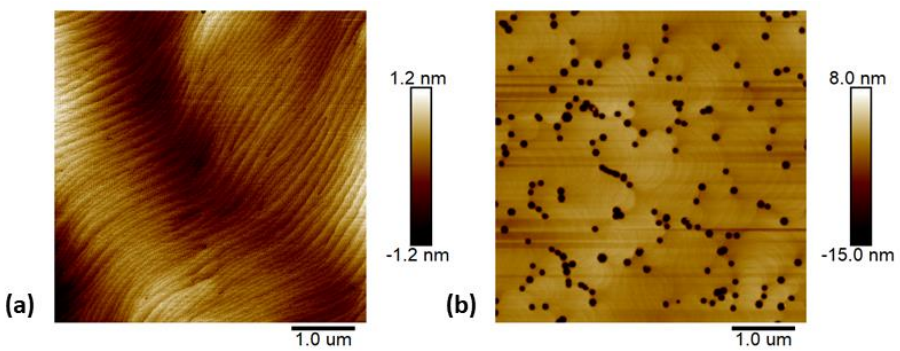


*Fig. 3.10. AFM images of (a) GaN buffer layer and (b) sample with 20 QWs. Images were taken by Dimension Icon AFM in semicontact mode, using ASPIRE tips.*

Electrical and transport properties of free carriers in GaN buffer layers were examined by Hall measurement. With this technique, we are able to examine the doping type (p-type or n-type), free carrier concentration and their mobility.

The PL is very important for the characterization of our structures. In our laboratory, we have the possibility to use two different laser excitation wavelengths 325 nm and 375 nm, respectively. It is important to note that at a room temperature with these two different excitation wavelengths we excite directly InGaN QWs (375 nm) or barriers over the GaN bandgap (325 nm). Differences in obtained results help us to resolve the mechanism of creation of excitons, transport and their recombination. Another difference is in the penetration depth of incoming photons. When we use 375 nm excitation wavelength, we excite directly QWs and excite them all (even for samples with high number of QWs – up to 100) because the thickness of the single QW layer is only 1 – 2 nm. On the other hand, when 325 nm excitation wavelength is used, GaN barriers and thus only the upper part of the structure is excited (typically upper 10 QWs). Penetration depth in GaN for 325 nm wavelength was evaluated from the absorption coefficient (taken from [59]) to be approximately 90 nm, where ~63% of primary intensity of light is absorbed. Measurement at

both excitation wavelengths is very important and useful. When we want to use our structure as a scintillation detector (detection of high-energy photons or particles), we are dealing with excitation over GaN bandgap (the similar mechanism in PL at 325 nm excitation wavelength) and excitation of the whole structure, not only the upper part of the MQW region (information even about the quality of lower QWs as we can get from the PL measured at 375 nm excitation wavelength).

One of the promising application of our structure is a scintillation detector in the electron microscopes (detector of secondary or backscattered electrons). That is the reason why we use the CL as an another important luminescence characterization technique. We can change the penetration depth of incident electron beam by changing acceleration voltage. The penetration depth of electrons in GaN can be described by this equation [60]:

$$d = 10.46\, U^{1.68}$$

where U is acceleration voltage of electrons in keV and d is the penetration depth in nanometres.

CL measurement with different acceleration voltage of primary electrons shows different luminescence bands and their intensities (see Fig. 3.11). With 5 keV acceleration voltage (penetration depth is 160 nm) we excite only MQW region, so we can resolve luminescence band at 2.96 eV, which is QW excitonic band and broad band (so called QW defect band) with centre at 2.47 eV. When we use 15 keV acceleration voltage (990 nm penetration depth), we excite even GaN below the MQW region, so we can see GaN emission band at 3.4 eV. Broad defect band now has two contributions, QW defect band and yellow defect band, which comes from the GaN below the MQW region.

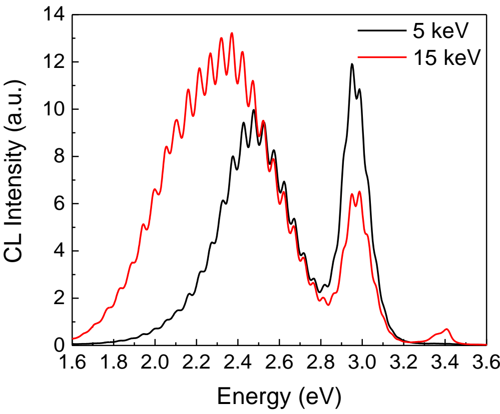


*Fig. 3.11. CL results measured on sample with 10 QWs (active region thickness about 100 nm) with two different acceleration voltages of primary electrons (5 and 15 keV).*

Time-resolved radioluminescence allows us to resolve kinetic properties of samples which are very important parameters of scintillation structures. We have used different measuring setups in collaboration with different laboratories, where they have different time resolution and different excitation source (for example laboratories in CERN, Claude Bernard

University Lyon 1 or Faculty of Biomedical Engineering of the Czech Technical University). The principle of the technique is usually based on time-correlated single photon counting (TCSPC) which is based on the detection of single photons and the measurement of their arrival times with respect to a reference signal. The reference signal goes directly from light source into the detector. Signal coming from the sample has some delay time, which is measured and analysed by multi-channel analyser. Delay time is plotted in a histogram, in which the channels on the x-axis represent time. TCSPC is a statistical method and requires a high repetitive source for accumulation a sufficient number of photons. As a source can be used pulsed laser diode (time-resolved photoluminescence) or pulses of X-ray (time-resolved radioluminescence). Time-resolved photoluminescence decay profile of sample with 50 QWs is shown in Fig. 3.12.

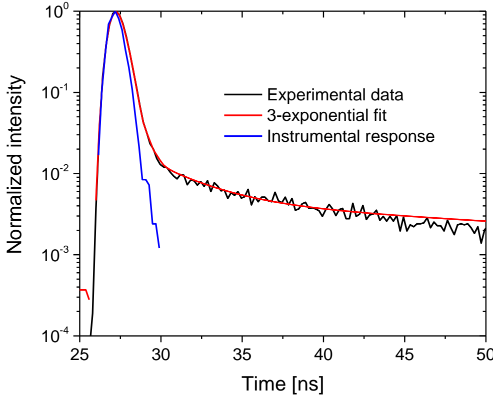


*Fig. 3.12. Time-resolved photoluminescence decay profile of sample with 50 QWs excited with 339 nm laser diode. Provided 3-exponential fit shows decay times: $\tau_1$ = 0.44 ns, $\tau_2$ = 1.8 ns and $\tau_3$ = 41.4 ns. Instrumental response in the same range as the fastest component of the excitonic band.*

# 4 Collection of Papers

This chapter collects seven original papers published in the impact journals, related to the dissertation topic. Papers are ordered with respect to the scintillation structure. The first four papers are devoted to technology of GaN buffer (papers [i], [ii]) and layers surrounding the InGaN/GaN MQW active region (papers [iii], [iv]), following three papers are devoted to technology and properties of InGaN/GaN MQW active region itself (papers [v], [vi] and [vii]). The first paper is focused on the growth of GaN nucleation and coalescence layer on the sapphire substrate. In the second paper, which was accepted for publication before the finish of this doctoral thesis, we have studied the growth of n-doped GaN layer and effect of different precursors (TMGa or TEGa) used for n-doped GaN growth. The third paper deals with the influence of Si doping of buffer and GaN capping layer on the luminescence and structural properties of the MQW active region. The fourth paper suggested the improvement of the scintillation structure quality by adding the low temperature GaN layer directly below the MQW region. The fifth paper studies the effect of different QW number (10 or 30 QWs) on the luminescence properties, especially cathodoluminescence properties. In the next paper, we have increased the QW number more (up to 70 QWs) and studied the effect of the thick active region on the luminescence and structural properties of the scintillation structure. The last paper introduced the new method of the growth interface between QW and barrier in the MQW region. The new method increased the indium content in InGaN QW layer which can be useful not only for scintillation applications but also for the LED structures emitting in the green spectrum. This process was successfully patented and the author of the doctoral thesis is the co-author of the patent, see [xii].

## 4.1 Improvement of luminescence properties of GaN buffer layer for fast nitride scintillator structures [i]

In this paper, we have studied the initial part of the GaN growth on the sapphire substrate. The nucleation and coalescence layer growth was studied. Nucleation layer, which is the wetting layer for the subsequent high temperature GaN growth, was studied and luminescence properties were improved by higher reactor pressure and longer layer growth with subsequent longer annealing. The next part of the paper deals with growth parameters of high temperature coalescence layer. The luminescence properties were improved by lower $NH_3$ flow (graded flow) during coalescence layer growth. The lower temperature also improved the quality. Very good quality of GaN buffer layers is necessary for the growth of MQW region and we have successfully improved undoped GaN quality, which was indicated by significant increase of the ratio of excitonic/YB luminescence intensity from 0.65 before optimization to 16.8 after the optimization. This paper was published in Journal of Crystal Growth (IF = 1.57, Q3, 7 citations).

Journal of Crystal Growth 464 (2017) 221–225

Contents lists available at ScienceDirect

Journal of Crystal Growth

journal homepage: www.elsevier.com/locate/jcrysgro

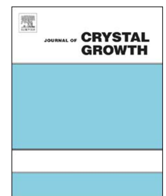

# Improvement of luminescence properties of GaN buffer layer for fast nitride scintillator structures

T. Hubáček[a], A. Hospodková[b,*], J. Oswald[b], K. Kuldová[b], J. Pangrác[b]

[a] *Institute of Mechatronics and Computer Engineering, TUL, Liberec, Czechia*
[b] *Institute of Physics CAS, v. v. i., Cukrovarnická 10, 162 00 Prague 6, Czechia*

ARTICLE INFO

'Communicated by' Dr. T.F. Kuech

*Keywords:*
A3. MOVPE
A3. GaN
B3. scintillators
A1. yellow band

ABSTRACT

We have optimized technology of GaN buffer layer growth with respect to the application in fast scintillation structures. The deep defect luminescence so called yellow band (YB) with decay time up to tens of microseconds is undesired for these applications and should be suppressed or at least the ratio of intensities of excitonic to YB maximum has to be considerably increased. The required photoluminescence properties were achieved by optimization of growth parameters of nucleation and coalescence layer on sapphire substrate. We have shown that decrease of $NH_3$ flow, decrease of coalescence temperature, increase of nucleation time and nucleation pressure lead to improvement of the structure and luminescence properties of the buffer layer. Results indicate a significant increased ratio of excitonic/YB luminescence intensity.

## 1. Introduction

The use of GaN as a material for optoelectronic devices has been increased since the first blue LEDs have been made in the early 1990s. Other prospective applications of nitride semiconductors are detectors of ionizing radiation and scintillators [1]. The advantages of GaN (ZnO as well) compared to other scintillation materials are wide band gap and high exciton binding energy. ZnO is used in scintillators for several decades. The advantages of GaN compared to ZnO are preparation with higher crystallographic quality and homogeneous epitaxial layers. It brings an advantage of better emission homogeneity over large area, high signal to noise ratio and narrower spectral range [2]. A demand for very fast scintillators with decay time of few nanoseconds was created in the last years due to the decreased size of integrated circuit structures down to a nanoscale and necessity of fast scanning electron microscopes for inspection machines in electronic industry. For these applications nitride heterostructures are highly promising.

The most important problem for creating nitride structures is the green-yellow band (YB) which is observed in the luminescence spectra. This deep defect luminescence with long decay time up to tens of microseconds is undesired, especially for fast luminescence applications, and should be suppressed or separated from the luminescence spectra or at least the ratio of intensities of excitonic to YB maximum has to be considerably increased.

YB is a deep defect luminescence which originates in GaN layer. Although many publications were devoted to the problem which type of defect or defect complexes could be responsible for it, the origin of defect-based luminescence is still under scientific discussion [3].

The structure which could be used for fast scintillation detectors is partly similar to nitride LED structures. Compared to LED it is necessary to grow a structure with higher number of QWs, so that the penetration of electrons to the heterostructure and active region with QWs have similar thickness. Only n-type doping is necessary to conduct excess electrons to the contacts. To prepare high quality InGaN/GaN MQW, it is necessary to grow them on a high quality buffer layer with optimized excitonic photoluminescence (PL) and suppressed YB luminescence or increased ratio of intensities of excitonic to YB maximum.

The aim of this work is to optimize the growth of the buffer layer, which will be suitable for the growth of scintillator structure. We have focused on the initial part of the buffer layer technology, which are the nucleation and the coalescence growth condition. A partial suppression of YB luminescence could be done with specific modification of the GaN growth technology. A very important step for obtaining high quality films is the growth of the nucleation layer (NL), which represents the wetting layer for the subsequent growth of the high temperature buffer layer [5]. The effect of temperature [6], reactor pressure [7] and V/III ratio [8,9] were studied by several groups during last twenty years. Thermal annealing of the nucleation layer is important to obtain suitable size and shape of islands of monocrystalline GaN [10]. The next step, coalescence of these islands, is also important. Change of growth temperature, reactor pressure and V/III ratio can influence the

* Corresponding author.
*E-mail address:* hospodko@fzu.cz (A. Hospodková).

http://dx.doi.org/10.1016/j.jcrysgro.2016.12.088

Available online 23 December 2016
0022-0248/ © 2017 Elsevier B.V. All rights reserved.

quality and optical properties of the high temperature buffer layer.

In this work we present incremental optimization of PL properties of GaN buffer layer by changing seven technological parameters. The nucleation layer technology and coalescence layer growth were optimized separately.

## 2. Experimental

All structures were prepared on Aixtron 3×2 CCS MOVPE System equipped by Laytec EpiCurveTT apparatus for in situ measurement of reflectivity. A true wafer temperature was measured in situ by EpiCurveTT. Trimethylgallium (TMGa) and ammonia ($NH_3$) were used as precursors with a hydrogen carrier gas. Sapphire substrate with c-plane orientation was baked out at 1045 °C for 300 s and afterwards nitrified by the $NH_3$ injection at 528 °C, which was also the temperature used for the nucleation layer growth. Optimization of the nucleation and coalescence layer growth with respect to photoluminescence properties was investigated. After the coalescence, the growth was finished by 2.4 µm of GaN high temperature buffer layer grown under the same growth conditions. The growth parameters which were kept fixed for the growth of the buffer layer are growth temperature 1036 °C, reactor pressure 250 mbar, total flow through the reactor 8 slpm, TMGa flow 1.1 $10^{-4}$ mol/min and V/III ration 1286. Twelve samples, which were prepared during the optimization process are presented in the Table 1 which summarizes the optimized growth parameters.

The PL was chosen as the main characterization method. The excitation with wavelength 325 nm is absorbed in approx. 100 nm of GaN, so the PL properties measured by this method are attributed only to the topmost part of the GaN buffer layer, which is exactly the region of interest when optimizing the buffer layer technology for subsequent active region growth. On the contrary, the X-ray diffraction give us average information from the whole buffer layer volume. Additionally, the PL measurements are more sensitive to the layer quality than X-ray diffraction as will be demonstrated in our conclusions. The PL spectra were measured at RT using confocal microscopy (LabRAM HR Evolution, excitation laser He-Cd λ=325 nm, objective 74CG, spot diameter 2 µm). Due to the different decay times of excitonic and YB luminescence, YB peak became saturated for higher excitation intensities, see Fig. 1. So that the intensity of measured spectra in the manuscript could be compared to each other, the PL measurement conditions as well as the excitation intensity were kept fixed (relative excitation intensity was 1, see Fig. 1).

## 3. Results and discussion

Several samples were prepared to study the influence of nucleation and coalescence layer growth conditions on PL properties of GaN grown on sapphire. Since qualitatively different results were obtained by optimization of coalescence and nucleation layer, we have presented the results into separate subsections. The last subsection presents PL results achieved by increased buffer layer thickness.

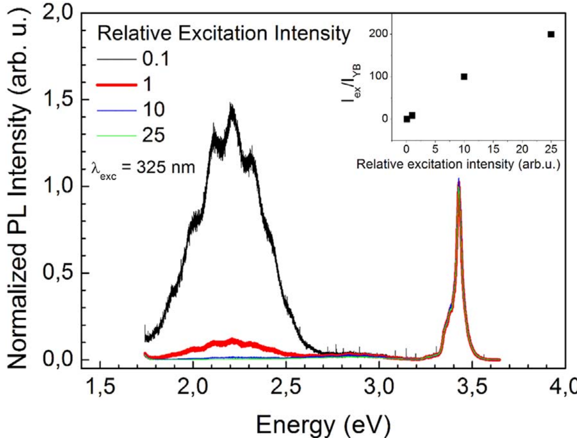


**Fig. 1.** Comparison of buffer layer PL spectra normalized to excitonic peak intensity excited by different excitation intensity. Relative contribution of YB luminescence is strongly decreasing with excitation intensity due to a long decay time and consequent saturation of this maximum. Rem.: spectra presented in Figs. 3–8 were recorded with relative excitation intensity I=1.

### 3.1. Coalescence layer growth

The first experiments were focused on the growth of coalescence layer. The aim was to increase the coalescence time, which is supposed to decrease the density of dislocations and improve the PL properties of formed GaN layer. We have investigated two possible ways to increase the coalescence time, by decreasing the V/III ratio ($NH_3$ flow) or decreasing the temperature during coalescence. The increase of coalescence time with decreased $NH_3$ flow is shown in Fig. 2(a).

Fig. 2(b) shows PL spectra of two samples with different ammonia flow during the growth of coalescence layer. A stronger PL improvement was achieved by decreased ammonia flow, which decreased YB luminescence intensity and enhanced excitonic luminescence. The lower V/III ratio during initial stage of coalescence leads to extended three-dimensional growth region. Therefore, there are larger islands with lower density. Screw dislocations are mainly created from the different step height of substrate and edge dislocations are generated from the coalescence process among the misoriented individual islands [11,12]. Lower V/III ratio during initial stage of coalescence layer growth helps to reduce edge or mixed edge dislocation density which

**Table 1**
Optimized growth parameters of presented samples, the thickness of coalescence and buffer layer is 2 µm for samples S1-S11 and 4 µm for sample S12.

| Sample | Nucleation | | | | Coalescence | | | $I_{ex}/I_{YB}$ratio |
|---|---|---|---|---|---|---|---|---|
| | Nucl. time (s) | Anneal. time (s) | Pressure (mbar) | Temperature (°C) | Temperature (°C) | $NH_3$ flow (sccm) | | |
| | | | | | | Initial | Final | |
| S1 | 160 | 30 | 200 | 530 | **1010** | **2900** | **2900** | 0.65 |
| S2 | 160 | 30 | 200 | 530 | 1010 | **2600** | **2600** | 1.65 |
| S3 | 160 | 30 | 200 | 530 | **990** | 2900 | 2900 | 1.92 |
| S4 | 160 | 30 | 200 | 530 | **990** | **2700** | **3200** | 2.70 |
| S5 | 160 | **30** | 200 | 530 | **970** | 2700 | 3200 | 2.77 |
| S6 | 160 | **60** | **200** | 530 | 970 | **2700** | 3200 | 2.91 |
| S7 | 160 | 60 | 200 | 530 | 970 | **2600** | 3200 | 1.78 |
| S8 | 180 | **90** | 200 | 530 | 970 | 2700 | 3200 | 3.87 |
| S9 | 160 | 60 | **500** | 530 | 970 | 2700 | 3200 | 6.08 |
| S10 | 160 | 60 | **600** | **530** | 970 | 2700 | 3200 | 5.37 |
| S11 | 160 | 60 | 600 | **545** | 970 | 2700 | 3200 | 6.52 |
| S12 | 160 | 60 | 600 | 545 | 970 | 2700 | 3200 | 16.80 |

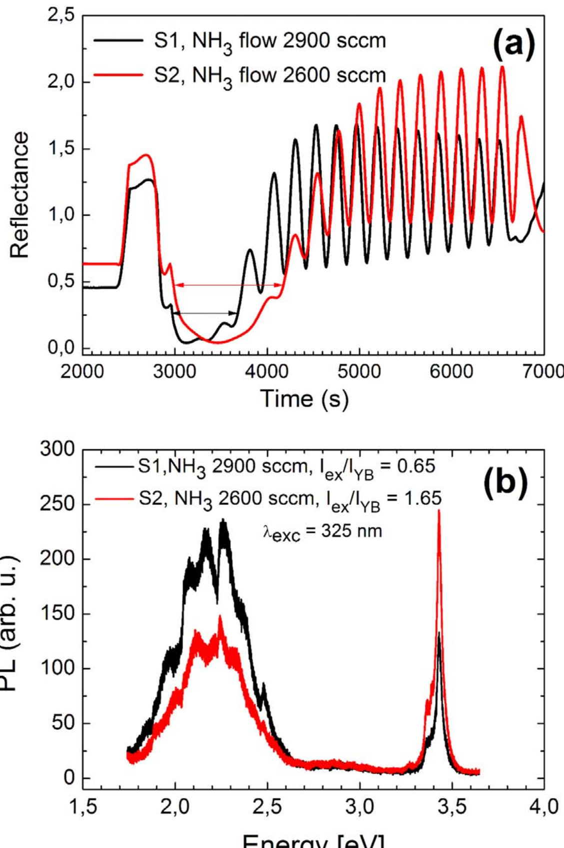


**Fig. 2.** Comparison of samples S1 and S2 with different $NH_3$ flow, 2900 sccm and 2600 sccm, during coalescence layer growth (a) reflectance measured at 633 nm during the sample growth. The coalescence time is marked by arrows, (b) comparison of PL spectra.

could lead to lower YB luminescence intensity and increased intensity of the excitonic peak. The screw dislocation density is not changed according to [12].

Another way to increase the coalescence time is to decrease the coalescence temperature. In our experiment both temperatures were decreased for sample S3, coalescence and as well as annealing temperature. PL spectra of GaN buffer S1 and S3 are shown in Fig. 3. The excitonic peak intensity remained almost unchanged. We suppose that this experiment did not help us to decrease the dislocation density because the lower mobility of addatoms during coalescence process was compensated by smaller monocrystal islands created

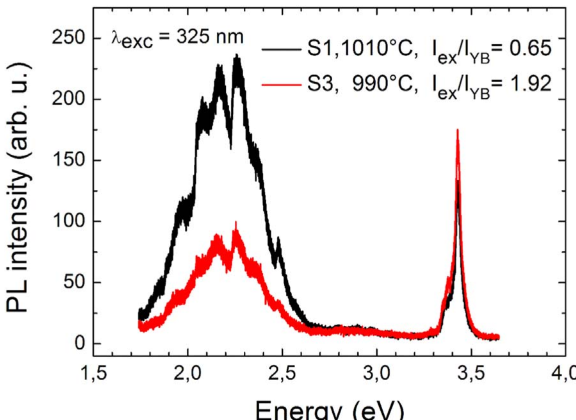


**Fig. 3.** PL spectra of samples S1 and S3 with different coalescence and annealing temperature of nucleation layer, 1010 °C and 990 °C.

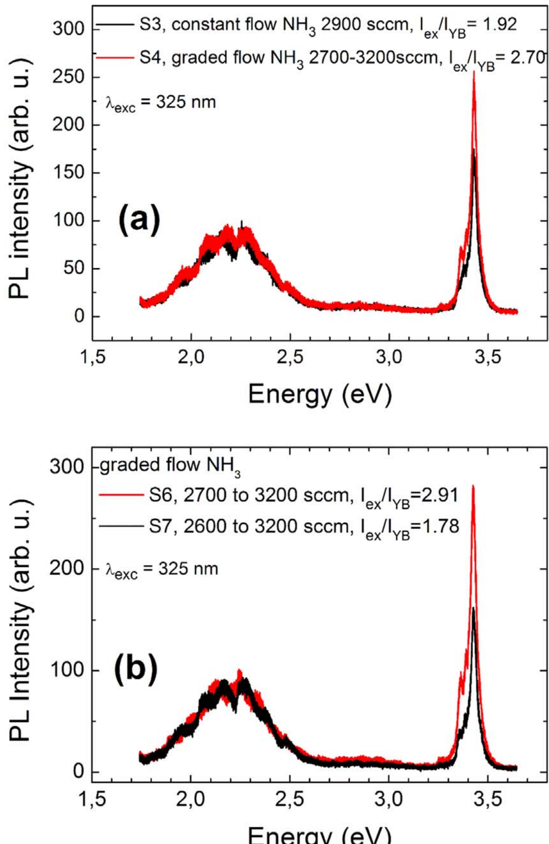


**Fig. 4.** PL spectra with graded $NH_3$ flow during coalescence with different initial $NH_3$ flow.

during annealing at lower temperature. On the other hand, considerable decrease of YB luminescence was achieved by decreasing the annealing and coalescence temperature by 20 °C. This decrease is similar to lowering $NH_3$ flow see Fig. 2(b) and may be caused by lower $NH_3$ decomposition at lower temperature. YB luminescence is probably not connected with dislocation density but with some point defect which are also influenced by V/III ratio.

Lowering the $NH_3$ flow may help to prolong the coalescence process as was demonstrated in Fig. 2(a), however, it is not optimal for further growth of the buffer layer after coalescence process. That is why we have used graded $NH_3$ flow during the coalescence layer growth. The PL results of sample with constant (S3) and with graded (S4) $NH_3$ flow are compared in Fig. 4(a), which show an improvement of excitonic maximum intensity. The $NH_3$ starting flow of 2700 sccm was found to be optimal for 970 °C growth temperature, see Fig. 4(b).

### *3.2. Nucleation layer and annealing*

After coalescence layer optimization, we have tried to improve the technological parameters for GaN nucleation on nitridated sapphire substrate and subsequent annealing. The aim was to decrease the density and increase the size of monocrystalline nuclei in the amorphous nucleation layer. The influence of three parameters, annealing time, reactor pressure and temperature on PL properties was investigated.

The most obvious way to increase the size of monocrystalline nuclei is to prolong the annealing time when the nuclei are developing. Adjusting proper time of nucleation layer growth and subsequent annealing is critical step for successful GaN growth on sapphire [13]. A scheme of structure after annealing is shown in Fig. 5(a). After sufficient annealing time, the monocrystalline nuclei are big enough to extend the amorphous nucleation layer surface and their extending

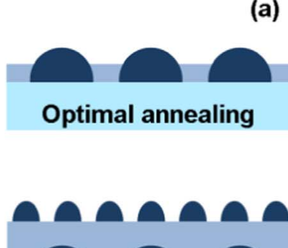


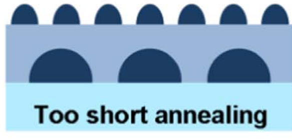


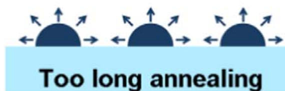


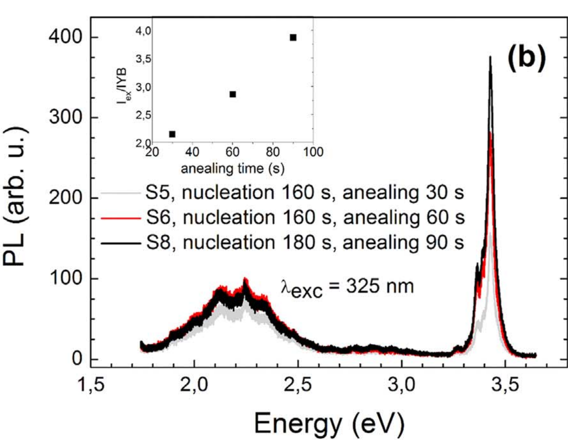


**Fig. 5.** Influence of annealing time. (a) Schematic drawing of GaN nuclei after annealing for optimal, short and long annealing time, (b) PL spectra of samples with different nucleation growth time/annealing time 160/30 s, 160/60 s and 180/90 s.

part become nuclei for subsequent high temperature monocrystalline epitaxy, amorphous nucleation layer enhances the lateral growth of islands and good quality of created layer is achieved. After short annealing time, monocrystalline nuclei do not reach the nucleation layer surface and poor crystalline or polycrystalline quality is obtained. Too long annealing time leads to depletion of wetting amorphous nucleation layer, 3D growth of islands occurs and rough surface is obtained. Fig. 5(b) shows PL results obtained on samples S5, S6 and S8 with different nucleation growth and annealing time. Longer nucleation and annealing time increases the size of the islands and less threading dislocations penetrate into high temperature buffer during the coalescence. Annealing time is correlated with nucleation growth times. Longer growth time needs longer annealing time as well. The highest intensity of excitonic maximum was achieved as expected for sample with longest annealing time, which is supposed to have lowest edge and mixed edge dislocation density. YB intensity is not affected.

The PL spectrum with different reactor pressure during the nucleation layer growth is shown in Fig. 6. The reactor pressures were 200, 500 and 600 mbar.

The increase of reactor pressure to 500 mbar has twice increased excitonic luminescence, for 600 mbar the increase is saturated (see Fig. 6). The mechanism of this improvement is not well understood. Higher reactor pressure at low growth temperature of the nucleation layer may improve the ammonia dissociation and improve the mobility of atoms, which could lead to more distant and bigger monocrystalline nuclei.

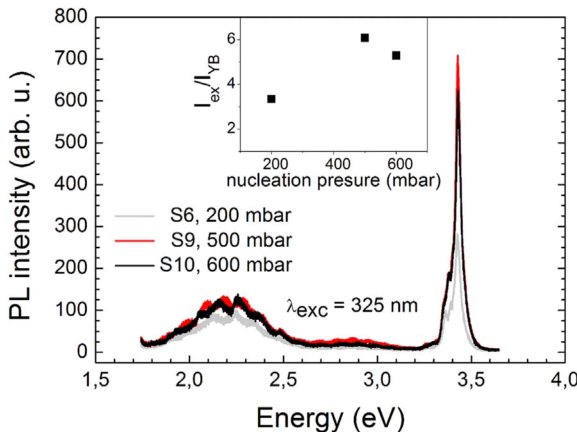


**Fig. 6.** PL spectrum of samples with different reactor pressures 200 mbar, 500 mbar and 600 mbar.

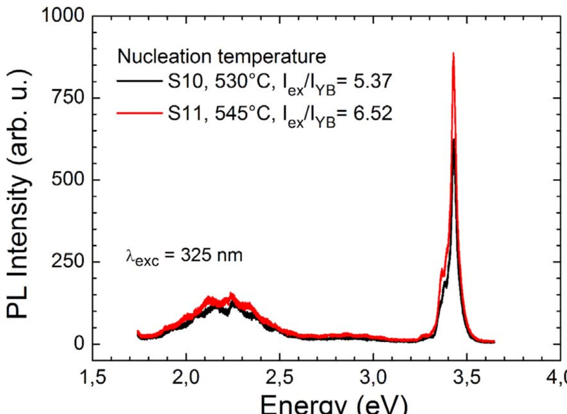


**Fig. 7.** PL spectrum of samples S10 and S11 with different nucleation temperature 530 °C and 545 °C.

Last technological parameter which was investigated was the growth temperature of nucleation layer. Two samples were prepared at 530 °C and 545 °C. PL spectrum of these samples is shown in Fig. 7. The small increase of excitonic peak intensity was observed for sample S11 with higher annealing and nucleation growth temperature. This increase is probably caused by bigger monocrystaline nuclei formed at slightly higher nucleation temperature.

### 3.3. Buffer layer thickness

To improve the top layer quality for the epitaxy of active region we

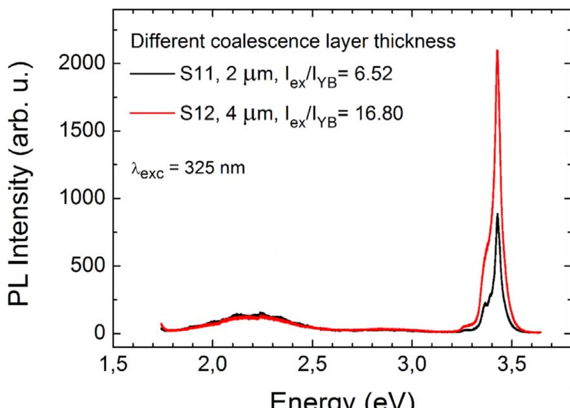


**Fig. 8.** PL spectra of samples S11 and S12 with different thickness of the buffer layer.

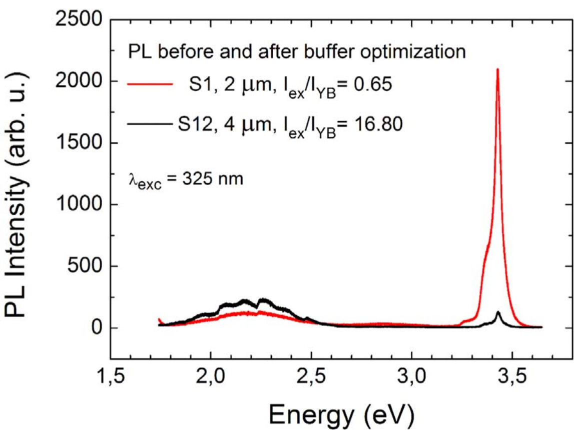


**Fig. 9.** Comparison of PL spectra before (S1) and after (S12) optimization of buffer layer growth.

have finally doubled the buffer layer thickness for sample S12. In the Fig. 8 is compared the PL of samples S11 and S12 prepared under the same technological conditions but differing in the buffer layer thickness. With increased buffer layer thickness considerable enhancement of the excitonic maximum was obtained, which is the sign of decreased dislocation density of the topmost GaN layer.

## 4. Conclusions

Nucleation and coalescence layer growth using the MOVPE technique was optimized with respect to their PL spectra.

The basic improvement of the nucleation layer was achieved through changing the nucleation time and annealing after the growth. Best results were obtained for the layer with 180 s nucleation time and 90 s annealing time. We have shown that the higher reactor pressure during nucleation and annealing process has positive influence on the excitonic luminescence. Best results were obtained with pressure 500 mbar. The cause is probably higher efficiency of ammonia decomposition, improved mobility of adatoms on the surface and subsequent increase of the monocrystalline nuclei size. The influence of the nucleation temperature was only week in the range of 530–545 °C.

The investigation of different parameters for the nucleation layer growth showed big influence on the excitonic luminescence but no significant influence on the YB luminescence. On the other hand, optimization of growth parameters of the coalescence layer had stronger impact on the YB luminescence. From these results we can suppose that the excitonic peak intensity is more influenced by the density of dislocations while the YB luminescence is caused by point or complex defects which are distributed randomly in epitaxial layer and are influenced by the growth parameters such as growth temperature or V/III ratio. Decreased concentration of nitrogen atoms or effective V/III ratio has suppressed the YB luminescence intensity. This is in agreement with results published in [4], where the origin of YB to be gallium vacancy is supposed to be caused by shallow donor ($V_{Ga}D$) complexes.

A comparison of the first sample and the last optimized sample is shown in Fig. 9. The quality of the growth layers was increased which indicates higher ratio excitonic/YB luminescence (0.65 for the first sample S1 and 16.8 for the last sample S12). We have also compared the density of dislocation of the first and the last sample. Derived from X-ray diffraction the density of edge and mixed edge dislocations has decreased only slightly from $1 \cdot 10^9$ cm$^{-3}$ to $0.9 \cdot 10^9$ cm$^{-3}$. This results suggest that decrease of the dislocation density is not the only reason for excitonic luminescence enhancement and also that PL measurements is much more sensitive method to evaluate the quality of the topmost region of the buffer layer. Further improvement of PL properties of the buffer layer could be achieved by optimization of the nitridation step which precedes the growth of nucleation layer [9,14,15] which might be a focus of future work.

## Acknowledgments

This work was supported by Grand Agency of the Czech Republic (GACR) project no. 16–11769S, by the MSMT NPU project no. LO1603 – ASTRANIT and by Student Grant Competition of Technical University of Liberec.

## References

[1] W. Lehmann, Edge emission of n-type conducting ZnO and CdS, Solid-State Electron. 9 (1966) 1107–1110 0.1016/0038-1101(66)90134-1.
[2] A. Hospodková, et al., InGaN/GaN multiple quantum well for fast scintillation application: radioluminescence and photoluminescence study, Nanotechnology 25 (2014) 455501 0.1088/0957-4484/25/45/455501.
[3] D.O. Demchenko, I.C. Diallo, M.A. Reshchikov, Yellow luminescence of gallium nitride generated by carbon defect complexes, Phys. Rev. Lett. 110 (2013) 087404. http://dx.doi.org/10.1103/PhysRevLett.110.087404.
[4] M.A. Reshchikov, H. Morkoç, Luminescence properties of defects in GaN, J. Appl. Phys. 97 (2005) 061301. http://dx.doi.org/10.1063/1.1868059.
[5] H. Morkoç, Handbook of Nitride Semiconductors and Devices (ISBN 9783527408382), Wiley-VCH Verlag GmbH & Co. KGaA, Weinheim, 2009, p. 2009.
[6] M.S. Yi, H.H. Lee, D.J. Kim, S.J. Park, D.Y. Noh, C.C. Kim, J.H. Je, Effects of growth temperature on GaN nucleation layers, Appl. Phys. Lett. 75 (1999) 2187–2189. http://dx.doi.org/10.1063/1.124959.
[7] J. Chen, S.M. Zhang, B.S. Zhang, J.J. Zhu, G. Feng, X.M. Shen, Y.T. Wang, H. Yang, W.C. Zheng, Effects of reactor pressure on GaN nucleation layers and subsequent GaN epilayers grown on sapphire substrate, J. Cryst. Growth 254 (2003) 348–352. http://dx.doi.org/10.1016/S0022-0248(03)01235-1.
[8] T. Yang, K. Uchida, T. Mishima, J. Kasai, J. Gotoh, Control of initial nucleation by reducing the V/III ratio during the early stages of GaN growth, Phys. Status Solidi A 180 (2000) 45. http://dx.doi.org/10.1002/1521-396X(200007)180:1 < 45:AID-PSSA45 > 3.0.CO;2-5.
[9] A.E. Wickenden, D.D. Koleske, R.L. Henry, R.J. Gorman, J.C. Culbertson, M.E. Twigg, The impact of nitridation and nucleation layer process conditions on morphology and electron transport in GaN epitaxial films, J. Electron. Mat. 28 (1999) 301–307. http://dx.doi.org/10.1007/s11664-999-0031-0.
[10] L. Sugiura, K. Itaya, J. Nishio, H. Fujimoto, Y. Kokubun, Effects of thermal treatment of low-temperature GaN buffer layers on the quality of subsequent GaN layers, J. Appl. Phys. 82 (1997) 4877–4882. http://dx.doi.org/10.1063/1.366350.
[11] S.T. Li, F.Y. Jiang, G.H. Fan, W.Q. Fang, L. Wang, The influence of growth mode on quality of GaN films and blue LED wafers grown by MOCVD, Physica B 391 (2007) 169–173. http://dx.doi.org/10.1016/j.physb.2006.09.014.
[12] S. Kim, J. Oh, J. Kang, D. Kim, J. Won, J.W. Kim, H.-K. Cho, Two-step growth of high quality GaN using V/III ratio variation in the initial growth stage, J. Cryst. Growth 262 (2004) 7–13. http://dx.doi.org/10.1016/j.jcrysgro.2003.10.009.
[13] M. Lada, A.G. Cullis, P.J. Parbrook, Effect of anneal temperature on GaN nucleation layer transformation, J. Cryst. Growth 258 (2003) 89–99. http://dx.doi.org/10.1016/S0022-0248(03)01517-3.
[14] S. Keller, B.P. Keller, Y.-F. Wu, B. Heying, D. Kapolnek, J.S. Speck, U.K. Mishra, S.P. DenBaars, Influence of sapphire nitridation on properties of gallium nitride grown by metalorganic chemical vapor deposition, Appl. Phys. Lett. 68 (1996) 1525–1527. http://dx.doi.org/10.1063/1.115687.
[15] K. Uchida, A. Watanabe, F. Yano, M. Kouguchi, T. Tanaka, S. Minagawa, Nitridation process of sapphire substrate surface and its effect on the growth of GaN, J. Appl. Phys. 79 (1996) 3487–3491. http://dx.doi.org/10.1063/1.361398.

## 4.2 Improvement of luminescence properties of n-GaN using TEGa precursor [ii]

This paper follows the first paper with respect to the study of GaN buffer layers. N-doped GaN layer is usually grown under the MQW region and due to the decrease of the formation energies of acceptor levels in n-doped GaN, intensity of defect bands (especially yellow band) are increased because the origin of the YB is recombination of electrons from shallow donor level and holes trapped in some kind of deep acceptor level (0.9 eV above valence band). After more than 20 years, there is still open discussion about the source of the acceptor level responsible for the YB. In our work, we have used different approach for the growth of n-doped GaN layer (different precursor). We were able to improve luminescence properties of n-doped GaN layers using TEGa precursor. Significant increase of excitonic band and consequence decrease of YB was observed. We have experimentally shown that both defects $C_N$ as well as $V_{Ga}$ can be responsible for YB luminescence. Using positron annihilation spectroscopy, we have identified presence of huge vacancy complexes in layers grown at $N_2$ atmosphere. This paper was published in Journal of Crystal Growth (IF = 1.57, Q3).

Journal of Crystal Growth 531 (2020) 125383

Contents lists available at ScienceDirect

Journal of Crystal Growth

journal homepage: www.elsevier.com/locate/jcrysgro

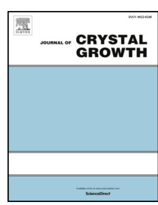

# Improvement of luminescence properties of n-GaN using TEGa precursor

T. Hubáček[a,b,*], A. Hospodková[a], K. Kuldová[a], M. Slavická Zíková[a], J. Pangrác[a], J. Čížek[c], M.O. Liedke[d], M. Butterilng[d], A. Wagner[d], P. Hubík[a], E. Hulicius[a]

[a] Institute of Physics CAS, v.v.i., Cukrovarnická 10, CZ-16200 Prague 6, Czech Republic
[b] Faculty of Mechatronics, Informatics and Interdisciplinary Studies, Technical University of Liberec, Studentská 2, CZ-46117 Liberec, Czech Republic
[c] Faculty of Mathematics and Physics, Charles University, V Holešovičkách 2, 18000 Praha 8, Czech Republic
[d] Institute of Radiation Physics, Helmholtz-Zentrum Dresden-Rossendorf Bautzner Landstr. 400, 01328 Dresden, Germany

ARTICLE INFO

Communicated by T.F. Kuech

*Keywords:*
A3. MOVPE
A1. TEGa precursor
B1. n-GaN
A1. yellow band
A1. $V_{Ga}$ defect

ABSTRACT

The aim of this work is to compare and improve optical and structural properties of GaN layers prepared using TMGa or TEGa precursors. MOVPE grown GaN buffer layers on sapphire substrates are usually grown from TMGa precursor at the temperatures above 1000 °C. These layers contain deep and shallow acceptor levels which are responsible for blue and yellow defect bands in luminescent spectra. Both defect bands are detrimental for all major nitride device applications. Especially n-doped GaN layers suffer from strong yellow defect bands. In this work, it is shown that yellow band photoluminescence intensity can be suppressed by using TEGa precursor during the growth of n–doped GaN layers. Different kinds of growth parameters, such as growth temperature or growth rate, have been studied. It is also shown that the change of carrier gas ($H_2$ or $N_2$) has very strong influence on the layer quality. $H_2$ carrier gas increased intensity of yellow band in sample grown from TEGa precursor while $N_2$ carrier gas had the same effect for sample grown from TMGa precursor. Variable energy positron annihilation spectroscopy showed creation of single $V_{Ga}$ in $H_2$ atmosphere and clustering of $V_{Ga}$ to big complexes $((V_{Ga})_3(V_N)_n)$ in $N_2$ atmosphere.

## 1. Introduction

Epitaxial GaN layers were first grown by Metal Organic Vapor Phase Epitaxy (MOVPE) technology in the late 1960 s by Manasevit and co-workers [1]. Layers were grown on c-plane sapphire substrates from trimethylgallium (TMGa), ammonia and a $H_2$ carrier gas. A significant breakthrough in nitrides growth was done in the late 1980s, when Amano and Akasaki invented a nucleation layer for the growth of nitrides on sapphire substrate [2]. This invention enabled to grow an active layer containing InGaN/GaN heterostructure on GaN buffer layer with sufficient quality. Since 1990s, GaN buffer layers grown on sapphire substrates have been extensively studied and the quality was improved. However, there are still a lot of open questions and unsolved problems today.

MOVPE grown GaN layers can be prepared from TMGa or TEGa precursors. TMGa is usually used for higher temperature growth while TEGa can be used at temperatures below 1000 °C. However, we have found that there are not many works comparing properties of GaN layers prepared using these two precursors. Therefore, one aim of this work is to contribute in this field and compare optical properties of GaN layers prepared from both precursors at different technological conditions.

GaN buffer layers are typically prepared from TMGa and ammonia precursors with a $H_2$ carrier gas at a growth temperature above 1000 °C, with V/III ratio between 1000 and 2000 and at growth pressure around 200 mbar. Silane is used for n-type doped GaN (similar growth conditions). GaN layers grown on sapphire substrate (the most common substrate for optoelectronic devices) have crystal structure with dislocation density around $10^8$ $cm^{-2}$. Undoped GaN layers are always unintentionally n-doped, due to impurities like oxygen or silicon; native defect formation cannot be excluded. All these defects and impurities in GaN are the cause of various bands in luminescent spectra. Many kinds of luminescent bands were described up to now, for example yellow band (YB) with the maximum around 2.2 eV or blue band (BB) with maximum around 2.9 eV. Most of them are described in review article [3].

The source of YB was attributed to some deep acceptor level [4]. Suppression of deep levels in GaN layers is a crucial point for all nitride applications, such as light emitting diodes (LEDs), high electron mobility transistors (HEMTs) or others. Deep levels (caused for example by carbon) can reduce electron mobility, which is detrimental for HEMTs [5]. In the active region of LEDs, they can be responsible for non-

* Corresponding author at: Institute of Physics CAS, v.v.i., Cukrovarnická 10, CZ-16200 Prague 6, Czech Republic.
*E-mail address:* hubacekt@fzu.cz (T. Hubáček).

https://doi.org/10.1016/j.jcrysgro.2019.125383
Received 24 September 2019; Received in revised form 25 November 2019; Accepted 27 November 2019
Available online 29 November 2019
0022-0248/ © 2019 Published by Elsevier B.V.

radiative recombination and decrease of the efficiency. For some other applications, such as fast scintillation detectors, non-radiative recombination is less detrimental than a radiative recombination, which has a long decay time [6,7]. In unintentionally n-doped GaN layers, the formation of acceptor levels is the most probable. Suppression of acceptor levels' formation in undoped GaN is difficult and in intentionally n-doped GaN layers is even more challenging (due to the lower formation energy of acceptor defects). Therefore, we have studied n-doped GaN layers in this work.

Undoped GaN layers grown from TMGa and triethylgallium (TEGa) were studied and compared in few works [8,9]. It was shown that GaN layers grown from TEGa have in some way better properties and layers contain less carbon. TEGa precursor is usually used for GaN growth when the growth temperature is lower than 1000 °C (typically during the growth of a barrier between InGaN quantum wells), because TEGa decomposition pathway involving β-hydrogen elimination can reduce carbon incorporation into GaN layers. Carbon usually sits on N lattice site ($C_N$) and acts as a deep acceptor 0.9 eV above the valence band [10]. Carbon atoms can be incorporated as an interstitial defect ($C_i$) or on Ga lattice site ($C_{Ga}$) as well, but the formation energies of these two defects are higher in usual growth conditions compared to $C_N$. So in GaN samples which are unintentionally n-doped, the $C_N$ defect will be the most probable [11]. YB was attributed to $C_N$ defect [10], $C_N$-$O_N$ complex [12], which is energetically favourable, or $C_N$-$Si_{Ga}$ [13] in n-type doped GaN especially. Another sources of YB, which were proposed in literature, were $V_{Ga}$-3H and $V_{Ga}$-$O_N$-2H complexes [14] or $V_{Ga}$-$O_N$ [15]. The source of the YB is still not clear and more experiments are needed.

In our work we will compare MOVPE grown n-type doped GaN layers grown from TMGa and TEGa precursor. Source of the YB will be discussed; suggestions for YB luminescence intensity suppression will be given and confirmed by the experiment. The supposed source of YB in n-type doped GaN layers will be also discussed and compared with our experimental results.

## 2. Experimental

Structures were prepared by MOVPE technology in Aixtron 3x2 CCS apparatus equipped with LayTec EpiCurveTT system for in situ measurement of reflectivity, temperature and curvature. Structures were grown on c-plane sapphire substrates baked out for 5 min at 1050 °C. Low temperature GaN nucleation layer was grown at 530 °C and then 3 μm thick high temperature GaN layer was grown with growth conditions described in our older publication [16]. GaN doped with silicon was grown on top with different growth parameters. Influence of these different growth parameters on quality of GaN layers will be discussed in this article. Description of growth parameters of studied samples is shown in Table 1.

Photoluminescence (PL) measurements were done at room temperature with 325 nm laser excitation wavelength. A confocal microscope LabRAM HR Evolution with He-Cd laser, objective 74 CG and spot diameter 2 μm was used. Penetration depth for this wavelength in GaN was evaluated from the absorption coefficient (taken from [17]) to approximately 90 nm, where ~63% of primary intensity of light is absorbed. All samples in this work have a thickness of upper n-GaN layer more than 400 nm, which is enough for the absorption of 99% of the incoming light.

Excitation intensity is very important parameter influencing the ratio of YB and excitonic maximum intensity (see Fig. 1(b)). We have used very low excitation intensity (0.05 $Wcm^{-2}$), so the YB in PL spectra before the optimization was dominant and the maximum YB intensity was higher compared to excitonic band.

Surface morphology was measured with an atomic force microscope (AFM) Dimension Icon. Semi contact mode with ASPIRE tips was used.

X-ray diffraction was used to evaluate the dislocation density of GaN layers. SmartLab of Rigaku with rotating Cu X-ray tube was used for the measurement. Omega scan (rocking curve) of the 0002 and 10–12 reflections was measured and FWHM of the curves was subtracted. For estimation of screw and edge + mixed dislocation densities, approach from Dunn and Koch was used [18].

Concentration of impurities in GaN layers was measured by secondary ion mass spectrometry (SIMS) by EAG Laboratories in USA.

Vacancy type point defects were studied by variable energy positron annihilation spectroscopy (VEPAS) which is a unique non-destructive method for detection of negatively charged or neutral vacancies in semiconductors [19]. VEPAS investigations were carried out on a pulsed slow positron beam MePS [20]. The energy of incident positrons was varied in the range from 1 to 16 keV. It corresponds to the mean positron penetration depth into GaN from 15 to 1250 nm calculated using the Makhovian positron implantation profile [21]. Positron lifetime spectra were measured using a digital spectrometer with time resolution of ≈250 ps (FWHM of resolution function). At least $10^7$ positron annihilation events were collected in each positron lifetime spectrum.

## 3. Results and discussion

Undoped GaN layers have in their luminescence spectra typically both defect bands, BB and YB (see Fig. 1(a)). GaN layers doped with silicon have much stronger YB (see Fig. 1(a)), because of an increase of transition probability between shallow donor and deep acceptor levels. Suppression of YB intensity will be studied in n-doped samples, where the YB intensity is more intensive.

Excitation intensity is very important parameter which influences the intensity of YB, BB, GaN excitonic bands and their ratio. In many publications the excitation intensity used is high enough to get strong excitonic band in PL spectra without significant contribution of BB or YB. In our work, we have intentionally used very low excitation intensity (0.05 $Wcm^{-2}$) during the PL measurement to get significant YB contribution to the PL spectra. The influence of the excitation intensity on the PL spectra of n-GaN layer is shown in Fig. 1(b).

### *3.1. TMGa – carrier gas and growth temperature*

Since TMGa is the most common precursor for the growth of GaN layers, we have prepared a set of samples at different temperatures and

**Table 1**
Description of samples grown from TMGa (named TMGx) and TEGa (named TEGx) precursor with the most important growth parameters of upper n-doped GaN layer.

| Sample | Carrier gas | Temperature (°C) | Growth rate (nm/s) | Sample | Carrier gas | Temperature (°C) | Growth rate (nm/s) |
|---|---|---|---|---|---|---|---|
| TMG1 | $H_2$ | 1065 | 0.24 | TEG1 | $H_2$ | 935 | 0.04 |
| TMG2 | $N_2$ | 1085 | 0.24 | TEG2 | $N_2$ | 950 | 0.04 |
| TMG3 | $H_2$ | 935 | 0.37 | TEG3 | $N_2$ | 920 | 0.04 |
| TMG4 | $N_2$ | 950 | 0.26 | TEG4 | $N_2$ | 880 | 0.04 |
| TMG5 | $H_2$ | 1065 | 0.08 | TEG5 | $N_2$ | 950 | 0.12 |
| TMG6 | $H_2$ | 1065 | 0.06 | TEG6 | $N_2$ | 950 | 0.08 |

Note: Different carrier gas changed slightly temperature due to different thermal conductivity of $N_2$ and $H_2$.

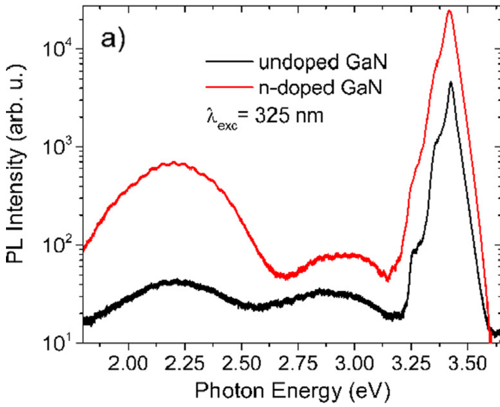


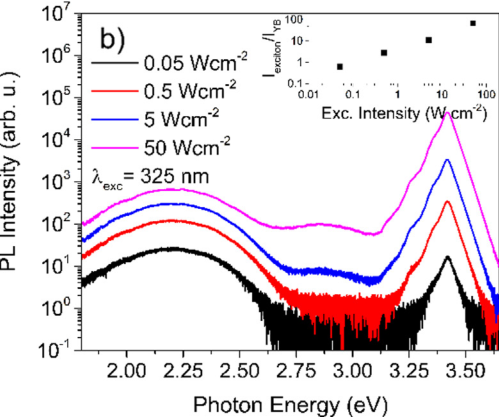


**Fig. 1.** (a) PL spectra of GaN layers (undoped GaN – black curve, n-doped GaN – red curve) with typical defect bands (BB around 2.9 eV and YB around 2.2 eV). (b) PL spectra of n-doped GaN layer with different excitation intensity. Ratio $I_{exciton}/I_{YB}$ increased from 0.64 (0.05 Wcm$^{-2}$) up to 66.3 (50 Wcm$^{-2}$).

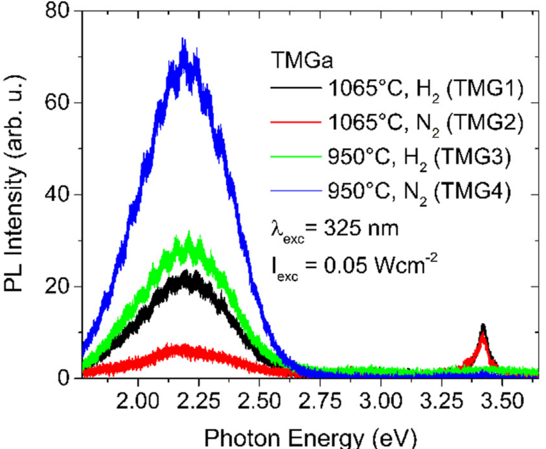


**Fig. 2.** Comparison of PL spectra of samples grown from TMGa precursor at different growth conditions.

with different carrier gasses using this precursor. Comparison of PL spectra of these samples is shown in Fig. 2.

The YB position was identical for all samples (2.19 eV) suggesting similar origin of YB luminescence. It can be seen that higher temperature (1065 °C) is essential for the growth of GaN using TMGa because of better molecule decomposition and lower carbon incorporation into the layers (as was observed in [22]). At lower temperature, the excitonic emission decreases rapidly for both carrier gasses (samples TMG3 and TMG4). Surprisingly, the best sample with respect to the YB suppression was obtained for $N_2$ carrier gas and high growth temperature (TMG2), although theoretical studies suggest that hydrogen is necessary for decomposition of TMGa [23]. Increase of carbon concentration using $H_2$ carrier gas was also observed in [24]. Unfortunately, the surface morphology of the sample TMG2 was rather poor with hillock formation.

On the opposite, the worst sample with respect to the PL properties was sample TMG4 grown at the lower temperature in $N_2$ atmosphere. This sample was proved to have the highest C concentration $3{\cdot}10^{17}$ cm$^{-3}$ according to SIMS results (background concentration $3{\cdot}10^{16}$ cm$^{-3}$). These results confirm the hypothesis of $C_N$ defect being the source of the YB here. Transport properties were worse as well. Carrier concentration was three times lower compared to sample TMG1 ($1.04{\cdot}10^{18}$ cm$^{-3}$ and $3.82{\cdot}10^{17}$ cm$^{-3}$) due to the compensation effect of carbon. That is why the lower growth temperature in $N_2$ atmosphere could be suggested for the growth of highly resistive C compensated layers in HEMT heterostructures, where the poor luminescence properties are not important.

### 3.2. TEGa – carrier gas

Since the lower temperature growth is essential for preparation of some heterostructures and TMGa does not seem to be suitable for the growth at lower temperatures we have also prepared a set of GaN samples from TEGa precursor. During the previous growth from TMGa precursor, we observed big influence of carrier gas type on luminescence and structural properties. At first, the influence of carrier gas was studied. Samples TEG1 with $H_2$ and TEG2 with $N_2$ carrier gases were grown at 950 °C. When $H_2$ carrier gas was used, huge increase of YB intensity was observed in PL spectra. The energy of YB maximum was 2.19 eV (the same energy as in previous samples). Excitonic band intensity was not influenced by different carrier gas. PL spectra of both samples are shown in Fig. 3.

Since the decrease of YB intensity was not accompanied by sufficient increase of excitonic luminescence, we can suppose that some kind of non-radiative recombination has been increased in sample TEG2.

Higher carbon incorporation into layers, when the hydrogen carrier gas was used, was observed in [5]. It was suggested that higher concentration of $C_N$ defect is caused by hydrogen due to the lowering of $C_N$ formation energy when the Fermi level rises (due to hydrogen interstitials acting as donors and enhanced formation of C-H complexes) [11]. On the other hand, SIMS analysis did not show any increase of carbon contamination in our GaN layer grown with $H_2$ carrier gas (concentration at the background – $3{\cdot}10^{16}$ cm$^{-3}$). This suggests that different deep level than $C_N$ defect could be responsible for enhanced

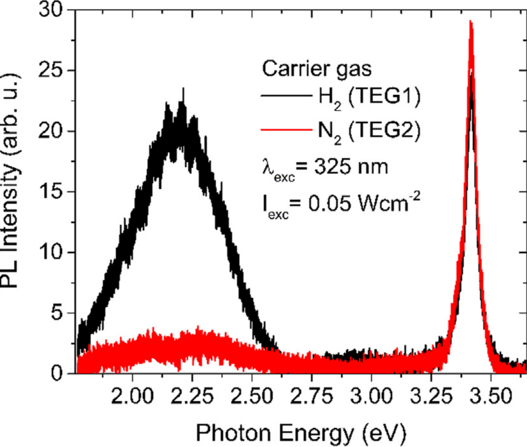


**Fig. 3.** PL spectra of samples grown from TEGa precursor at 950 °C with $H_2$ (black curve) and with $N_2$ (red curve) carrier gas.

YB luminescence in this case, for example $V_{Ga}$ complex with hydrogen, which has lower formation energy than Ga vacancy alone [25]. On the other hand, the position of the YB energy maximum (2.19 eV) and the shape of the YB, which is exactly the same for all studied samples, suggest the same origin of the YB, which was recognized to be the $C_N$ defect according to our previous results. However, according to literature transition levels of both $C_N$ and $V_{Ga}$ related defects are very similar (around 0.9 eV above the valence band maximum) and with theoretical and experimental uncertainties, it is therefore hard to distinguish which defect contributes to the YB luminescence.

Both samples TEG1 and TEG2 were characterized by VEPAS to confirm or exclude our suspicion that the difference in YB intensity is caused by different $V_{Ga}$ concentration. The lifetime of positron annihilated in the free state is significantly shorter than that for a positron localized in vacancy, because electron density in vacancy is reduced. Consequently, positron lifetime increases with increasing open volume of vacancy. That is why positron lifetime spectroscopy can give us not only the estimation of vacancy concentration but also the information about the vacancy size or type.

The dependence of the mean positron lifetime on the kinetic energy $E$ of incident positrons is shown in Fig. 4. The mean positron penetration depth $z_{mean}$ (top axis in Fig. 4) is related to the energy of incident positrons [26]

$$z_{mean} = \frac{A}{\rho}E^b,$$

where $b \approx 1.6$, $A \approx 4$ µg cm$^{-2}$ keV$^{-b}$ and ρ is the mass density (ρ = 6.15 g cm$^{-3}$ for GaN). Positron lifetime on the surface is considerably increased since positron is trapped at image potential on the surface [26]. At low energies $E \approx 1$ keV majority of positrons is annihilated in the surface state ($z_{mean} \approx 7$ nm) and measured positron lifetime is therefore close to the value for the surface state. With increasing energy positrons penetrate deeper into the GaN film and the fraction of positrons diffusing back to the surface gradually decreases. This is reflected by gradual decrease of the mean positron lifetime from the surface value to a plateau value corresponding to the situation that all positrons are annihilated inside the GaN film. Hence, the mean positron lifetime characteristic for the GaN film is the value measured at high energies ($E > 12$ keV). From inspection of Fig. 4 one can conclude that sample TEG2 exhibits higher mean positron lifetime than sample TEG1.

The lifetime of trapped positrons measured in sample TEG1 ($H_2$ carrier gas) is in good agreement with the lifetime of positron trapped in $V_{Ga}$ defect [27,28] while lifetime of trapped positrons in sample TEG2 ($N_2$ carrier gas) is remarkably higher.

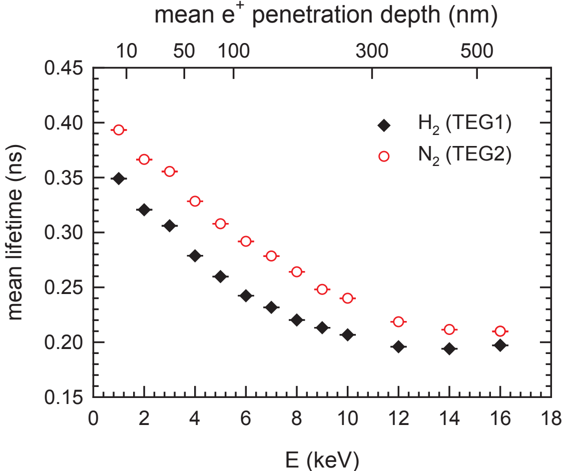


**Fig. 4.** The dependence of the mean positron lifetime on the energy of incident positrons. Top horizontal axis shows the mean positron penetration depth.

Using the two state simple trapping model [29] and the specific positron trapping rate $\nu_v = 10^{15}$ s$^{-1}$ typical for negatively charged vacancies in semiconductors [19] the concentration of $V_{Ga}$ of $1{\cdot}10^{17}$ cm$^{-3}$ was estimated for the TEG1 sample. $V_{Ga}$ defect is probably associated with hydrogen due to lower formation energy of $V_{Ga}$ + H complex [25]. Surprisingly, the lifetime of trapped positron in sample TEG2 ($N_2$ carrier gas) was significantly higher, which means that positron must be trapped by different type of point defect with open volume larger than that for monovacancy. The measured lifetime around 295 ps value is in good agreement with theoretically calculated lifetime of positron trapped in $(V_{Ga})_3(V_N)_n$ complex, where n is in the range 1–3. The number of nitrogen atoms in the complex is uncertain since they have relatively low impact on lifetime of trapped positrons. The concentration of $(V_{Ga})_3(V_N)_n$ complexes in the TEG2 film was estimated to be around $3{\cdot}10^{16}$ cm$^{-3}$, using the simple two state trapping model [29] with the specific trapping rate $\nu_c = 3\nu_v$ [30]. Hence, according to VEPAS results the concentration of $V_{Ga}$ in TEG2 is insignificant and must be much lower than the concentration of $(V_{Ga})_3(V_N)_n$ complexes. These results suggest that while in hydrogen atmosphere single gallium vacancies are formed, comparable number of vacancies is clustered into vacancy complexes when nitrogen is used as carrier gas. The mechanism of vacancy clustering is not clear, yet.

The results of positron annihilation on samples TEG1 and TEG2 are also well supported by PL and transport measurement. Recent publication showed that complexes of $V_{Ga}$ and $V_N$, such as $(V_{Ga})(V_N)$ or $(V_{Ga})_3(V_N)_3$, are major intrinsic non-radiative centres in undoped and Mg-doped GaN respectively [31]. Our PL results suggest increase of non-radiative recombination in sample TEG2 since the integral luminescence has been decreased in comparison to sample TEG1, see Fig. 3. The excitonic luminescence intensity is the same for both samples. Thus, it could be expected that the defect band luminescence was replaced by some non–radiative recombination process. The hypothesis that $V_{Ga}$ are responsible for defect band luminescence in sample TEG1 is directly supported by positron annihilation suggesting much higher single $V_{Ga}$ concentration in comparison to sample TEG2.

Transport measurements of our two samples showed lower mobility of free carriers for sample TEG1 (379 cm$^2$/Vs for sample TEG1 and 566 cm$^2$/Vs for sample TEG2) at the same concentration of free carriers (around $1.2{\cdot}10^{18}$ cm$^{-3}$). It also partly supports the positron annihilation results since mobility is expected to be more sensitive to defect concentration than defect size.

VEPAS results showed that nitrogen carrier gas support clustering of $V_{Ga}$ defects with $V_N$ defects. Understanding of this phenomenon is very important for nitride community and it will need more investigation.

### 3.3. TEGa – growth temperature

In the next step, we have studied the influence of the growth temperature on luminescence and structural properties. At temperature above 1000 °C, the growth from TEGa precursor was not possible due to many pre–reactions in the gas phase. At lower temperature (below 1000 °C) the growth was accomplished as usual when a barrier is grown. We have prepared set of samples with different growth temperatures 950 °C, 920 °C and 880 °C. Comparison of PL spectra is shown in Fig. 5. Slight increase of YB intensity (energy of the maximum intensity at 2.19 eV) and consequently decrease of the excitonic band was observed when the growth temperature was decreased. However, the influence of the growth temperature is much lower than the influence of the type of carrier gas observed in previous experiment. For TMGa precursor the higher carbon incorporation into the GaN layers was observed at lower temperatures [22,32]. The same trend is expected for TEGa precursor and this measurement confirms the hypothesis about the $C_N$ defect responsible for the YB.

Surface morphology is shown in Fig. 6. No significant change was observed when the growth temperature was lowered to 920 °C. But at the lowest temperature (880 °C), we observed significant change in the

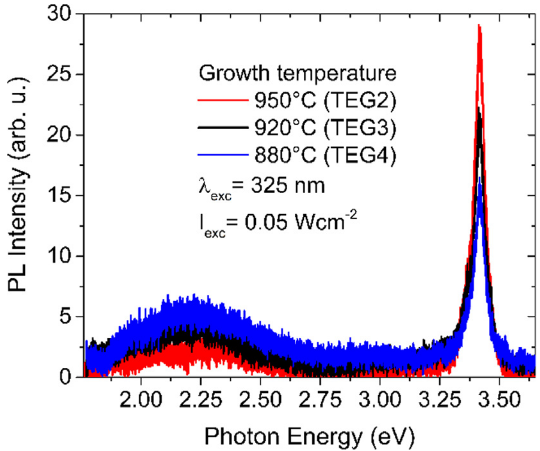


**Fig. 5.** PL spectra of three samples with different growth temperatures 950 °C, 920 °C and 880 °C.

surface morphology. The growth temperature was low enough to open V-pits around threading dislocations reaching the surface. The same phenomenon was observed in our previous work, where lower growth temperature was used [33].

### *3.4. Growth rate (TEGa and TMGa precursor)*

One drawback of the growth from TEGa precursor is the growth rate, which is significantly lower than for the growth from TMGa precursor. We have tried to increase the growth rate by increased TEGa flow, but as we expected, deterioration of luminescence properties was observed, YB intensity was increased and excitonic band luminescence was suppressed, see Fig. 7(a).

Although the positive effect of decreased growth rate on luminescence properties is already known and many times published we have found that this rule is not always valid. The lowest growth rate from TMGa precursor (sample TMG6) caused increase of non-radiative centre generation as can be seen in Fig. 7(b), where PL properties of samples TMG1, TMG5 and TMG6 are compared. As expected, three times slower growth rate (compare samples TMG1 and TMG5) improved luminescence properties (increased excitonic band and decreased YB). Another reduction of the growth rate (sample TMG6) led to vanishing of excitonic band, indicating many non-radiative centres created in the layer. Moreover, at such low growth rate quality of surface morphology decreased very significantly, resulting in impossible utilization of these growth conditions in various nitride applications, although YB suppression was observed (probably due to worse quality and many non-radiative centres).

## 4. Conclusions

Comparison of PL spectra of the best samples grown from TMGa (sample TMG5) and TEGa (sample TEG2) precursor is shown in Fig. 8. Despite of the fact that the growth rate is very similar in both samples, better results were obtained when TEGa precursor was used. The $I_{exciton}/I_{YB}$ ratio increases from 1.8 to 9.6. Surface morphology of sample TEG2 is very good and it is shown in Fig. 6 (left image). Dislocation density was $1.2{\cdot}10^8$ cm$^{-2}$ for screw type and $6.4{\cdot}10^8$ cm$^{-2}$ for edge and mixed type.

In conclusion, luminescent and structural properties of n-doped GaN layers grown from TMGa and TEGa precursors with different technological parameters were studied. The growth temperature influenced dominantly the excitonic luminescence intensity, especially when TEGa was used for the growth. Excitonic luminescence was enhanced for higher growth temperatures (950 °C).

As conclusion from our results we can suppose that both carbon as well as $V_{Ga}$ related defects can cause the YB luminescence. In case of TMGa decreasing growth temperature increased carbon contamination of layers and YB luminescence was enhanced.

Yellow band luminescence was also strongly influenced by the type of carrier gas. In case of TMGa, the choice of suitable carrier gas depends on the growth temperature. For lower growth temperature (950 °C), $H_2$ is suggested to obtain layers with better optical properties. $N_2$ carrier gas increased significantly the carbon concentration (up to $3{\cdot}10^{17}$ cm$^{-3}$ observed by SIMS) and YB emission at lower growth temperature. This technology could be used for the growth of high resistive layers in HEMT structures. On the other hand, $N_2$ carrier gas has opposite influence on YB luminescence (decrease of YB intensity) for samples grown from TMGa at higher temperature (1065 °C) or for samples grown from TEGa. At these samples the dominant role in YB luminescence take single $V_{Ga}$ related defects. $N_2$ carrier gas suppresses considerably $V_{Ga}$ concentration which are transformed to $(V_{Ga})_3(V_N)_n$ non-radiative defects. The consequence of lower $V_{Ga}$ concentration is suppressed YB luminescence.

Both luminescence bands, excitonic as well as YB, were influenced by the growth rate, when $NH_3$ partial pressure was kept the same. In case of TEGa, decreasing the growth rate suppressed the YB luminescence, while excitonic luminescence was enhanced. In case of TMGa precursor, for very low growth rate both luminescence bands were suppressed suggesting increased ratio of non-radiative recombination.

The best optical and structural results were obtained for sample TEG2 prepared from TEGa precursor in $N_2$ atmosphere, at 950 °C, reactor pressure 150 mbar, V/III ratio 10,000 and with slow growth rate 0.04 nm/s.

## Declaration of Competing Interest

The authors declare that they have no known competing financial

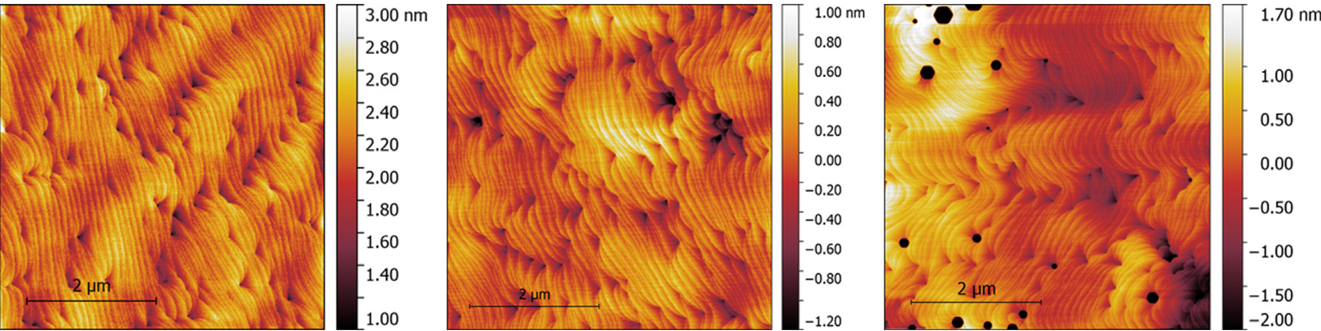


**Fig. 6.** AMF images of set of samples with different growth temperatures (from left to right 950 °C, 920 °C and 880 °C) grown from TEGa precursor and with $N_2$ carrier gas. Opened V-pits were observed at the lowest temperature (880 °C). RMS roughness was evaluated in Gwyddion software to be 0.224 nm, 0.258 nm and 5.598 nm, respectively.

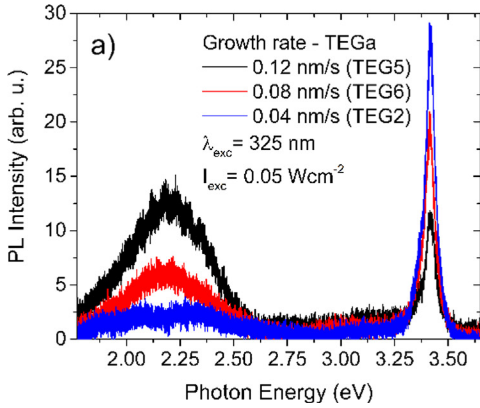


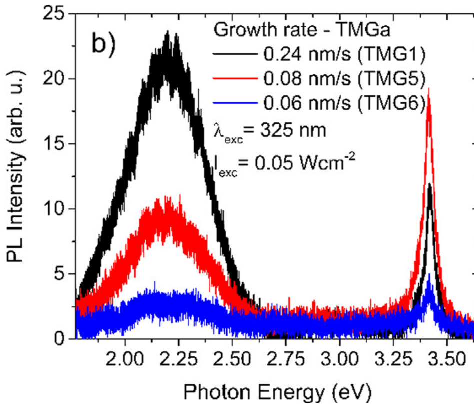


**Fig. 7.** Comparison of PL spectra of three samples with different growth rate (a) with TEGa precursor and (b) TMGa precursor.

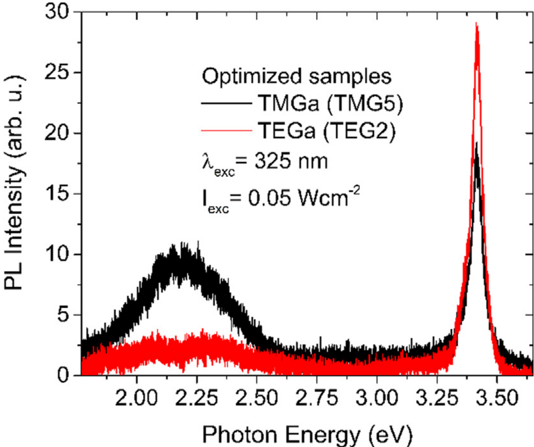


**Fig. 8.** Comparison of PL spectra of optimized samples grown from TMGa (black curve) and TEGa (red curve) precursor.

interests or personal relationships that could have appeared to influence the work reported in this paper.

## Acknowledgement

The authors acknowledge project TH02010014 and NPU project LO1603. The authors wish to thank Dr. Alexej Vetushka and Dr. Pavel Machek from the Institute of Physics, Czech Academy of Sciences for AFM and X-ray diffraction measurements. J. Čížek acknowledges support by the Czech Science Foundation (project 18-09347S). The MePS facility has partly been funded by the Federal Ministry of Education and Research (BMBF) with the grant PosiAnalyse (05K2013). The support of the ELBE team at HZDR is greatly acknowledged.

## References

[1] H.M. Manasevit, The use of metalorganics in the preparation of semiconductor materials: growth on insulating substrates, J. Cryst. Growth 13 (14) (1972) 306–314.
[2] H. Amano, N. Sawaki, I. Akasaki, Y. Toyoda, Metalorganic vapour phase epitaxial growth of a high quality GaN film using an AlN buffer layer, Appl. Phys. Lett. 48 (1986) 353–355.
[3] M.A. Reshchikov, H. Morkoc, Luminescence properties of defects in GaN, J. Appl. Phys. 97 (2005) 061301.
[4] T. Ogino, M. Aoki, Mechanism of Yellow Luminescence in GaN, Jpn. J. Appl. Phys. 19 (1980) 2395.
[5] F. Kaess, S. Mita, J. Xie, P. Reddy, A. Klump, L.H. Hernandez-Balderrama, S. Washiyama, A. Franke, R. Kirste, A. Hoffmann, R. Collazo, Z. Sitar, Correlation between mobility collapse and carbon impurities in Si-doped GaN grown by low pressure metalorganic chemical vapour deposition, J. Appl. Phys. 120 (2016) 105701.
[6] A. Hospodková, M. Nikl, O. Pacherová, J. Oswald, P. Brůža, D. Pánek, B. Foltynski, E. Hulicius, A. Beitlerová, M. Heuken, InGaN/GaN multiple quantum well for fast scintillation application: radioluminescence and photoluminescence study, Nanotechnology 25 (2014) 455501.
[7] T. Hubáček, A. Hospodková, K. Kuldová, J. Oswald, J. Pangrác, V. Jarý, F. Dominec, M. Slavická Zíková, F. Hájek, E. Hulicius, A. Vetushka, G. Ledoux, Ch. Dujardin, M. Nikl, Advancement toward ultra-thick and bright InGaN/GaN structures with a high number of QWs, CrystEngComm 21 (2019) 356.
[8] A. Saxler, D. Walker, P. Kung, X. Zhang, M. Razeghi, J. Solomon, W.C. Mitchel, H.R. Vydyanath, Comparison of trimethylgallium and triethylgallium for the growth of GaN, Appl. Phys. Lett. 71 (1997) 3272.
[9] K.-M. Song, D.-J. Kim, Y.-T. Moon, S.-J. Park, Characteristics of GaN grown by metalorganic chemical vapour deposition using trimethylgallium and triethylgallium, J. Cryst. Growth 233 (2001) 439–445.
[10] J.L. Lyons, A. Janotti, C.G. Van de Walle, Carbon impurities and the yellow luminescence in GaN, Appl. Phys. Lett. 97 (2010) 152108.
[11] J.L. Lyons, A. Janotti, C.G. Van de Walle, Effects of carbon on the electrical and optical properties of InN, GaN, and AlN, Phys. Rev. B 89 (2014) 035204.
[12] D.O. Demchenko, I.C. Diallo, M.A. Reshchikov, Yellow luminescence of gallium nitride generated by carbon defect complexes, Phys. Rev. Lett. 110 (2013) 087404.
[13] S.G. Christenson, W. Xie, Y.Y. Sun, S.B. Zhang, Carbon as a source for yellow luminescence in GaN: isolated $C_N$ defect or its complexes, J. Appl. Phys. 118 (2015) 135708.
[14] J.L. Lyons, A. Alkauskas, A. Janotti, C.G. Van de Walle, First-principle theory of acceptors in nitride semiconductors, Phys. Status Solidi B 252 (2015) 900–908.
[15] Z. Xie, Y. Sui, J. Buckeridge, A.A. Sokol, T.W. Keal, A. Walsh, Prediction of multiband luminescence due to the gallium vacancy-oxygen defect complex in GaN, Appl. Phys. Lett. 112 (2018) 262104.
[16] T. Hubáček, A. Hospodková, J. Oswald, K. Kuldová, J. Pangrác, Improvement of luminescence properties of GaN buffer layer for fast nitride scintillator structures, J. Cryst. Growth 464 (2017) 221–225.
[17] J.F. Muth, J.D. Brown, M.A. Johnson, Z. Yu, R.M. Kolbas, J.W. Cook, J.F. Schetzina, Absorption coefficient and refractive index of GaN, AlN and AlGaN alloys, MRS Internet J. Nitride Semicond. Res. 4 (S1) (1999) G5.2.
[18] C.G. Dunn, E.F. Koch, Comparison of dislocation densities of primary and secondary recrystallization grains of Si-Fe, Acta Metall. 5 (1957) 548.
[19] R. Krause-Rehberg, H.S. Leipner, Positron Annihilation in Semiconductors Vol. 127 Springer-Verlag, Berlin, 1999.
[20] A. Wagner, M. Butterling, M.O. Liedke, K. Potzger, R. Krause-Rehberg, Positron annihilation lifetime and Doppler broadening spectroscopy at the ELBE facility, AIP Conf. Proc. 1970 (2018) 040003.
[21] Ch. Hugenschmidt, Positrons in surface physics, Surf. Sci. Rep. 71 (2016) 547–594.
[22] D.D. Koleske, A.E. Wickenden, R.L. Henry, M.E. Twigg, Influence of MOVPE growth conditions on carbon and silicon concentrations in GaN, J. Cryst. Growth 242 (2002) 55–69.
[23] K. Sekiguchi, H. Shirakawa, Y. Yamamoto, M. Araidai, Y. Kangawa, K. Kakimoto, K. Shiraishi, First-principles and thermodynamic analysis of trimethylgallium (TMG) decomposition during MOVPE growth of GaN, J. Cryst. Growth 468 (2017) 950–953.
[24] J.-L. Zhang, J.-L. Liu, Y. Pu, W.-Q. Fang, M. Zhang, F.-Y. Jiang, Effect of carrier gas on Carbon Incorporation in GaN, Chin. Phys. Lett. 31 (2014) 037102.
[25] C.G. Van de Walle, Interactions of hydrogen with native defects in GaN, Phys. Rev. B 56 (1997) 10020R–10023R.
[26] M.J. Puska, R.M. Nieminen, Theory of positrons in solids and on solid surfaces, Rev. Mod. Phys. 66 (1994) 841–899.
[27] K. Saarinen, in: M.O. Manasreh (Ed.), III-V Nitride Semiconductors: Electrical Structural and Defect Properties, Elsevier, Amsterdam, 2000, p. 109.
[28] K. Saarinen, J. Nissilä, J. Oila, V. Ranki, M. Hakala, M.J. Puska, P. Hautojärvi, J. Likonen, T. Suski, I. Grzegory, B. Lucznik, S. Porowski, Observation of Ga vacancies and negative ions in undoped and Mg-doped GaN bulk crystals, Phys. B 273–274 (1999) 33–38.
[29] R.N. West, Positron studies of condensed matter, Adv. Phys. 22 (1973) 263–383.
[30] R.M. Nieminen, J. Laakkonen, Positron trapping rate into vacancy clusters, Appl. Phys. 20 (1979) 181–184.
[31] S.F. Chichibu, A. Uedono, K. Kojima, H. Ikeda, K. Fujito, S. Takashima, M. Edo,

K. Ueno, S. Ishibashi, The origins and properties of intrinsic nonradiative recombination centers in wide bandgap GaN and AlGaN, J. Appl. Phys. 123 (2018) 161413.

[32] N.A. Fichtenbaum, T.E. Mates, S. Keller, S.P. DenBaars, U.K. Mishra, Impurity incorporation in heteroepitaxial N-face and Ga-face GaN films grown by metalorganic chemical vapour deposition, J. Cryst. Growth 310 (2008) 1124–1131.

[33] F. Dominec, A. Hospodková, T. Hubáček, M. Zíková, J. Pangrác, K. Kuldová, A. Vetushka, E. Hulicius, Influence of GaN buffer layer under InGaN/GaN MQWs on luminescent properties, J. Cryst. Growth 507 (2019) 246–250.

## 4.3 Influence of Si doping of GaN layers surrounding InGaN quantum wells on structure photoluminescence properties [iii]

InGaN/GaN heterostructures suffer from a quite huge internal piezoelectric field which results in tilting of the band structure and consequently worse overlap of electrons and holes confined in QWs. Influence of different position of Si doped layer around MQW region on luminescence and structural properties was studied. It was found that the dominant influence of Si doping is in a modification of the tilt of the band structure. Both luminescence bands, excitonic and defect band, were influenced and we have suggested the mechanism of defect band (observed in our luminescence spectra) which could be recombination between holes confined in QWs and defect states located near the upper InGaN/GaN QW interface. The paper was published in Journal of Crystal Growth (IF = 1.57, Q3, 3 citation).

Journal of Crystal Growth 506 (2019) 8–13

Contents lists available at ScienceDirect

Journal of Crystal Growth

journal homepage: www.elsevier.com/locate/jcrysgro

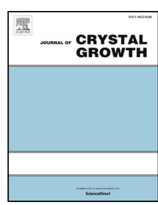

# Influence of Si doping of GaN layers surrounding InGaN quantum wells on structure photoluminescence properties

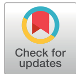

M. Zíková[a,*], A. Hospodková[a], J. Pangrác[a], T. Hubáček[a], J. Oswald[a], K. Kuldová[a], F. Hájek[a], G. Ledoux[b], C. Dujardin[b]

[a] Institute of Physics CAS, v. v. i., Cukrovarnická 10, 162 00 Prague 6, Czech Republic
[b] Université Lyon, Université Claude Bernard Lyon 1, CNRS, Institut Lumière Matière UMR 5306, F-69100 Villeurbanne, France

ARTICLE INFO

Communicated by Yasuyuki Miyamoto

*Keywords:*
A1. Low dimensional structures
A3. MOVPE
A3. InGaN/GaN quantum wells
B2. Luminescent defect band

ABSTRACT

In this work, the influence of Si doping position on the photoluminescence (PL) properties of InGaN/GaN quantum wells (QWs) is studied. A set of samples with different positions of Si doping with respect to the multi quantum well (MQW) active region was prepared and studied by PL, SIMS and AFM and structure band alignments were simulated. Based on our experiments and band structure simulations, we show that the dominant influence of Si doping is in modification of the tilt of the band structure. However, the minor influence of lower dislocation density or unintentional doping of a few lowest QWs in the case of a Si doped buffer layer cannot be excluded. A probable origin of the defect band luminescence and its high sensitivity to the band structure tilting is explained. Based on gained understanding, proper Si doping position for particular applications is suggested. In the case of LED structures, the n-type buffer layer and p-type capping layer help improve the emission efficiency. In the case of an InGaN/GaN MQW structure designed for scintillators, the n-type doping immediately under the MQW region is not required, since it strongly increases the QW defect band luminescence which becomes dominant in the spectrum.

## 1. Introduction

Nitride heterostructures for luminescence applications have the disadvantage of the presence of a piezoelectric field which causes tilting of the band structure. The polarization of InGaN/GaN interfaces and the electric field between them cause opposite tilting of the band structure of InGaN and GaN layers. This polarization field causes worse overlap of electrons and holes confined in a quantum well (QW) and subsequently suppresses the intensity of QW luminescence especially for structures with an increased In content or thicker quantum wells (QWs). This complicates achieving efficient emission of luminescence from laser diodes in green spectral region. It is known that the effect of polarization field can be suppressed and QW luminescence can be enhanced by suitable doping of surrounding layers [1] or GaN barriers. The tilt of a band structure influenced by doping of surrounding layers is also used to improve luminescent properties and to suppress Auger recombination in light emitting diodes (LEDs) [2,3]. We have found that tilting of a band structure does not only influence the main QW excitonic emission, but also the QW defect band (DB) which is harmful for some InGaN/GaN multi quantum well (MQW) applications [4]. This slow defect band is not a problem for applications with high intensity of excitation, such as light emitting or laser diodes, but at low excitation densities it may become dominant in the luminescence spectrum. To find a way how to suppress the defect band luminescence would be very beneficial for applications which need to have fast luminescence response and work at low excitation densities, such as scintillators. In this work we investigate structures with InGaN/GaN QWs with different Si doping of surrounding GaN layers and its influence on photoluminescent (PL) properties of these structures. The aim is to explain how the polarization field may influence particular luminescence bands and to find optimal layer doping to improve the PL properties (decreasing QW DB or increasing the QW excitonic band).

## 2. Experimental

We prepared a set of samples with n-type doping using $SiH_4$. The doped layers were prepared at different positions with respect to the active MQW region. Samples were prepared on Aixtron 3 × 2 CCS MOVPE System equipped by Laytec EpiCurveTT apparatus for in situ measurement of reflectivity, curvature and wafer temperature. Structures were grown on sapphire substrates with exact c-plane orientation. Trimethylgallium (TMGa) and ammonia ($NH_3$) were used as

* Corresponding author.
*E-mail address:* zikova@fzu.cz (M. Zíková).

https://doi.org/10.1016/j.jcrysgro.2018.10.013

Available online 05 October 2018
0022-0248/ © 2018 Elsevier B.V. All rights reserved.

**Table 1**
n-type concentration and Si doping position for different samples.

| Sample | A | B | C | D | E* |
|---|---|---|---|---|---|
| QW cap layer | – | $9\cdot10^{17}\,cm^{-3}$ | $9\cdot10^{17}\,cm^{-3}$ | – | – |
| QW buffer layer | $1.1\cdot10^{18}\,cm^{-3}$ | – | $1.1\cdot10^{18}\,cm^{-3}$ | – | $1.1\cdot10^{18}\,cm^{-3}$ |

* In sample E the Si doped layer was 150 nm below the MQW region.

precursors with a hydrogen carrier gas for the growth of buffer layers, triethylgallium (TEGa), trimethylindium (TMIn) and ammonia with nitrogen carrier gas were used for the growth of the MQW region including barriers. MQW structures with 2 × 5 QWs were prepared with a graded composition of In in InGaN QWs by temperature profiling during the QW growth (the temperature for the main part of QW was 730 °C) and with temperature increased to 820 °C for the growth of GaN barriers. The mean content of In was about 4% with slightly lower value on the QW edges due to a temperature ramp. This content was determined by SIMS measurement and is in agreement with the results obtained from HRTEM analysis. The whole MQW active region was grown under $N_2$ atmosphere at a reactor pressure of 400 mbar and $NH_3$ flow rate of 4 l/min. MQW structures were prepared on buffer layers with optimized technology with respect to the PL properties [5]. The upper 1000 nm of the buffer layer were grown with a lower growth rate and n-doped by Si in the case of sample A. Sample B has Si doped capping layer, both buffer and capping layers are doped in the case of structure C and structure D was grown without any intentional Si doping. Si doping level and position for different samples are summarized in Table 1. When there was no intentional doping in the structure, we assumed n-type concentration due to impurities in the order of $1\cdot10^{17}\,cm^{-3}$.

A semiconductor laser LD-375 emitting at 375 nm was used for the PL excitation. The PL signal was detected by a GaAs photo-multiplier tube. The resulting PL was detected using a combination of a double monochromator SDL-1 and a GaAs photo-multiplier tube. Synchronous detection technique was implemented by chopping the laser beam at a modulation frequency of about 35 Hz and by employing a lock-in amplifier. The excitation intensity was $10\,Wcm^{-2}$. The He-Cd laser emitting at 325 nm was focused on the sample with a cassegrain objective CG74 (spot diameter 2 μm) and the backscattered light was collected into the LabRam spectrometer equipped with a grating having 1800 grooves/mm. The excitation intensity was $0.5\,Wcm^{-2}$. Both PL measurements were done at room temperature.

The PL measurements for excitation emission maps were performed on a homemade apparatus. The sample was illuminated by a EQ99X laser-driven light source filtered by a Jobin Yvon Gemini 180 monochromator. The exit slit from the monochromator was then reimaged on the sample by two 100 mm focal length, 2 in. diameter $MgF_2$ lenses. The whole apparatus was calibrated by means of a Newport 918D Low power calibrated photodiode sensor over the range 190–1000 nm. The resolution of the system was 4 nm. The light emitted from the sample was collected by an optical fiber connected to a Jobin-Yvon TRIAX320 monochromator equipped with a cooled CCD detector. At the entrance of the monochromator, different long pass filters could be chosen in order to eliminate the excitation light. The resolution of the detection system was 2 nm.

Hall effect measurement in van der Pauw configuration (for a GaN buffer layer) and SIMS measurement (for both GaN buffer and cap layers) were used for determination of n-type concentration of Si doped layers. Measurement was carried out on 700 nm thick layers grown with adequate growth parameters.

## 3. Results and discussion

A set of samples A-E with different positions of Si doped GaN with respect to the InGaN/GaN MQW region was prepared. In the PL spectra in Fig. 1, two main peaks can be identified: excitonic band (EB) at around 420 nm originating in InGaN QWs and the so-called defect band at around 500 nm whose origin is unclear, although we know from our previous results that it is related to QW states [6]. The aim was to study how the position of Si doping influences the PL properties of such a structure with QWs.

The position of Si doping strongly influences both luminescence bands; the EB as well as the DB. The strongest excitonic maximum was obtained for sample C with Si doping in both surrounding layers below and above the MQW region for both excitation wavelengths, see Fig. 1(a) and (b), 375 nm exciting directly to the QWs and 325 nm exciting to GaN barriers. More pronounced dominance of excitonic band of sample C was observed for stronger excitation to GaN barriers in Fig. 1(b). There could be several possible ways how the Si doping could influence the PL properties of the MQW structure, such as surface quality of the buffer layer before the MQW formation, residual doping of the MQW region, deterioration of a crystal structure or influence of Si doping on the polarization field and change of the MQW band structure tilt. We have investigated these possible cases in order to find the dominant cause.

First, we have checked the residual doping of the MQW region by SIMS, which proved that two lowest InGaN QWs in the structure are slightly doped due to the residual memory effect of the reactor, see Fig. 2. Si contamination causes enhancement of the yellow band (YB) in GaN luminescence [7], so it may also enhance the DB luminescence of QWs. On the other hand, the residual doping does not seem to be a

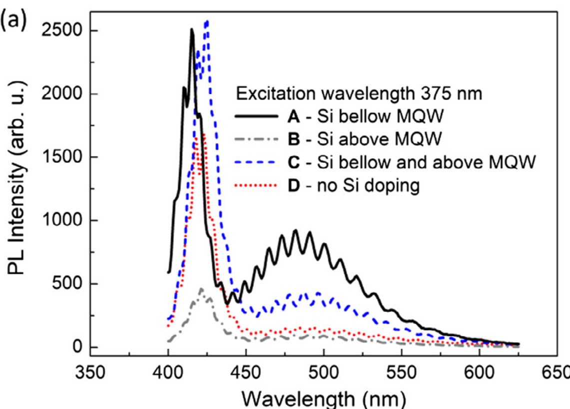


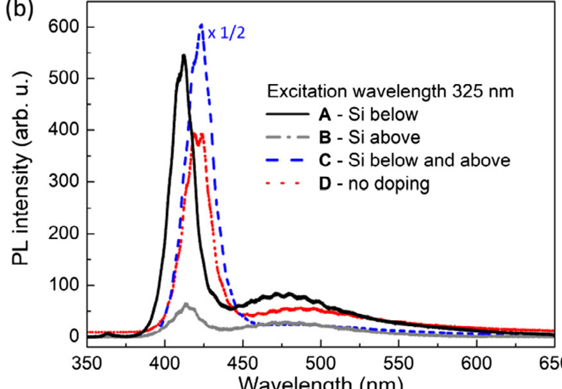


**Fig. 1.** PL spectra of samples with different position of Si doping with respect to the MQW region for excitation (a) directly to the QW with 375 nm excitation wavelength and (b) to GaN barriers with excitation wavelength 325 nm.

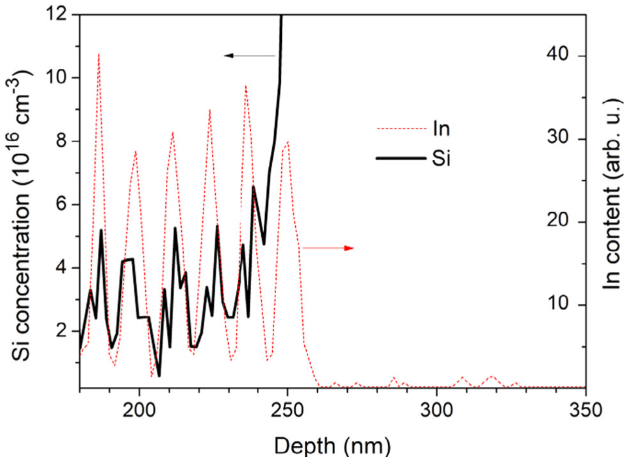


**Fig. 2.** Si concentration profile measured by SIMS, In profile is shown as a QW marker.

problem since the strongest excitonic maximum with lowered DB intensity was observed for sample C which has Si doping both below and above the MQW active region.

To compare different internal electric fields in the MQW region of samples A–D, conduction and valence band profiles were simulated by Nextnano software [8,9]. In all cases n-doping due to impurities (oxygen and silicon) in GaN was assumed [10,11] at a level of $1{\cdot}10^{17}\,\text{cm}^{-3}$. Fermi level pinning on the surface was assumed to be 0.7 eV below the conduction band [12]. Results of simulations of structures A–D are shown in Fig. 3. If we compare these results with PL properties of the samples, we can say that higher PL intensity for both, the EB as well as the DB, was achieved for samples with increasing energy of valence and conduction bands towards the surface over the whole QW region. The opposite tilt of band structure or balanced electric field in the QW region resulted in lower EB and even more significantly suppressed DB intensity. The enhancement of wavefunction overlap with Si doping of the buffer layer was also calculated and experimentally proved in [13]. The band structure tilt, which is caused by balancing the Fermi level between surface states and buffer layer, seems to have influence on PL properties, but other suggested reasons have to be investigated.

One of the possible reasons related to the Si doping of the buffer layer which can influence the PL properties of a structure is a change of surface morphology of epitaxial layers and their crystal quality. We have checked the surface quality of doped and undoped buffer layers by AFM. Although in some cases an improvement of surface morphology with Si doping was reported [14], no significant difference in roughness of our structures with and without Si doping was observed, see Fig. 4. However, approximately two times higher density of threading dislocations of $1.1 \cdot 10^{9}\,\text{cm}^{-3}$ as estimated by XRD (the examples of orifices of these types of dislocations on the surface are marked by arrows) can be found in the sample without Si doping. A higher density of dislocations could increase the nonradiative recombination rate and thus suppress the intensity of both luminescence bands.

In order to determine whether the increased PL intensity can be caused by improved crystallographic properties of sample with Si doped buffer layer or whether it is caused by an electric field between surface states and the doped buffer layer, we grew sample E with Si doped layer shifted deeper into the buffer leaving 150 nm of undoped region below the MQW. The tilt of the band structure of sample E should be almost identical to structure D with undoped buffer layer according to the simulation, see Fig. 5(a). The crystallographic quality should be similar to structure A with 1000 nm of Si doped buffer layer. The PL spectra of both samples D and E are identical (see Fig. 5(b)), therefore an improved crystallographic quality as a cause of PL spectrum enhancement for samples with Si doped buffer layer can be excluded. According to this experiment, the PL spectrum is dominantly influenced by the band structure tilting.

Both QW PL bands are enhanced by Si doping below the MQW region, but the DB is even more sensitive to the Si doping level than the EB maximum. As can be seen in Fig. 5(b) and in Fig. 1, the absent Si doping in the buffer layer has a significant effect on the DB which is practically missing in the PL spectra. As mentioned in the introduction, for some applications working at low excitation densities, suppressing the DB luminescence is highly required. Since the DB becomes dominant for low excitation intensities [4], we have measured excitation emission maps of samples A, B and D also under very low excitation intensity, see Fig. 6. It is evident that in case the buffer layer is not doped the suppression of the QW DB is so efficient that it is practically missing also for the low excitation intensity. The only observable defect luminescence is the YB PL originating in GaN layers. This YB PL is observed for resonant excitation energy around 360 nm and is relatively strong for sample B with Si doped capping layer. It is known that Si doping enhances the defect band, so the YB PL intensity increases for this sample when excited from the surface. The highest intensity of QW excitonic maximum was achieved for sample B with Si doped capping layer in the case of very low excitation intensity.

The tilt of the band structure in the MQW region of samples A and C

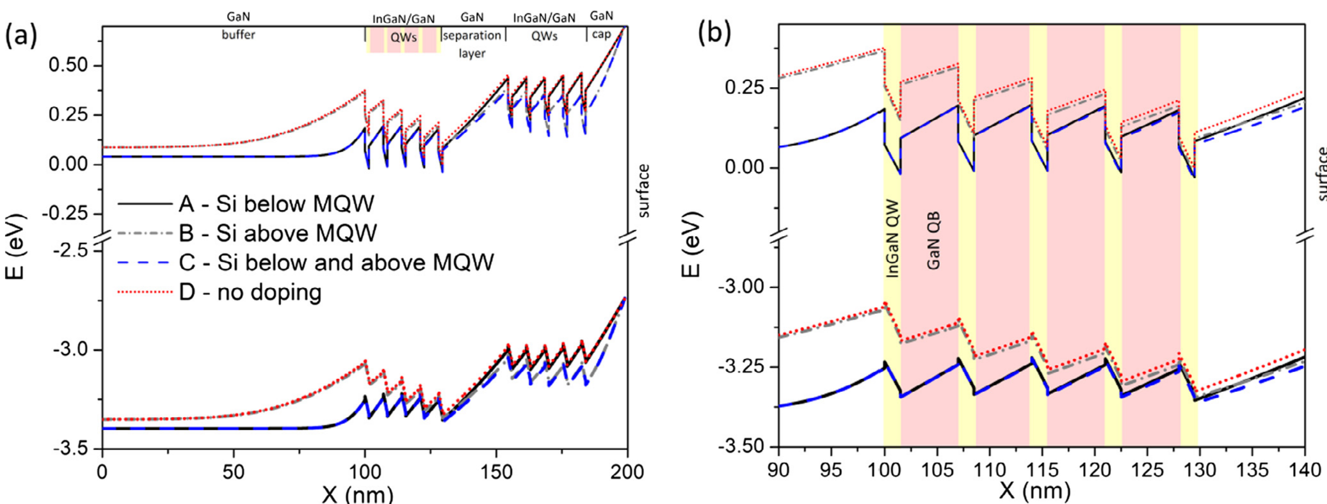


**Fig. 3.** Simulated band structures of samples A-D by NextNano software: (a) the whole region and (b) first five QWs, the doping levels are as written in Table 1, unintentional doping of GaN was assumed to be $1 \cdot 10^{17}\,\text{cm}^{-3}$.

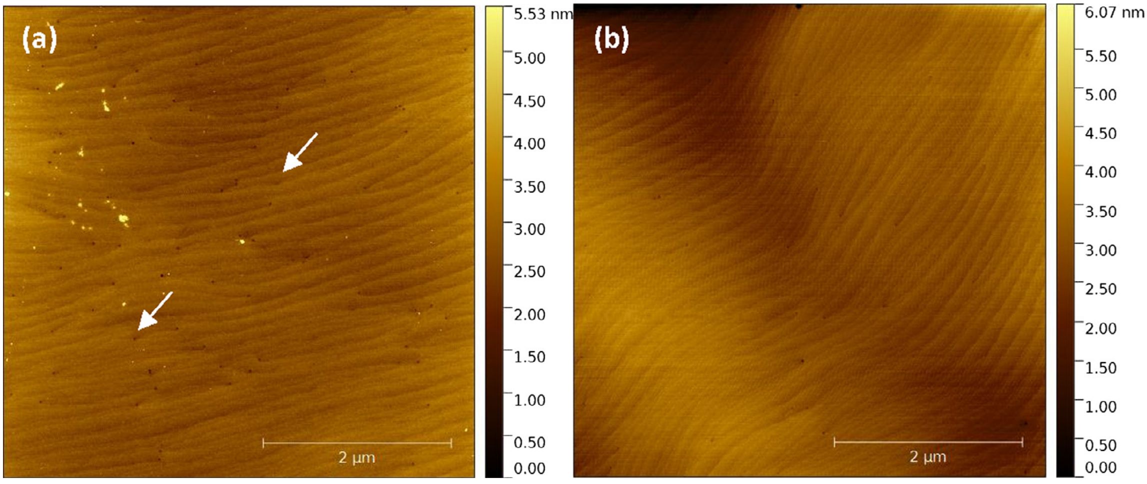


**Fig. 4.** AFM images of GaN buffer layers (a) without Si doping (b) doped with Si to n-type concentration of $1.1 \cdot 10^{18}\,cm^{-3}$. Some examples of threading dislocations penetrating to the sample surface are marked by arrows. Two times higher density of dislocations ($1.1 \cdot 10^{9}\,cm^{-3}$) was found in the undoped buffer layer.

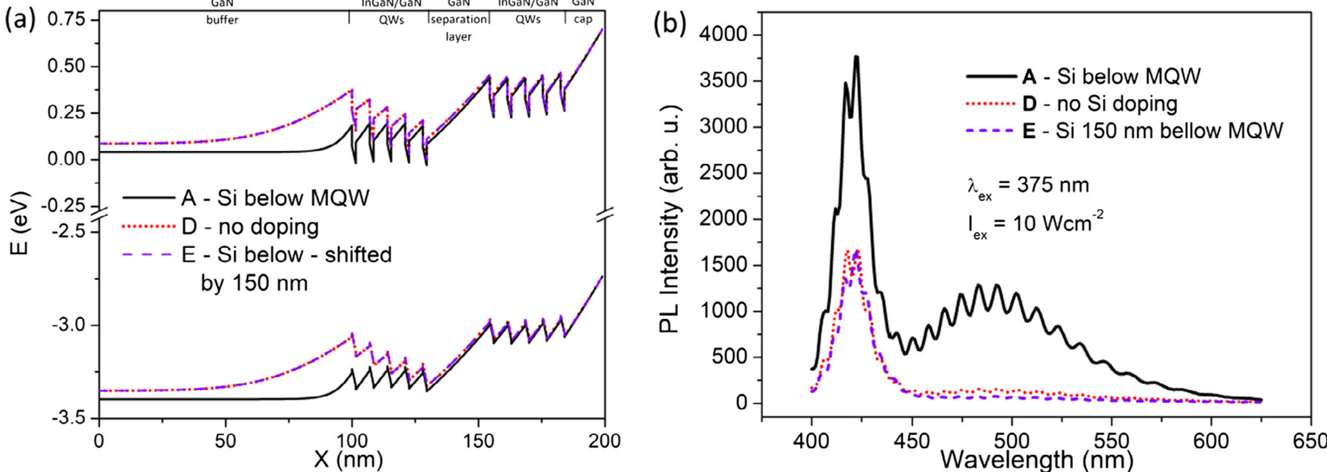


**Fig. 5.** (a) Simulated band structure of samples A, E and D, (b) PL of structures A, E and D.

is similar to the conventional tilt used in light emitting diodes (LEDs) with p-type doping on the top and n-type doping of the buffer electron emitter. It is known that this built-in electric field enhances the overlap of electrons and holes in QW, which are partly separated by the polarization (mostly piezoelectric field). Similar enhancement of excitonic emission based on this mechanism was also observed for our samples A and C compared to sample D, see the schematic drawing in Fig. 7. The tilt of the band structure and the shifted position of the carrier wave functions in QWs can also be responsible for an even stronger suppression of the DB. The upper InGaN/GaN QW interface is known to be technologically complicated. QWs are usually grown at temperatures lower than the ones used for the barrier layers. Lower temperature for InGaN is necessary for incorporation of In, while for GaN growth higher temperatures are necessary to get smooth surface and low density of point defects. To suppress the In desorption during the temperature increase for the barrier growth after the QW formation, we cover the

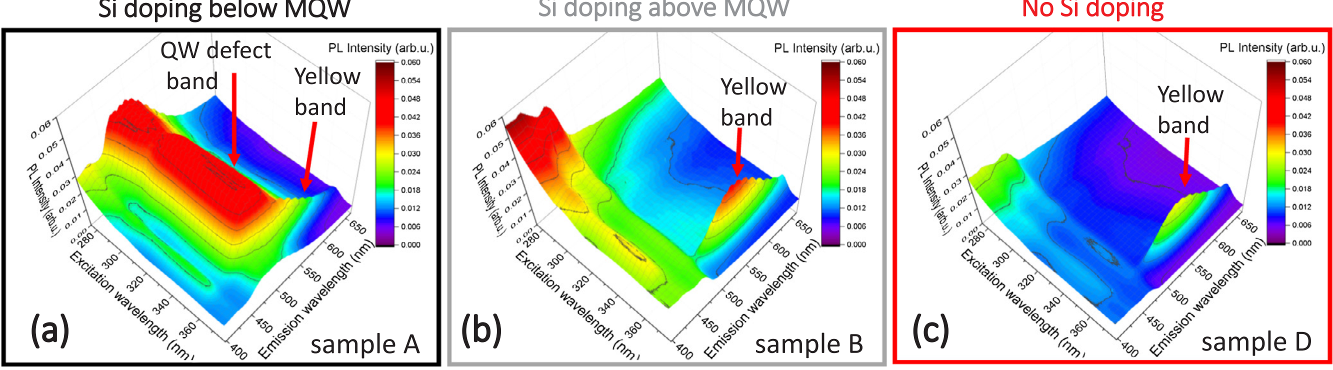


**Fig. 6.** Excitation emission PL maps measured at low excitation intensity for structures with (a) Si doped buffer layer (b) Si doped capping layer of the MQW region and (c) without any intentional doping.

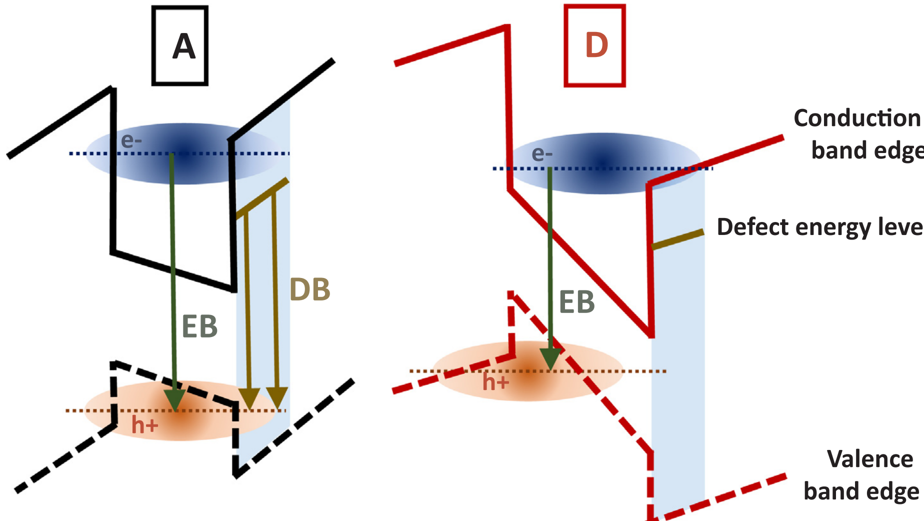


**Fig. 7.** Schematic drawings of band structures of a single InGaN/GaN QW situated in different internal electric fields (samples A and D) – suggested mechanism of DB luminescence suppression with increased band structure tilt.

InGaN QW with a thin GaN protection layer grown at the same temperature as the one of the QW growth. Compared to GaN grown at higher temperature, this thin layer may contain higher density of point defects which could serve as traps for carriers. In case of sample A, the decreased tilt of the band structure enhances penetration of holes into this interface and thus the recombination of holes with electrons trapped in the defect states of the low temperature GaN protection layer. That is why this defect band is so strongly enhanced in the case of sample A. The balanced electric field or even slightly opposite tilt in the MQW region of samples B, D and E strongly suppresses the DB. Sample C is somewhere between these cases.

Based on the understanding how the Si doping position influences the PL properties, we can suggest the optimal Si doping position for different applications. In case of LED structures, working at high excitation densities when the excitonic band is the most important, the n-type buffer layer helps improve the emission efficiency. On the other hand, in the case of InGaN/GaN MQW structure designed for scintillator applications, the n-type doping immediately under the MQW region is not required, since it strongly increases the QW DB luminescence which becomes dominant in the spectrum at low excitation intensities. Doping of upper GaN layers may be beneficial for this application.

## 4. Conclusions

In this work we have studied the influence of Si doping position on the PL properties of InGaN/GaN QWs. A set of samples with different positions of Si doping with respect to the MQW active region was prepared and studied by PL, SIMS and AFM. Structure band alignment was simulated by Nextnano software. Based on our experiments and band structure simulations, we can conclude that the dominant influence of Si doping is in a modification of the tilt of the band structure. However, the minor influence of lower dislocation density or unintentional doping of a few lowest QWs in the case of a Si doped buffer layer cannot be excluded.

We have suggested an explanation for high sensitivity of the DB luminescence to the band structure tilting. We suppose that the origin of DB luminescence is a recombination between holes confined in QWs and electrons trapped in defect states of the low temperature GaN layer near the upper InGaN/GaN QW interface. The tilt of the band structure prevents penetration of the hole wave function to the upper InGaN/GaN interface, thus the DB luminescence is efficiently suppressed.

Understanding the mechanism how the doping of layers surrounding the MQW region influences the luminescence properties can help us design proper doping for particular applications. In case of LED structures working at high excitation densities where the DB is negligible in comparison to the EB QW emission, the n-type buffer layer and p-type capping help improve emission efficiency. On the other hand, in the case of InGaN/GaN MQW structures designed for scintillator applications, the n-type doping immediately under the MQW region is not required, since it strongly increases the QW DB luminescence which becomes dominant in the PL spectrum for a low excitation intensity. Si doping of covering layer may improve the PL properties.

## Acknowledgements

The authors acknowledge the support of the GACR project no. 16-11769S and MSMT project no. NPU LO1603 – ASTRANIT. Partial support of the EC project H2020-TWINN-2015 no. 690599 - ASCIMAT is also gratefully acknowledged.

## References

[1] M.J. Davies, P. Dawson, F.C.-P. Massabuau, R.A. Oliver, M.J. Kappers, C.J. Humphreys, The effects of Si-doped prelayers on the optical properties of InGaN/GaN single quantum well structures, Appl. Phys. Lett. 105 (2014) 092106.
[2] Z.Q. Li, M. Lestrade, Y.G. Xiao, Z.S. Li, Improvement of performance in p-side down InGaN/GaN light-emitting diodes with graded electron blocking layer, Jpn. J. Appl. Phys. 50 (2011) 080212.
[3] F. Akyol, D.N. Nath, S. Krishnamoorthy, P.S. Park, S. Rajan, Suppression of electron overflow and efficiency droop in N-polar GaN green light emitting diodes, Appl. Phys. Lett. 100 (2012) 111118.
[4] A. Hospodková, M. Nikl, O. Pacherová, J. Oswald, P. Brůža, D. Pánek, B. Foltynski, E. Hulicius, A. Beitlerová, M. Heuken, InGaN/GaN multiple quantum well for fast scintillation application: radioluminescence and photoluminescence study, Nanotechnology 25 (2014) 455501.
[5] T. Hubáček, A. Hospodková, J. Oswald, K. Kuldová, J. Pangrác, Improvement of luminescence properties of GaN buffer layer for fast nitride scintillator structures, J. Cryst. Growth 464 (2017) 221.
[6] A. Hospodková, J. Oswald, M. Zíková, J. Pangrác, K. Kuldová, K. Blažek, G. Ledoux, C. Dujardin, M. Nikl, On the correlations between the excitonic luminescence efficiency and the QW numbers in multiple InGaN/GaN QW structure, J. Appl. Phys. 121 (2017) 214505.
[7] In-Hwan Lee, In-Hoon Choi, C.R. Lee, S.K. Noh, Evolution of stress relaxation and yellow luminescence in GaN/sapphire by Si incorporation, Appl. Phys. Lett. 71 (1997) 1359.
[8] A. Trellakis, T. Zibold, T. Andlauer, S. Birner, R.K. Smith, R. Morschl, P. Vogl, The 3D nanometer device project nextnano: concepts, methods, results, J. Comput. Electron. 5 (2006) 285.
[9] S. Birner, S. Hackenbuchner, M. Sabathil, G. Zandler, J.A. Majewski, T. Andlauer, T. Zibold, R. Morschl, A. Trellakis, P. Vogl, Modeling of semiconductor nanostructures with nextnano3, Acta Phys. Pol. A 110 (2006) 111.
[10] C.G. Van de Walle, J. Neugebauer, First-principles calculations for defects and impurities: applications to III-nitrides, J. Appl. Phys. 95 (2004) 3851.

[11] Ch. Sasaoka, F. Miyasaka, T. Koil, M. Kobayashi, Y. Murase, Y. Ando, M.G. Ganchenkova, R.M. Nieminen, Nitrogen vacancies as major point defects in gallium nitride, Phys. Rev. Lett. 96 (2006) 196402.
[12] D. Segev, C.G. Van de Walle, Origins of Fermi-level pinning on GaN and InN polar and nonpolar surfaces, Europhys. Lett. 76 (2006) 305.
[13] M.J. Davies, Ph. Dawson, F.C.-P. Massabuau, A. Le Fol, R.A. Oliver, M.J. Kappers, C.J. Humphreys, A study of the inclusion of prelayers in InGaN/GaN single- and multiple-quantum-well structures, Phys. Status Solidi B 252 (2015) 866–872.
[14] C. Sasaoka, F. Miyasaka, T. Koi, M. Kobayashi, Z. Murase, Y. Ando, A.A. Yamaguchi, Surface morphologies and optical properties of Si doped InGaN multi-quantum-well grown on vicinal bulk GaN(0001) substrates, Jpn. J. Appl. Phys. 52 (2013) 115601.

## 4.4 Influence of GaN buffer layer under InGaN/GaN MQWs on luminescent properties [iv]

Commercial available LED structures are grown with InGaN underlayer or InGaN/GaN superlattice under the MQW active region for increasing luminescence efficiency. The mechanism of that improvement is still not well understood and publications with new explanations are published every year. In this work we have compared structures with different buffer layers and studied photoluminescence properties. SIMS analysis showed that after decreasing of the growth temperature to the growth of InGaN layers, impurities, such as oxygen, iron or zinc, are incorporated into InGaN layers. We grew set of samples with low temperature (LT) GaN buffer layer under different growth conditions and found that LT GaN buffer layer increases excitonic emission from QWs and decreases defect band. LT GaN layer did not influence contamination incorporation and the increase of PL was explained by increased size of V-pits. This suggestion was proved by two samples grown with $N_2$ and $H_2$ carrier gas. In conclusion, we have shown that PL improvement can be done by LT GaN buffer layer without any indium and this approach can be used either in LED community or for our scintillation structure. The paper was published in Journal of Crystal Growth (IF = 1.57, Q3, 2 citation).

Journal of Crystal Growth 507 (2019) 246–250

Contents lists available at ScienceDirect

Journal of Crystal Growth

journal homepage: www.elsevier.com/locate/jcrysgro

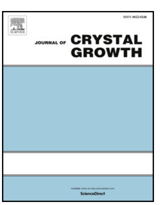

# Influence of GaN buffer layer under InGaN/GaN MQWs on luminescent properties

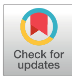

Filip Dominec, Alice Hospodková*, Tomáš Hubáček, Markéta Zíková, Jiří Pangrác, Karla Kuldová, Aliaksei Vetushka, Eduard Hulicius

*Institute of Physics CAS, v. v. i., Cukrovarnická 10, 162 00 Prague 6, Czech Republic*

ARTICLE INFO

*Keywords:*
A1. Low dimensional structures
A1. V-pits
A3. Metalorganic vapor phase epitaxy
B2. InGaN/GaN quantum wells
B2. GaN buffer layer
B3. Scintillators

ABSTRACT

Although InGaN layers or InGaN/GaN superlattices are commonly used as efficiency improving buffers for LED structure production, there is still a controversy and active discussion about the mechanisms improving the luminescence properties of InGaN QWs grown above such buffers. In this manuscript it is shown that presence of In in the buffer layer is not the primary reason for photoluminescence improvement which can be also achieved by introduction of GaN buffer layer grown at lower temperature under nitrogen atmosphere. SIMS analysis suggests that low temperature buffer layer does not influence the impurity incorporation and hence the PL improvement is caused by suppressed contamination of MQW region grown above the low temperature buffer. AFM images for two samples that differ mostly in morphology however supports another explanation in which formation of larger V-pits is the main reason for the luminescence improvement.

## 1. Introduction

It was observed that with increased number of InGaN/GaN quantum wells (QWs) their photoluminescence (PL) efficiency is increased. Usually PL improvement was observed until 10 InGaN/GaN QWs [1], but some works have reported PL improvement even for 30 QW structure [2]. The nonlinear improvement of PL efficiency with increased QW number was a motivation to develop buffer layers containing indium which were also reported to enhance the PL of InGaN/GaN multiple QW (MQW) structures [3–8]. The most common types of such buffers are InGaN layers [3–5] or InGaN/GaN superlattices [6–8]. Although these buffer layers are already commonly used for LED structure production, there is still controversy and active discussion about the mechanisms improving the luminescence properties of InGaN QWs grown above such buffers. Several possible mechanisms are suggested, such as strain relaxation [3,7,8], enhanced impurity incorporation [5] or increased size of V-pits [4,6]. During the growth of InGaN layers, hexagonal V-pits form around threading dislocations reaching the sample surface (Fig. 2). Their depth and diameter are determined by the thickness of the layer grown at sufficiently low temperature [9] and/or after switching the $H_2$ carrier gas to $N_2$ [10–12]. It was suggested that sufficiently wide V-pits represent an effective barrier for carriers in QWs and may prevent excitons from approaching the threading dislocation, thus preventing their non-radiative recombination [13].

Although different mechanisms of PL improvement were suggested, previous works assumed the presence of In in buffer layers to be a necessary condition for the PL enhancement.

The defect band (DB) emission was not studied before. Majority of published works focus on QW emission, since the luminescence of DB is very low under excitation conditions used for LEDs or laser diodes. Recently, new application of InGaN/GaN MQW structure as fast scintillators has emerged [14]. Scintillators consisting of InGaN/GaN MQWs, see Fig. 1, present a promising technology for radiation detection and imaging owing to their high efficiency of blue light emission upon irradiation. The fast electron-hole recombination in MQWs takes place within few nanoseconds, however the temporal resolution of our samples is deteriorated by an additional spectral component, the already mentioned DB which has much longer decay time. Unfortunately, it becomes dominant in the emission spectrum at very low excitation power densities that are typical for some scintillator operation.

Convincing arguments exist to assume that the DB arises from within the MQW active region [2], in contrast to other weaker spectral components that are emitted from impurities of the GaN buffer, denoted in the literature as yellow band and blue band. The DB central energy is sensitive to the MQW thickness and composition; in particular, DB is found systematically 300–400 meV below the narrower spectral emission of the MQW exciton. In addition, depth-resolved

* Corresponding author.
*E-mail address:* hospodko@fzu.cz (A. Hospodková).

https://doi.org/10.1016/j.jcrysgro.2018.11.025

Available online 23 November 2018
0022-0248/ © 2018 Elsevier B.V. All rights reserved.

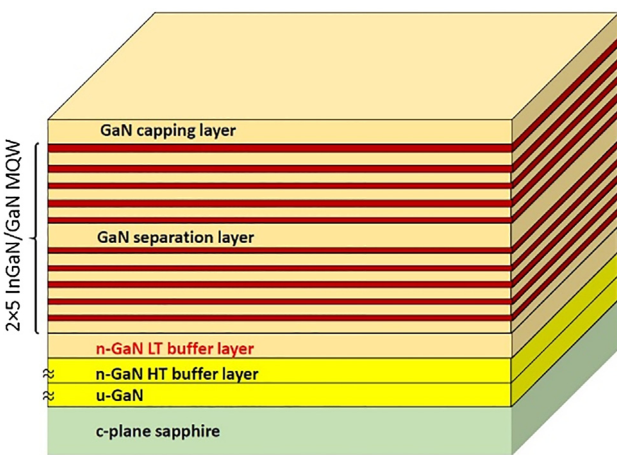


**Fig. 1.** Schematic of InGaN/GaN MQW structure.

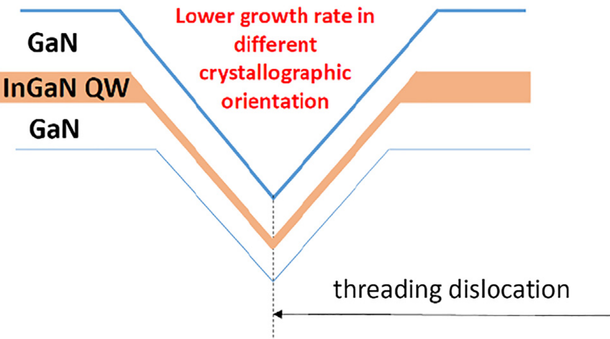


**Fig. 2.** Schematic cross-section of a V-pit [5].

cathodoluminescence measurements corroborate the spatial overlap of DB emission with the MQW structure [2]. The exact source of DB has not been conclusively identified yet.

In this paper, we investigated several modifications of the GaN buffer layer below the MQWs that do not contain In, with the aim to elucidate mechanism of InGaN/GaN PL enhancement, to judge whether presence of In is necessary condition for the PL improvement and also to eliminate the harmful DB luminescence.

## 2. Experimental

We prepared all discussed structures on sapphire substrates with Aixtron 3x2″ CCS MOVPE system, equipped by Laytec epicurveTT in-situ monitoring. All samples were grown on c-oriented $Al_2O_3$ substrates, baked out and nitrified by $NH_3$ prior to the growth of 25 nm thick nucleation layer. TMGa precursor was used for the growth of 3.4 µm thick GaN high-temperature buffer layer (HTB). TEGa was subsequently used as gallium source for the low-temperature buffer layer (LTB), for the active region of the MQW structure, and for the GaN capping layer. Upper part of HTB and LTB ($\sim 10^{18}$ $cm^{-3}$) was doped by Si from $SiH_4$.

The active MQW region contained (2 × 5) of $In_xGa_{1-x}N$ (x = 0.04–0.06) 1.5 nm thick QWs, formed by introduction of TMIn into the reactor, and separated by 6 nm thick GaN barriers. The structure is schematically depicted in Fig. 1 and important sample growth parameters are summed up in Table 1.

PL was measured at room temperature by confocal microscope with excitation wavelength $\lambda_{exc}$ = 325 nm, and power density ~0.5 W/cm$^2$ with spot diameter 2 µm, which partly saturated the DB luminescence. Atomic Force Microscopy (AFM) images were taken by Dimension Icon AFM in semicontact mode, using ASPIRE tips.

Secondary ion mass spectroscopy (SIMS) were provided by EAG laboratories.

**Table 1**
Sample growth parameters.

| Sample | Thickness of LT buffer layer included under MQW (nm) | Growth parameters of the buffer layer adjacent to MQW | | |
|---|---|---|---|---|
| | | Pyrometer temperature (°C) | Group-III precursor | Carrying gas |
| A | 0 | 1065 | TMGa | $H_2$ |
| B | 30 | 820 | TEGa | $N_2$ |
| C | 30 | 800 | TEGa | $N_2$ |
| D | 60 | 820 | TEGa | $N_2$ |
| E | 60 | 820 | TEGa | $H_2$ |

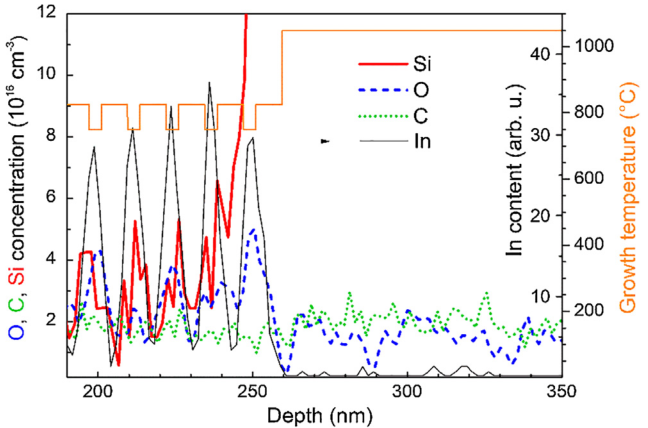


**Fig. 3.** SIMS composition profiles of InGaN/GaN MQW sample without LTB with detail on concentrations of indium, silicon, oxygen and carbon, with an overlay showing the growth temperature of each layer.

## 3. Results and discussion

### 3.1. SIMS analysis

Since we consider chemical contamination can be one of possible source for DB emission (beside native defects or their complexes), we performed a secondary ion mass spectroscopy (SIMS) analysis on a MQW sample of type **A** (i.e. one without LTB). Fig. 3a shows that some elements, notably oxygen, exhibit propensity to accumulate in the InGaN layers. Increased oxygen incorporation was also reported earlier [15] and was explained by more favorable stoichiometric conditions for incorporation of oxygen atoms to the N sites due to the insufficient decomposition of $NH_3$. However, our results do not support this hypothesis since increased incorporation in InGaN layers is found also for silicon which is dominantly incorporated in group III sites. Particularly, high concentration of Si in the lowermost QW is due to $SiH_4$ buffer doping and reactor memory effect. On the other hand, no influence was observed for carbon incorporation which similarly as oxygen incorporates in the N sublattice. Therefore, the simultaneous increase of O and Si impurity concentration on both Ga/In and N sites appears to result from easier impurity incorporation at lower temperature.

Even more striking spike of concentration at the bottom edge of the MQW region can be found for iron (see solid line in Fig. 4a), which can be explained by large Fe atoms floating on the surface during high-temperature epitaxial growth of the GaN buffer layer [16] and subsequent incorporation at the edge of MQW structure upon the reduction of growth temperature which is essential for the InGaN QW growth. An elevated concentration correlated with the InGaN QWs was also found for zinc (see solid line in Fig. 4b), which may be either due to lower temperature (as for iron), or, alternatively, traces of zinc may be introduced with the TMIn precursor.

Because the SIMS results suggested increased contaminant

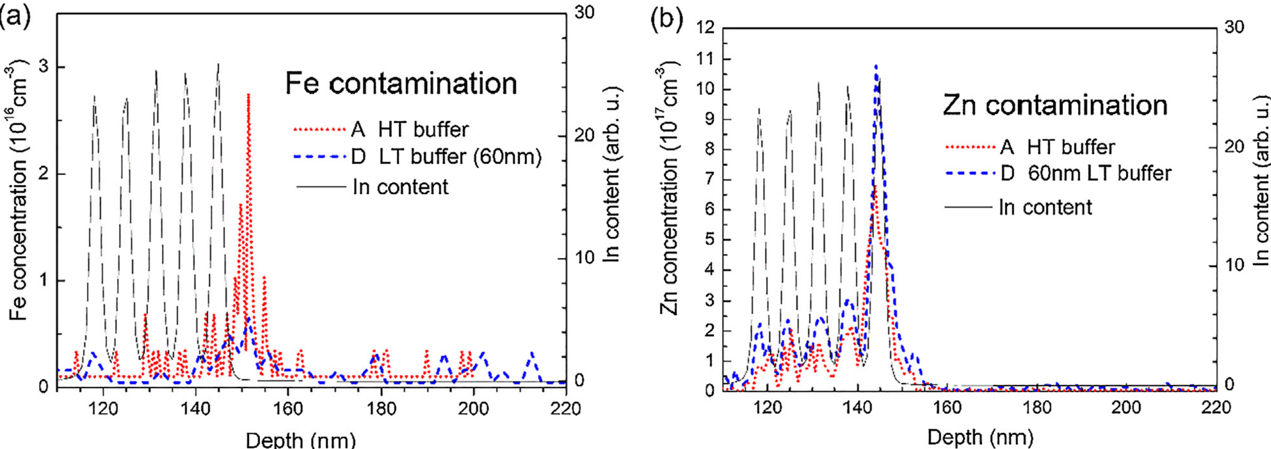


**Fig. 4.** Comparison of SIMS composition profiles of InGaN/GaN MQW samples with and without 60 nm thick LTB grown at 820 °C: (a) Detail on concentration of iron, (b) Detail on concentration of zinc.

concentration in InGaN layers, we have prepared set of samples **B-E** (see Table 1) containing different types of GaN LTB layers. The original motivation was to allow the surfacing atoms to incorporate during the growth into LTB and to prevent them from contaminating the active MQW region. Although InGaN layers were reported to improve the PL properties in LEDs, we did not use any In in the buffer layer to avoid further increase of the strain in the exceptionally thick scintillating MQW structure. Sample D with 60 nm thick LTB grown at $N_2$ atmosphere was sent for SIMS analysis to check Fe and Zn incorporation in the structure with LTB. However, according to the results shown in Fig. 4a, b (dotted lines), no expected increased Fe or Zn concentration in LTB layer was observed. The possible explanation is that it is not the lower growth temperature, but presence of In which may enhance the impurity segregation in the first QW layers. Similar hypothesis was also recently suggested in [5].

Nevertheless the SIMS results show surprisingly high unintentional Zn concentration which might be a very important information for other MOVPE technological laboratories. The source of this unintentional Zn contamination was not recognized, yet. Both samples were grown from different bubblers of TMIn precursor and according to SIMS results, changing the TMIn source did not apparently influenced the Zn concentration (see Fig. 4b).

### 3.2. Effect of LTB layer growth temperature and thickness on PL

In samples A, B and C, we have included 30 nm thick low-temperature GaN buffer layer directly under the MQWs. In Fig. 5 the PL results obtained from traditionally grown MQW sample A (with HTB only) and from samples B and C featuring a 30 nm LTB layer, grown at 820 °C and 800 °C, respectively, are compared. Comparing the samples A and B we observed a 40% increase of peak PL intensity, accompanied by 50% suppression of the defect band.

According to these results, we can conclude that decreasing the growth temperature of LTB layer prepared under N2 atmosphere either suppresses or deactivates defects in MQW region responsible for the non-radiative recombination and for recombination causing the DB.

As demonstrated in Fig. 6, keeping the LTB growth temperature constant at 820 °C, but doubling its thickness can further increase by ~ 30% the luminescence intensity for both the exciton MQW as well as for the unwanted DB. This suggests that the non-radiative recombination is suppressed with increasing thickness of the buffer layer, but it does not influence defects responsible for the DB luminescence.

Since the influence of LTB on incorporation of contaminants into the MQW can be excluded according to SIMS measurement, the PL improvement with introduction of LTB from Figs. 5 and 6 must have different interpretation. A possible reason could be enhanced V-pit

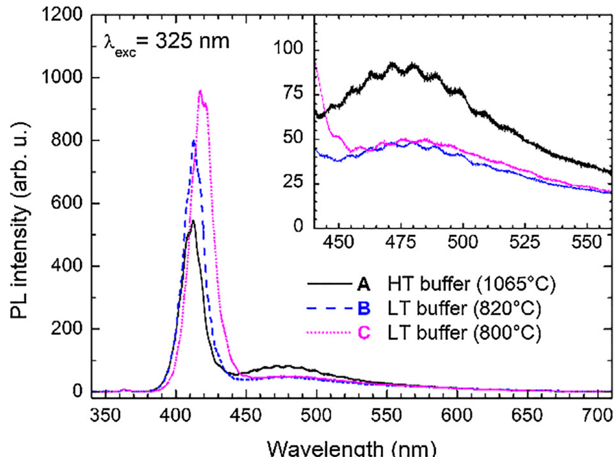


**Fig. 5.** PL of MQW structure with HTB only (**A**) and with addition of LTB grown at different temperatures of 820 °C and 800 °C (B, C).

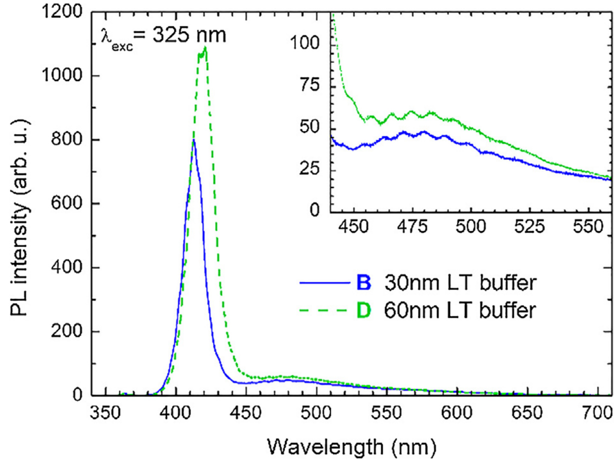


**Fig. 6.** PL of MQW structures with different LTBs thicknesses 30 nm and 60 nm (samples B, D).

formation during the LTB growth.

### 3.3. Effect of the LTB layer on V-pit diameter and depth

Surface morphology acquired from a parallel series of samples A, B

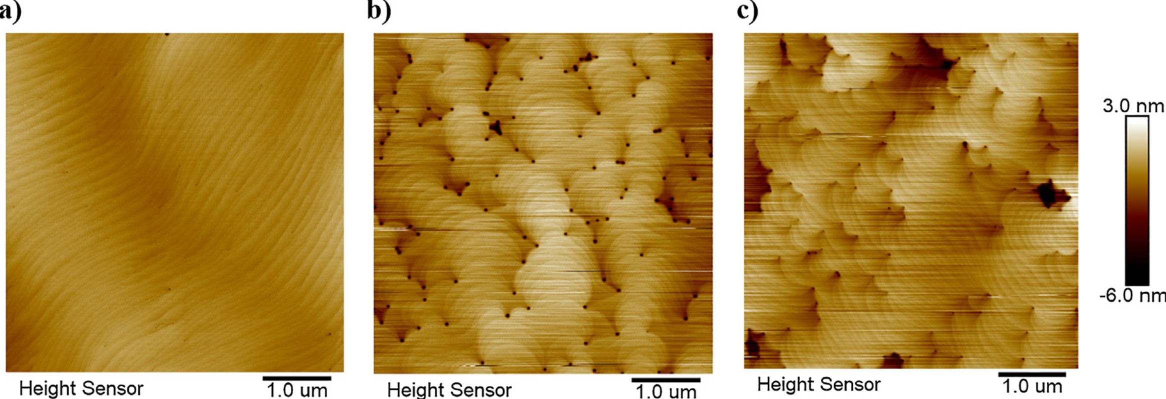


**Fig. 7.** AFM images of the GaN layers, with growth interrupted exactly before MQW layers. (a) HTB surface corresponding to the high-temperature buffer layers, grown at high temperature of 1060 °C, with H2 as the carrying gas. No V-pits form at the dislocation ends. (b) LTB surface corresponding to sample D, grown at low temperature 820 °C with N2 as the carrying gas. (c) LTB surface corresponding to sample E, grown at low temperature of 810 °C with H2 as the carrying gas.

and D with growth terminated exactly before the MQW active region is shown by AFM, see Fig. 7.

Comparing these AFM images with PL results of samples A, B and D (Figs. 5 and 6) suggests that the size of V-pits is positively correlated with luminescence efficiency. Additionally, it can be noticed that bigger V-pits are also correlated with a small red shift which we have also observed on other set of our samples. The reason is probably lower In incorporation on V-pit walls and consequently higher In content on flat, luminescent part of QW structure. Similar correlation of enhanced luminescence of MQW structures with increased V-pit size was also recently published by other groups [17–19].

To tell apart the effects of contamination and V-pit size, we have grown an additional sample **E** with 60 nm thick LTB and other growth parameters identical to sample **D**, except for the carrier gas - $H_2$ being kept for both the HTB and LTB. Use of hydrogen for sample **E** LTB partially suppresses the V-pits formation: Although V-pits are visible and have nearly the same density (c.f. Fig. 7b, c), they are much shallower than when nitrogen was used, as demonstrated by AFM profiles in Fig. 8. Suppressed V-pit formation under $H_2$ atmosphere was also previously observed [6–8]. The possible reason may be increased migration od adsorbed atoms on epitaxial surface under H2 atmosphere and the type of carrier gas probably also influences the growth rate in different crystal planes.

In Fig. 9 the PL results of both MQW structures grown with different carrying gases $N_2$ and $H_2$ are compared. Growing the LTB of sample **E** with $H_2$ carrying gas yielded much weaker exciton emission and

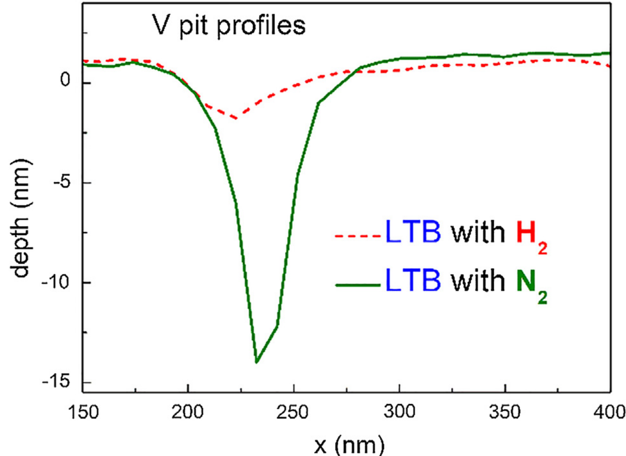


**Fig. 8.** V-pits in the LTB are deeper and larger when prepared with $N_2$ carrying gas.

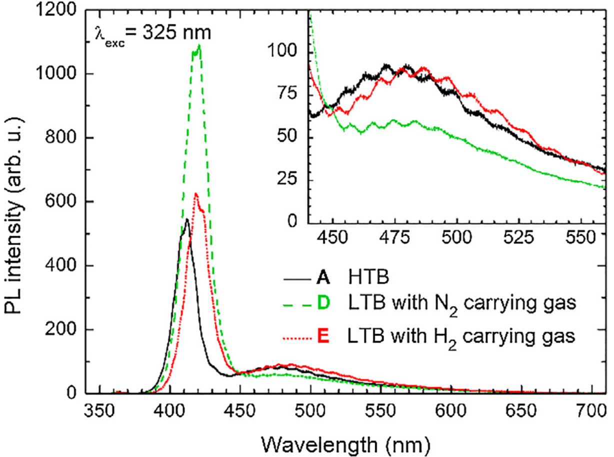


**Fig. 9.** Comparison of PL from samples **D** and **E**, with similar buffers differing mostly by the carrying gas. For comparison, PL of sample **A** with HTB only has been added.

stronger DB emission, which makes it almost as bad as sample **A** without any LTB. Supposing that hydrogen does not increase the presence of any contaminant segregation on epitaxial surface during the LTB growth, we can conclude that the PL enhancement as well as weak DB suppression is probably not caused by enhanced incorporation of impurities at lower growth temperature of buffer layer, but by increased V-pit size in InGaN/GaN MQW region. Bigger V-pits prevent penetration of electrons and holes into the region around dislocations with increased defect formation and consequently increased non-radiative or defect luminescent recombination

## 4. Conclusions

In this manuscript it is shown that the presence of In in the buffer layer is not the primary reason for the PL improvement which can be also achieved by introduction of GaN buffer layer grown at lower temperature under nitrogen atmosphere. In a series of samples where a low-temperature buffer layer is added to separate the MQW structure from the high-temperature buffer beneath it, we confirmed that the luminescence efficiency of the exciton recombination improved and simultaneously the undesired defect band was suppressed. The effect of this low-temperature buffer layer was more pronounced when the growth temperature was further reduced, or when its thickness was doubled.

SIMS analysis has shown that the concentration of some unwanted

elements such as oxygen or silicon is increased in InGaN layers, occurrence of others such as iron or zinc is correlated with the beginning of the MQW growth. However, SIMS analysis of structures with LTB layers bellow MQW region did not prove enhanced impurity incorporation in LTB region. No significant influence of LTB on impurity concentration was observed in the MQW region. Hence, PL improvement is not caused by suppressed contamination of MQW region grown above low temperature buffer.

Instead, on the comparison of similar samples featuring LTB grown in the $N_2$ and $H_2$ atmosphere, we have shown that the improvement of luminescence is clearly linked with the formation of V-pits during the low-temperature growth in $N_2$. Bigger V-pits more effectively separate electrons and holes in InGaN QWs from regions around dislocations with increased defect concentration. The growth conditions of InGaN layers are simultaneously conditions for the V-pit development. This is the reason why the In containing buffer layers were identified to improve the PL properties of MQWs previously.

Based on the results presented, we conclude that addition of a low-temperature GaN buffer is clearly desirable for MOVPE growth of InGaN/GaN MQW LED or scintillators.

## Acknowledgments

The authors acknowledge support from MEYS project NPU LO1603 – ASTRANIT and from the Czech Science Foundation project no. 16-15569S. Partial support of EC project H2020-TWINN-2015 no. 690599 (ASCIMAT) is also gratefully acknowledged.

## References

[1] D.-J. Kim, Y.-T. Moon, K.-M. Song, C.-J. Choi, Y.-W. Ok, T.-Y. Seong, S.-J. Park, Structural and optical properties of InGaN/GaN multiple quantum wells: the effect of the number of InGaN/GaN pairs, J. Cryst. Growth 221 (2000) 368–372.
[2] A. Hospodková, J. Oswald, M. Zíková, J. Pangrác, K. Kuldová, K. Blažek, G. Ledoux, C. Dujardin, M. Nikl, On the correlations between the excitonic luminescence efficiency and the QW numbers in multiple InGaN/GaN QW structure, J. Appl. Phys. 121 (2017) 214505.
[3] N. Nanhui, W. Huaibing, L. Jianping, L. Naixin, X. Yanhui, H. Jun, D. Jun, S. Guangdi, Enhanced luminescence of InGaN/GaN multiple quantum wells by strain reduction, Solid-State Electron. 51 (2007) 860–864.
[4] M.J. Davies, F.C.-P. Massabuau, P. Dawson, R.A. Oliver, M.J. Kappers, C.J. Humphreys, Effects of an InGaN prelayer on the properties of InGaN/GaN quantum well structures, Phys. Status Solidi C 11 (2014) 710–713.
[5] C. Haller, J.-F. Carlin, G. Jacopin, D. Martin, R. Butte, N. Grandjean, Burying non-radiative defects in InGaN underlayer to increase InGaN/GaN quantum well efficiency, Appl. Phys. Lett. 111 (2017) 262101.
[6] K. Sugimoto, Y. Denpo, N. Okada, K. Tadatomo, Effect of superlattice on light output power of InGaN-based light-emitting diodes fabricated on underlying GaN substrates with different dislocation densities, Phys. Status Solidi C 13 (2016) 270–273.
[7] S.J. Leem, Y.C. Shin, K.C. Kim, E.H. Kim, Y.M. Sung, Y. Moon, S.M. Hwang, T.G. Kim, The effect of the low-mole InGaN structure and InGaN/GaN strained layer superlattices on optical performance of multiple quantum well active layers, J. Cryst. Growth 311 (2008) 103–106.
[8] Q. Mu, M. Xu, X. Wang, Q. Wang, Y. Lv, Z. Feng, X. Xu, Z. Ji, Influence of the InGaN/GaN quasi-superlattice underlying layer on photoluminescence in InGaN/GaN multiple quantum wells, Physica E 76 (2016) 1–5.
[9] S.R. Jeon, S.J. Lee, S.H. Jung, S.H. Lee, J.H. Baek, H. Jeong, O.H. Cha, E.K. Suh, M.S. Jeong, Effect of V-shaped defects on structural and optical properties of AlGaN/InGaN multiple quantum wells, J. Phys. D: Appl. Phys. 41 (2008) 13.
[10] Y.D. Zhu, T.P. Lu, X.R. Zhou, G.Z. Zhao, H.L. Dong, Z.G. Jia, X.G. Liu, B.S. Xu, Effect of hydrogen treatment temperature on the properties of InGaN/GaN multiple quantum wells, Nanoscale Res. Lett. 12 (2017) 321.
[11] Y.B. Tao, Z.Z. Chen, T.J. Yu, Y. Yin, X.N. Kang, Z.J. Yang, G.Z. Ran, G.Y. Zhang, Improvement of structural and luminescence properties in InGaN/GaN multiple quantum wells by symmetrical thin low temperature-GaN layers, J. Cryst. Growth 318 (2011) 509–512.
[12] F. Scholz, J. Off, E. Fehrenbacher, O. Gfrörer, G. Brockt, Investigations on structural properties of GaInN-GaN multi quantum well structures, Phys. Status Solidi A 180 (2000) 215.
[13] A. Hangleiter, F. Hitzel, C. Netzel, D. Fuhrmann, U. Rossow, G. Ade, P. Hinze, Suppression of nonradiative recombination by V-shaped pits in GaInN/GaN quantum wells produces a large increase in the light emission efficiency, Phys. Rev. Lett. 95 (2005) 127402.
[14] A. Hospodková, M. Nikl, O. Pacherová, J. Oswald, P. Brůža, D. Pánek, B. Foltynski, E. Hulicius, A. Beitlerová, M. Heuken, InGaN/GaN multiple quantum well for fast scintillation application: radioluminescence and photoluminescence study, Nanotechnology 25 (2014) 455501.
[15] N. Okada, F. Ishida, Y. Mitsui, K. Tadatomo, H. Mangyo, Y. Kobayashi, H. Ono, K. Ikenaga, Y. Yano, K. Matsumoto, Evaluation of performance of InGaN/GaN light-emitting diodes fabricated using $NH_3$ with intentionally added $H_2O$, Jap. J. Appl. Phys. 48 (2009) 062102.
[16] Z.H. Feng, B. Liu, F.P. Yuan, J.Y. Yin, D. Liang, X.B. Li, Z. Feng, K.W. Yang, S.J. Cai, Influence of Fe-doping on GaN grown on sapphire substrates by MOCVD, J. Cryst. Growth 309 (2007) 8–11.
[17] N. Okada, H. Kashihara, K. Sugimoto, Y. Yamada, K. Tadatomo, Controlling potential barrier height by changing V-shaped pit size and the effect on optical and electrical properties for InGaN/GaN based light-emitting diodes, J. Appl. Phys. 117 (2015) 025708.
[18] K. Sugimoto, N. Okada, S. Kurai, Y. Yamada, K. Tadatomo, Separation of effects of InGaN/GaN superlattice on performance of light-emitting diodes using mid-temperature-grown GaN layer, Jpn. J. Appl. Phys. 57 (2018) 062101.
[19] S. Kurai, K. Okawa, R. Makio, G. Nobata, J. Gao, K. Sugimoto, N. Okada, K. Tadatomo, Y. Yamada, Nanoscopic spectroscopy of potential barriers formed around V-pits in InGaN/GaN multiple quantum wells on moderate temperature GaN pit expansion layers, J. Appl. Phys. 124 (2018) 083107.

## 4.5 InGaN/GaN Structures: Effect of the Quantum Well Number on the Cathodoluminescent Properties [v]

Very thick active region is necessary for some applications of our scintillation structure. In this paper, we have studied structures with different number of QWs (10 and 30 QWs). From the PL and CL measurements it was found out that sample with 30 QWs has stronger excitonic luminescence than sample with 10 QWs. The main cathodoluminescence signal originates only from the lowest part of the interaction volume of the incident electrons, which was found out from the CL measurement with different acceleration voltage. This observation is important for design of the scintillation structure, where active region should overlap the main CL region to get the most intensive luminescence for specific primary electron energy. Enhancement of the luminescence intensity in sample with 30 QWs was explained by bigger V-pits and screening of the non-radiative centres located around threading dislocations (in the middle of V-pits). The paper was published in Physica Status Solidi B in May 2018 (IF = 1.45, Q3, 3 citations).

# InGaN/GaN Structures: Effect of the Quantum Well Number on the Cathodoluminescent Properties

*Alice Hospodková,* Tomáš Hubáček, Jiří Oswald, Jiří Pangrác, Karla Kuldová, Matěj Hývl, Filip Dominec, Gilles Ledoux, and Christophe Dujardin*

**In this work we compare luminescence results obtained on InGaN/GaN multiple quantum well (QW) structures with 10 and 30 QWs. The aim is to increase the intensity of faster blue QW emission and decrease the luminescence of the QW defect band, showing a slower luminescence decay time, which is undesired for fast scintillator applications. We demonstrate that increasing the number of InGaN QWs is an efficient method to reach this goal. The luminescence improvement of the sample with higher number of QWs is explained by the influence of the increased size of V-pits with increased QW number. Thinner QWs on the side wall of V-pits serve as barriers which separate carriers from dislocations penetrating through the V-pit centre, supressing thus the non-radiative and radiative recombination on defects. Based on cathodoluminescence (CL) results, the scintillator structure design is discussed. Scintillator structures with higher number of QWs can take advantage of both, improved luminescence efficiency and thicker active region.**

## 1. Introduction

InGaN/GaN quantum well (QW) structures have been widely used for LEDs and lasers since early 1990s. More recently, the application of nitride heterostructures as fast scintillators for detectors of ionizing radiation have emerged.[1] The advantages of nitride heterostructures compared to other scintillation materials are: high radiation resistance, high exciton binding energy, and consequently short luminescence decay time as well as high luminescence efficiency. A demand for very fast, efficient scintillators with decay time of a few nanoseconds has emerged in recent years due to the need for fast scanning electron microscopes for inspection machines in the electronic industry. High energy calorimetry and time of flight imaging, such as positron emission tomography, would also greatly benefit from a drastic improvement of the scintillating timing performances.[2,3] For these applications nitride heterostructures are highly promising.[4,5]

Structures designed for scintillating applications require large QW numbers covering the particle penetration depth. In this work we concentrate our effort on the growth of structures with higher numbers of QWs than typically used in LED in order to increase the thickness of the active region. We have identified two bands in PL spectra of our structures, the faster blue and a slower defect bands, which differ by most properties, such as by their spectral position and width, lifetime, and sensitivity to diverse type of excitation. The fast blue QW band has luminescence time in the order of nanoseconds and has probably still excitonic nature, as our QWs are designed to be shallow and thin.[6] The slower defect band has luminescence response in the microsecond time scale which is not desired in fast scintillator applications. Although luminescent nitride structures have been widely used for a long time, the luminescent properties of the defect bands in bulk GaN and InGaN/GaN QW structures are not well understood, because this defect band can be observed only for very low excitation densities which are not subject of interest for LED focused research. However, for scintillator application the luminescence properties have to be optimized for excitation densities approx. $10^{18}$ to $10^{22}$ $cm^{-3}s^{-1}$, which are several order of magnitude lower than in the case of typical LED excitation ($10^{24}$–$10^{28}$ $cm^{-3}s^{-1}$).[6] Many works have focused on the defects in GaN responsible for the slow "yellow band."[7,8] To the best of our knowledge, the origin of the blue or green defect bands from InGaN QWs has not been explained so far.

In order to optimize scintillation efficiency and timing performances in the multilayer system, we study the effect of QW number on intensity of fast blue QW emission and on the luminescence of QW defect band. We discuss the comparison of morphological (AFM) and luminescence properties of structures grown with 10 and 30 QWs in the active region. The luminescence of the structures was studied by both photoluminescence (PL) with low excitation density and cathodoluminescence (CL) measurements. CL was measured to investigate

Dr. A. Hospodková, T. Hubáček, Dr. J. Oswald, Dr. J. Pangrác, Dr. K. Kuldová, M. Hývl, Dr. F. Dominec
Institute of Physics
Czech Academy of Sciences
v.v.i., Cukrovarnická 10, 16200 Praha 6, Czech Republic
E-mail: hospodko@fzu.cz

Dr. G. Ledoux, Prof. C. Dujardin
Université Lyon
Université Claude Bernard Lyon 1
CNRS
Institut Lumière Matière UMR 5306
F-69100 Villeurbanne, France

The ORCID identification number(s) for the author(s) of this article can be found under https://doi.org/10.1002/pssb.201700464.

**DOI: 10.1002/pssb.201700464**



© 2017 WILEY-VCH Verlag GmbH & Co. KGaA, Weinheim

the luminescence properties of structures at different depths given by the penetration depth of incident electron with different kinetic energies.

## 2. Experimental Section

Structures with InGaN/GaN MQWs (see **Figure 1**) have been prepared by an Aixtron $3 \times 2$ CCS MOVPE system equipped with a Laytec epicurveTT apparatus for in situ measurement of reflectivity. Two structures were prepared: one with $2 \times 5$ InGaN QWs (structure A) and one with $6 \times 5$ InGaN QWs (structure B) in the active region. Each group of five QWs was followed by a 25 nm thick separation layer with the purpose of decreasing the strain energy in the active region and also to increase the thickness of the scintillator active region. Both structures were prepared on 2.5 μm thick GaN buffer layer with the same technology of preparation. More details about the buffer layer growth can be found in Ref. [9].

The true wafer temperature was measured in situ by a EpiCurveTT. Trimethylgallium (TMGa) and ammonia ($NH_3$) were used as precursors with a hydrogen carrier gas for the growth of buffer layers. Triethylgallium (TEGa), trimethylindium (TMIn), and ammonia with a nitrogen carrier gas were used for the growth of the MQW region, including barriers. Structures were grown on sapphire substrates with *c*-plane orientation, further details about the structure growth can be found in Ref. [10]. The In content in $In_xGa_{1-x}N$ QWs ranged from $x = 0.06–0.08$, with QW thicknesses around 1.3 nm and GaN barrier thicknesses around 5.7 nm. Thickness was estimated from the simulation of X-ray diffraction data and the In concentration was found from SIMS results.

The PL spectra were measured at RT using confocal microscopy (LabRAM HR Evolution, excitation laser He—Cd $\lambda = 325$ nm, objective 74 CG, spot diameter 2 μm). The excitation with the 325 nm wavelength takes place predominantly in upper 100 nm of the structure. Low excitation density 0.5 W cm$^{-2}$ was used to simulate typical excitation densities required for scintillator applications.

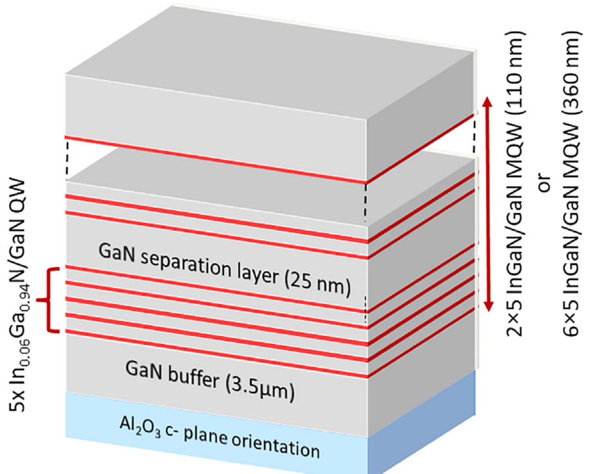


**Figure 1.** Scheme of InGaN/GaN MQW structure.

CL was measured to investigate the spatial differences of luminescence properties at different depths of the QW region. The acceleration voltage of the electrons was 2–15 keV, with the spot size 1 mm$^2$ and emission current 1 μA, kept constant for all acceleration voltages. Luminescence was collected by an optical fiber connected to an ANDOR Shamrock163 monochromator equipped with a 150 gr mm$^{-1}$ grating and coupled with an ANDOR Newton 920 CCD camera.

The AFM topography measurements were performed in QNM semi-contact mode using Dimension Icon AFM. To ensure precise visualization of the pits, we chose to employ conical Aspire CFM tips with high tip aspect ratio and nominal tip radius of ≈8 nm. All results shown were done with horizontal scan direction.

## 3. Results and Discussion

As the active region of structures A and B were designed as scintillator for fast electron microscopy imaging, the main characterization method was CL with the acceleration voltage in the range 2–15 keV. CL spectra of sample A ($2 \times 5$ QWs) and sample B ($6 \times 5$ QWs) can be found in **Figure 2**a and b, respectively.

Both spectra have two main maxima, the blue, QW maximum at 445 nm and a broad defect band at 500–650 nm. Interesting feature of the broad defect band is, that it shifts together with the blue QW luminescence band according to the changes of QW parameters. This phenomenon was observed on more than forty QW samples with different QW parameters. The energy difference of blue and defect bands keeps in the range 380–470 meV. Thus we can attribute both bands to the luminescence of InGaN/GaN QW.

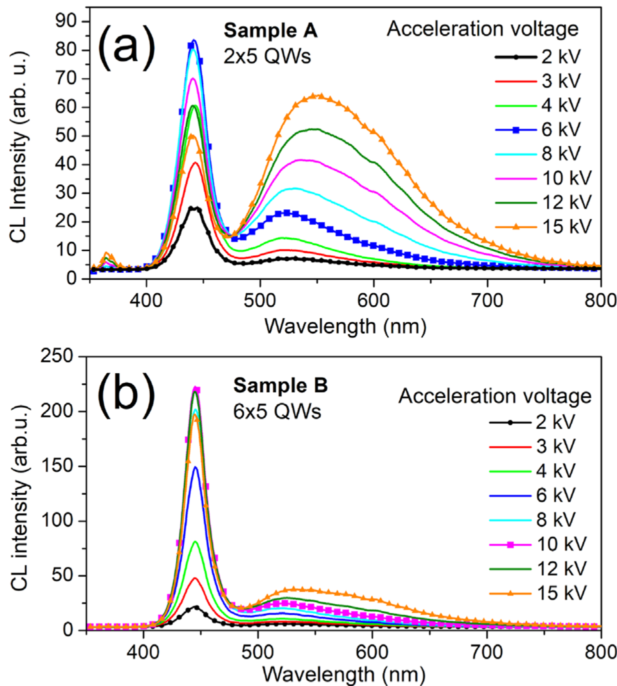


**Figure 2.** CL spectra measured with acceleration voltages 2–15 keV of (a) sample A with $2 \times 5$ QWs and (b) sample B with $6 \times 5$ QWs.

 © 2017 WILEY-VCH Verlag GmbH & Co. KGaA, Weinheim

The broad defect band may belong to transitions between QW states and defect levels in InGaN or GaN barriers.[10]

This defect band has a slow decay time, and therefore need to be suppressed for fast scintillator applications. The increase of long wavelength shoulder at high acceleration voltages is caused by buffer GaN yellow band contribution. A weak peak at 365 nm originating from the GaN buffer layer can be also noticed for higher acceleration voltages, especially for sample A with its thinner active region. The presence of the GaN peak is a sign that the electron beam is penetrating through the active region into the GaN buffer layer. Two main differences can be noticed between the CL of both samples: First, sample A has stronger defect band maximum. Second, the maximal intensity of CL is achieved at lower acceleration voltage in case of sample A.

The reason for the second feature is the different thicknesses of the active layer, 120 nm with 10 QWs and 360 nm with 30 QWs for samples A and B, respectively. Maximal intensities of the QW blue peak of samples A and B as a function of the acceleration voltage are shown in **Figure 3**. Maximal intensities for sample A is achieved at 7 keV incident electron energy, while for sample B it is at 10 keV (shown by arrows in Figure 3).

After reaching these maxima, the CL intensity gradually decreases with increasing acceleration voltage, although the penetration depth (**Figure 4**b) and a total volume in which the electrons interact with the structure is increasing. The reason for this is that the CL originates only in the hatched part of incident region, see Figure 4a.

From the penetration depth calculated according to Ref. [11] for the acceleration voltage at which the CL efficiency starts to decrease and from the thickness of the active region (110 nm and 360 nm for sample A or sample B, respectively), we can estimate the approximate thickness of main CL region shown in Figure 4a. Let us assume the structure A with 10 QWs and the active region starting 110 nm below the sample surface. CL intensity of this structure starts to decrease for acceleration voltages above 7 kV (see Figure 3), so we can suppose that at this voltage the main CL region start to be plunged under the active region and the thickness of the main CL region can be estimated

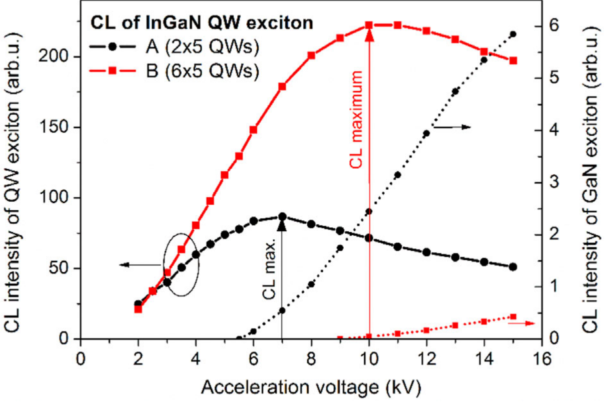


**Figure 3.** CL peak intensity of the QW (solid lines) and GaN buffer exciton (dotted lines) as a function of electron acceleration voltage for samples A and B. Arrows shows the voltage when maximal CL intensity is achieved. Presence of GaN exciton (dotted lines) is a sign of electron penetration under the active region.

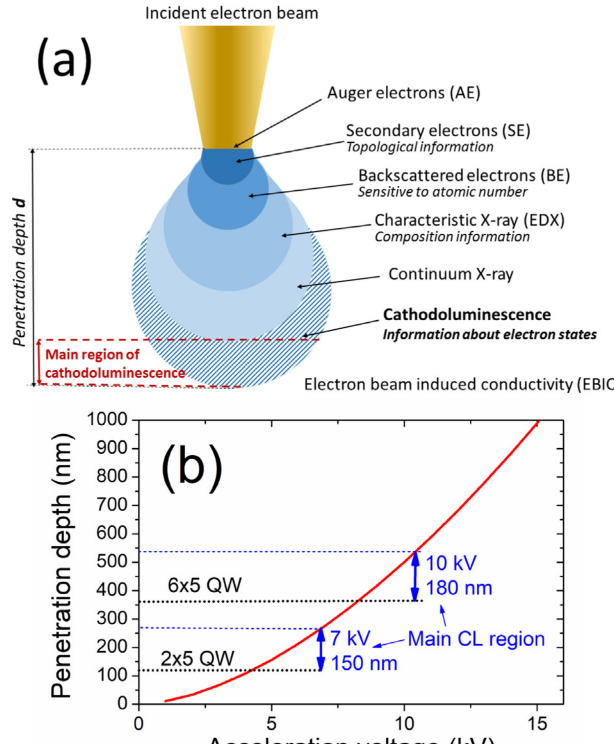


**Figure 4.** a) Scheme of the interaction of the incident electron beam with the structure. The region, where CL originates, is hatched. b) Penetration depth of electrons as a function of acceleration voltage calculated according to Ref. [11]. The active layer thicknesses of sample A with $2 \times 5$ InGaN QWs and sample B with $6 \times 5$ InGaN QWs are shown. With increasing acceleration voltage behind the CL maximum, the main region of CL becomes plunged under the active region and hence the CL efficiency of the structure decreases.

as the difference between the penetration depth at 7 kV and depth of the active region, see Figure 4b. According to this estimation, the main CL region thickness is around 150 nm for electron energy 7 keV and 180 nm for electrons with kinetic energy 10 keV.

With respect to these results, it is important to design scintillator structures in such way that the active region overlaps with the main CL region.

Another important difference between sample A and sample B, which can be noticed in Figure 2a and b is a stronger blue band and weaker defect band maximum for sample B with its higher number of InGaN QWs. The stronger enhancement of the blue maximum with increasing acceleration voltage for sample B is also apparent in Figure 3a. For direct comparison, two CL spectra with the same acceleration voltage are shown in **Figure 5**a. Although the volume of the excited active region is the same, superior CL properties (higher intensity of the blue band and a lower intensity of the defect band) are seen for sample B with higher QW number. This result suggest that the top QW layer of sample B have higher luminescence efficiency than top layers of sample A. The PL with excitation wavelength 325 nm (excitation to approx. 100 nm thick top region from the sample surface) shows even higher enhancement of the blue maximum


© 2017 WILEY-VCH Verlag GmbH & Co. KGaA, Weinheim

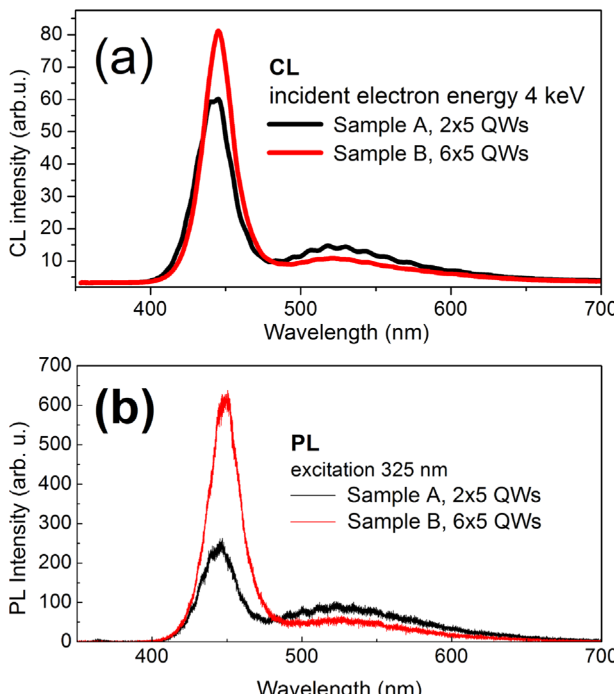


**Figure 5.** Comparison of (a) CL and (b) PL spectra of sample A with $2 \times 5$ InGaN QWs and sample B with $6 \times 5$ InGaN QWs. Excitation wavelength 325 nm to GaN barrier and the excitation power density 0.5 $Wcm^{-2}$ were used. In both types of luminescence, the same volume (only 10 QWs from the active region) should be excited.

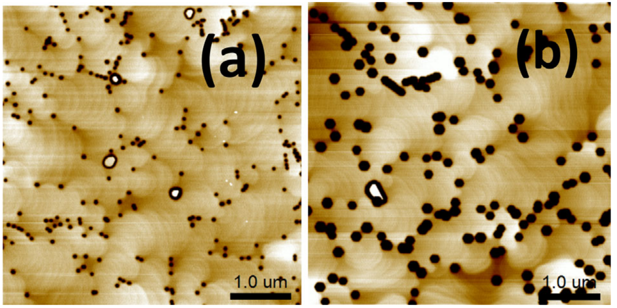


**Figure 6.** AFM surface images of (a) sample A with $2 \times 5$ InGaN QWs and (b) sample B with $6 \times 5$ InGaN QWs.

of sample B in comparison to sample A, however, we cannot exclude that slightly different volumes of the active region are excited in the case of the CL and PL measurements. For both types of luminescence, the blue band luminescence is enhanced and the defect band is lower in the case of higher numbers of QWs. Similar behavior was also observed in Ref. [9], where the deeper part of MQW active region with a lower number of underlying QWs was found to have larger contributions to the defect band luminescence.

Several explanations for PL improvement with increased number of QWs have been suggested such as gradual relaxation in QW region and consequently decreased strain in upper QWs,[12,13] improved crystallographic quality for structures with higher number of QWs in upper part of the active region,[14,15] screening of internal electric field caused by Si doped layer[9] or improved interface roughness caused by Si during the growth of first QW layers.[16] Another possible explanation is suppression of thermionic emission and recapture of carriers in structures with higher number of QWs which was also supported by theoretical model.[17]

Based on our AFM results, we suggest an alternative explanation, which takes into account the different size of V-pits in the structures with different numbers of QWs, as seen in **Figure 6**.

Recently, V-pits have been found to have a positive effect on the InGaN PL properties.[18–20] Several explanations were suggested, one of which is strain relaxation and reduction in QW region. The V-pits may also benefit from hole injection, as holes can transport through V-pits and into the QWs due to the lower polarization field on the side walls.[21,22] However, the most probable reason for PL enhancement by V-pits is the passivation of dislocations, which reduce the non-radiative recombination rate. Our V-pit density $9.6 \cdot 10^8\,cm^{-2}$ is very similar to our dislocation density estimated according to XRD results $9 \times 10^8$–$1 \times 10^9\,cm^{-2}$. This is in agreement with previously reported results which show that V-pits originates on dislocations.[22] The slower growth rate of V-pit sidewalls leads to thinner QWs with less indium content than on the sidewalls. Because of this, the potential of thinner sidewall QWs will be higher than that of *c*-plane QWs, and thus will effectively separate carriers from dislocations situated in the middle of V-pits.[23] This has the effect of not only suppressing the non-radiative recombination on dislocations, but also decreasing the defect band intensity due to the higher concentration of defects near dislocations. This explains why the bigger V-pits of sample B with the average V-pit diameter around 200 nm can more effectively decrease the defect band intensity as was observed on CL and PL results.

## 4. Conclusion

We have studied the luminescence characteristics of the InGaN/GaN multiple quantum well structures with 10 and 30 QWs in the active region. The main characterization method used was CL, but was also supported by other methods, namely PL and AFM.

We have shown that increasing the number of InGaN QWs is an efficient method to improve the luminescence properties of MQW structure. With higher QW number in the structure the intensity of fast blue QW emission is enhanced and luminescence of the QW defect band is suppressed. We explain the luminescence improvement by influence of increased size of V-pits with increased QW number, as the bigger V-pits can more effectively separate carriers from dislocations in the middle of V-pits reducing so non-radiative recombination and luminescence on defects decorating dislocations in their neighborhood. Suppression of non-radiative recombination and defect band luminescence leads to enhancement of blue QW luminescence.

Based on measured dependence of CL intensity on the primary electron energy, the most effective region where CL takes place has an approximate thickness of 180 nm and is buried 360–530 nm under the surface for incident electrons energy 10 keV and thickness 150 nm buried 120–270 nm for


© 2017 WILEY-VCH Verlag GmbH & Co. KGaA, Weinheim

incident electron energy 7 keV. According to these results, it is important to design scintillator structures in such way that the active region is overlapping the main CL region.

## Acknowledgements

The authors acknowledge support from MSMT project no. NPU LO1603–ASTRANIT and by the GACR project no. 16-11769S. Partial support of EC project H2020-TWINN-2015 no. 690599 (ASCIMAT) and by MSMT project no. LM2015087 is also gratefully acknowledged.

## Conflict of Interest

The authors declare no conflict of interest.

## Keywords

cathodoluminescence, GaN, InGaN, quantum wells, scintillators

Received: August 25, 2017
Revised: November 7, 2017
Published online:

[1] P. Pittet, G. N. Lu, J. M. Galvan, J. M. Bluet, I. A. Ismail, J. Y. Giraud, J. Balosso, *Opt. Mater.* **2009**, *31*, 1421.
[2] P. Lecoq, E. Auffray, S. Brunner, H. Hillemanns, P. Jarron, A. Knapitsch, T. Meyer, F. Powolny, *IEEE Trans. Nucl. Sci.* **2010**, *57*, 2411.
[3] S. Gundacker, E. Auffray, B. Frisch, P. Jarron, A. Knapitsch, T. Meyer, M. Pizzichemi, P. Lecoq, *J. Instrum.* **2013**, *8*, P07014.
[4] A. Hospodková, M. Nikl, O. Pacherová, J. Oswald, P. Brůža, D. Pánek, B. Foltynski, E. Hulicius, A. Beitlerová, M. Heuken, *Nanotechnology* **2014**, *25*, 455501.
[5] G. Balakrishnan, *Nanotechnology* **2015**, *26*, 090501.
[6] T. J. Badcock, M. Ali, T. Zhu, M. Pristovsek, R. A. Oliver, A. J. Shields, *Appl. Phys. Lett.* **2016**, *109*, 151110.
[7] S. Nakamura, M. Senoh, N. Iwasa, S. Nagahama, *Jpn. J. Appl. Phys.* **1995**, *34*, L797.
[8] G. Pozina, J. P. Bergman, B. Monemar, T. Takeuchi, H. Amano, I. Akasaki, *J. Appl. Phys.* **2000**, *88*, 2677.
[9] T. Hubácek, A. Hospodková, J. Oswald, K. Kuldová, J. Pangrác, *J. Cryst. Growth* **2017**, *464*, 221.
[10] A. Hospodková, J. Oswald, M. Zíková, J. Pangrác, K. Kuldová, K. Blažek, G. Ledoux, C. Dujardin, M. Nikl, *J. Appl. Phys.* **2017**, *121*, 214505.
[11] O. Kurniawan, V. K. S. Ong, *Scanning* **2007**, *29*, 280.
[12] N. Nanhui, W. Huaibing, L. Jianping, L. Naixin, X. Yanhui, H. Jun, D. Jun, S. Guangdi, *Solid-State Electron.* **2007**, *51*, 860.
[13] M. J. Davies, F. C. -P. Massabuau, P. Dawson, R. A. Oliver, M. J. Kappers, C. J. Humphreys, *Phys. Status Solidi C* **2014**, *11C*, 710.
[14] S. J. Leem, Y. C. Shin, K. C. Kim, E. H. Kim, Y. M. Sung, Y. Moon, S. M. Hwang, T. G. Kim, *J. Cryst. Growth* **2008**, *311*, 103.
[15] Q. Mu, M. Xu, X. Wang, Q. Wang, Y. Lv, Z. Feng, X. Xu, Z. Ji, *Physica E* **2016**, *76E*, 1.
[16] C. Sasaoka, F. Miyasaka, T. Koi, M. Kobayashi, Y. Murase, Y. Ando, A. A. Yamaguchi, *Jpn. J. Appl. Phys.* **2013**, *52*, 115601.
[17] P. Hurst, P. Dawson, S. A. Levetas, M. J. Godfrey, I. M. Watson, G. Duggan, *Phys. Status Solidi B* **2001**, *228B*, 137.
[18] K. Sugimoto, Y. Denpo, N. Okada, K. Tadatomo, *Phys. Status Solidi C* **2016**, *13C*, 270.
[19] X. Wu, J. Liu, Z. Quan, Ch. Xiong, Ch. Zheng, J. Zhang, Q. Mao, F. Jiang, *Appl. Phys. Lett.* **2014**, *104*, 221101.
[20] Z. J. Quan, L. Wang, C. D. Zheng, J. L. Liu, F. Y. Jiang, *J. Appl. Phys.* **2014**, *116*, 183107.
[21] Y. Li, F. Yun, X. Su, S. Liu, W. Ding, X. Hou, *J. Appl. Phys.* **2014**, *116*, 123101.
[22] X. Wu, J. Liu, F. Jiang, *J. Appl. Phys.* **2015**, *118*, 164504.
[23] A. Hangleiter, F. Hitzel, C. Netzel, D. Fuhrmann, U. Rossow, G. Ade, P. Hinze, *Phys. Rev. Lett.* **2005**, *95*, 127402.

 © 2017 WILEY-VCH Verlag GmbH & Co. KGaA, Weinheim

## 4.6 Advancement toward ultra-thick and bright InGaN/GaN structures with a high number of QWs [vi]

In this article, we have studied structures with QWs number up to 70 QWs. Scintillation structures need to have thick active region (more than 1 μm) and we have studied the effect of higher QW number on the luminescence properties. The structure with 70 QWs had almost 800 nm thick active region which is up to now the highest reported QW number in the nitride community. PL intensity increased with higher QW number (as was observed in previous article) but for sample above 50 QWs the PL intensity started to decrease. This decrease was attributed to too big V-pits (strong V-pits coalescence and increase of non-radiative recombination). The best diameter of V-pits was found 200 – 300 nm (sample with 40 QWs). The decay time of the structures was measured as well and it was shown that structures had the fast excitonic band with the decay time from 0.25 ns (for sample with 10 QWs) to 1.1 ns (for sample with 60 QWs). In conclusion, we have reported InGaN/GaN structures with the highest QW number and active region thickness, but for reaching 1 μm thick active region we cannot increase only number of QWs because V-pits of the high QW number structures are too big, but we will have to find a way how to control V-pits size. The paper was published in CrystEngComm (IF = 3.38, Q1, 2 citation).

Published on 26 November 2018. Downloaded by Institute of Physics of the Czech Academy of Sciences on 10/18/2019 6:33:26 AM.

CrystEngComm

PAPER

View Article Online
View Journal | View Issue

Cite this: CrystEngComm, 2019, 21, 356

# Advancement toward ultra-thick and bright InGaN/GaN structures with a high number of QWs†

Tomáš Hubáček, *[ab] Alice Hospodková,[a] Karla Kuldová, [a] Jiří Oswald,[a] Jiří Pangrác,[a] Vitězslav Jarý,[a] Filip Dominec,[a] Markéta Slavická Zíková,[a] František Hájek,[a] Eduard Hulicius,[a] Alexej Vetushka,[a] Gilles Ledoux,[c] Christophe Dujardin [c] and Martin Nikl[a]

InGaN/GaN multiple quantum well structures are studied as potential candidates for superfast scintillation detectors and show the leading decay time of around 1 ns and intense luminescence. Photoluminescence properties of these structures with quantum well (QW) numbers ranging from 10 to 60 are described and discussed. It is shown that with increased QW number, the luminescence efficiency of the whole structure increases due to the V-pits of a sufficient size suppressing non-radiative recombination. Suppression of the non-radiative recombination near dislocations is demonstrated by the cathodoluminescence measured at different acceleration voltages. The optimal V-pit size is found to be in the range from 200 to 300 nm, which is obtained for structures with 40 QWs. On the other hand, when the V-pit size exceeds the optimal value, the PL intensity decreases by strong V-pit coalescence, which is observed for structures with 60 QWs. For further increasing the active region thickness, which helps to enhance the detection efficiency of high-energy irradiation, it is necessary to find a way to control the V-pit size. Excitation–emission maps are measured to elucidate how efficiently the structures are excited depending on the light wavelength and the QW number. It is shown that the wavelength for most efficient excitations of InGaN/GaN QWs is 362 nm. With increasing number of QWs, their fast excitonic luminescence is considerably enhanced, whereas slow defect band luminescence is suppressed. Time-resolved measurements with soft X-ray excitation also support our conclusions, showing suppressed non-radiative recombination for structures with higher QW numbers. The fastest decay component increases from 0.25 ns for a structure with 10 QWs to 1.1 ns for a structure with 60 QWs.

Received 25th October 2018,
Accepted 26th November 2018

DOI: 10.1039/c8ce01830h

rsc.li/crystengcomm

## 1. Introduction

Nitride semiconductor heterostructures are widely used for light-emitting and laser diodes (LEDs and LDs) as well as for high-power and high-frequency applications. Recently, new applications for InGaN/GaN multiple quantum well (MQW) heterostructures have emerged.[1,2] It is shown that these heterostructures, if properly designed, can work as very efficient fast scintillators with long lifetime due to their radiation resistance. Although this application does not have a huge market compared to LEDs, LDs or high-electron-mobility transistors (HEMTs), there is still very high demand for fast scintillators and detectors of ionizing radiation due to the expansion of new diagnostic methods in medicine, electron microscopy and nuclear physics.[3,4] There is a particular lack of fast scintillators with short decay times in the order of few nanoseconds.[5] Although InGaN/GaN MQW heterostructures have been intensively studied for several decades, this new application with different requirements needs completely different design of the heterostructure, which opens new problems that have not been solved yet. The first problem is low excitation intensity. For LED structures, high level of excitation causes a problem with non-radiative Auger recombination;[6,7] in the case of scintillators, the opposite problem with extremely low intensity of excitation has to be solved. Under such conditions, the excitonic QW luminescence can have even lower intensity than different kinds of defect bands originating either in GaN (yellow band) or in InGaN QWs. These defect bands are usually not observed under high intensity of excitation due to their saturation.[8,9] Since they have slow

[a] Institute of Physics CAS, v.v.i., Cukrovarnická 10, CZ-16200, Prague 6, Czech Republic. E-mail: hubacekt@fzu.cz
[b] Faculty of Mechatronics, Informatics and Interdisciplinary Studies, Technical University of Liberec, Studentská 2, CZ-46117, Liberec, Czech Republic
[c] Institut Lumière Matière, UMR55306 Université Claude Bernard, Lyon 1-CNRS, France

† Electronic supplementary information (ESI) available. See DOI: 10.1039/c8ce01830h



This journal is © The Royal Society of Chemistry 2019

Published on 26 November 2018. Downloaded by Institute of Physics of the Czech Academy of Sciences on 10/18/2019 6:33:26 AM.

decay in the microsecond time scale, they are detrimental for fast scintillator applications.[1]

Another challenge for scintillator structure design is the demand for thick active regions with a higher number of QWs compared to that for LED structures due to the high penetration depth of ionizing radiation. For some applications, the active region is required to be thicker than 1 μm. Since no other application needs such thick active regions, the highest reported QW number to date is thirty.[10–12] Herein, we report results obtained on QW structures with different thicknesses of the active region ranging from 110 nm for structures with 10 QWs to 800 nm for structures containing 70 QWs. We will discuss the consequences of thick active regions such as the formation of huge V-pits, their influence on PL properties and possibilities to control their size. The effect of the QW number on the decay time will be shown.

## 2. Experimental

Structures were prepared on the Aixtron 3 × 2 CCS MOVPE system equipped with LayTec EpiCurveTT apparatus for *in situ* measurement of reflectivity, curvature and true wafer temperature. Buffer layers were grown with trimethylgallium (TMGa) and ammonia ($NH_3$) precursors with a hydrogen carrier gas. The MQW region was prepared from triethylgallium (TEGa), trimethylindium (TMIn) and ammonia precursors with a nitrogen carrier gas. Structures were grown on sapphire substrates with standard *c*-plane orientation. A low-temperature GaN nucleation layer was grown at 550 °C at the reactor pressure of 600 mbar. Subsequently, 3 μm-thick GaN buffer was grown. More details about growth parameters of GaN buffer layer are described in our previous publication.[13] Before the growth of the MQW active region, a 1 μm-thick GaN layer doped with silicon was added (target doping $1 \times 10^{18}$ $cm^{-3}$). The MQW active region consisted of 10 to 70 QWs (In content close to 5%) separated by GaN quantum barriers (QB). The thicknesses of QW and QB were around 1.5 nm and 5 nm, respectively. After each stack of five QWs and QBs, 25 nm-thick GaN separation layer with the same growth temperature as for QB was grown to decrease the strain energy in the structure and prevent the misfit dislocation generation. The whole structure was always capped with a 12 nm-thick GaN layer to isolate QWs from the surface states.

Photoluminescence (PL) spectra were measured at RT at two different excitation wavelengths. For 325 nm excitation wavelength, a confocal microscope (LabRAM HR Evolution, He–Cd laser, objective 74 CG, spot diameter 2 μm) was used. For 375 nm excitation wavelength, a semiconductor laser LD-375 was used and the detection was done using a combination of a double monochromator SDL-1 and a GaAs photomultiplier tube.

The excitation–emission map measurements were performed on a homemade apparatus. The sample was illuminated by an EQ99X laser driven xenon lamp filtered by a Jobin Yvon Gemini 180 monochromator. The exit slit from the monochromator was then reimaged on the sample by two 100 mm focal length two-inch diameter $MgF_2$ lenses. The whole apparatus was calibrated by means of a Newport 918D Low power calibrated photodiode sensor over the range of 190–1000 nm with the resolution of the system being 4 nm. The emitted light from the sample was collected by an optical fibre connected to a Jobin-Yvon TRIAX320 monochromator equipped with a cooled CCD detector. At the entrance of the monochromator, different long pass filters can be chosen to eliminate the excitation light. The resolution of the detection system is 2 nm.

Atomic force microscopy (AFM) images were taken by Dimension Icon AFM in semicontact mode using ASPIRE tips.

Panchromatic cathodoluminescence images were recorded by a custom setup with Hamamatsu photomultiplier tube H7711-13 attached to Philips/FEI XL30 scanning electron microscope, where SEM images were also taken.

Time-resolved radioluminescence (TRRL) was measured with soft X-ray pulses generated by a picosecond pulsed laser from Hamamatsu (illuminating the photocathode of X-ray tube) with pulse duration of 51 ps and emission at 379 nm. Detection was done by a PicoHarp 300 multichannel analyzer connected to a PMA 182 photomultiplier from PicoQuant. We used 10 nm bandpass filters to obtain response only from the excitonic band.

## 3. Results and discussion

We have verified our structures *via* X-ray diffraction (XRD) measurements, which confirmed that no relaxation occurred even in structures with the highest QW number. All structures are compressively strained with respect to the GaN buffer layer. XRD data of sample with 70 QWs are available in ESI.†

To establish the relation between the luminescence properties and the number of QWs, PL results of structures at two different excitation wavelengths (375 nm and 325 nm) have been obtained.

The excitation at 375 nm corresponds to energy below the GaN band gap and above the QW band gap. It thus penetrates deeply into the structure and we can obtain PL from all QWs similar to the case of excitation by ionizing radiation. Under this excitation, increased excitonic luminescence intensity without any saturation with QW number is observed (Fig. 1(b)). The results reported by other groups usually show decreased QW PL efficiency for QW number higher than ten. Herein, we report increased QW excitonic luminescence with the number of QWs up to 60. This demonstrates the properly designed structure parameters and technology. Contrary to the excitonic QW luminescence band intensity, the defect band (at 490 nm) intensity remains unaffected by the QW number, suggesting that the total number of defects leading to 490 nm band do not depend on the active region thickness. This further suggests that the defect band originates only in some part of the active region, most likely in the upper or in the bottom one.

Published on 26 November 2018. Downloaded by Institute of Physics of the Czech Academy of Sciences on 10/18/2019 6:33:26 AM.

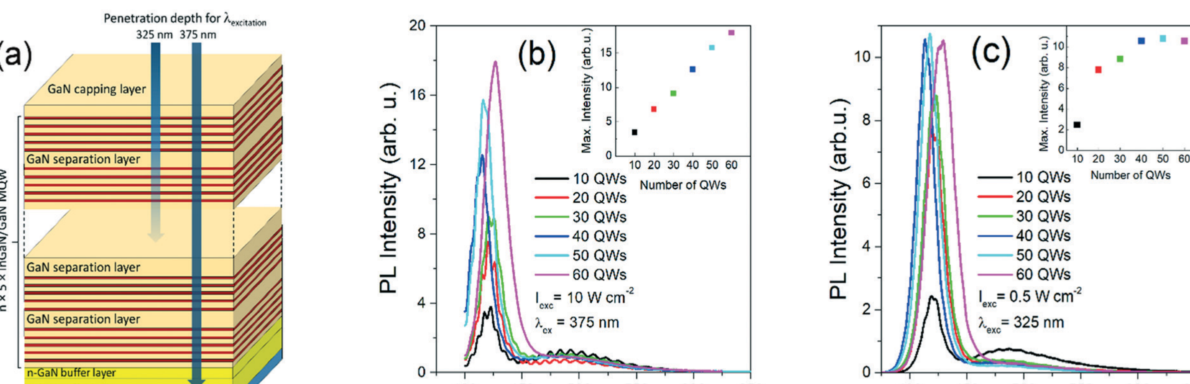


**Fig. 1** (a) A schematic drawing of the InGaN/GaN heterostructure. (b) PL results of structures with different QW numbers at 375 nm excitation (all QWs are excited) and (c) at 325 nm excitation (PL from 10 topmost QWs).

To identify the dominant region of the defect band luminescence, PL with excitation at 325 nm was measured. The light with the wavelength of 325 nm has energy above GaN band gap. It is thus highly absorbed in the structure. Approximately 90% of the excitation beam is absorbed in first 100 nm corresponding to about 10 topmost QWs. According to the results shown in Fig. 1(c), the defect band maximum is significantly suppressed for a structure with 20 QWs, which suggests that the defect band dominantly originates in few deepest QWs. Moreover, the excitonic maximum intensity of topmost 10 QWs is dependent on the QW number in the structure. It increases up to the structure with 40 QWs. This suggests that underlying QWs enhance the luminescence intensity of 10 topmost QWs. For samples with 60 QWs, the luminescence intensity starts to decrease. A similar increase in the PL intensity with underlying QWs or InGaN/GaN superlattice has been reported in previous research; it is ascribed by authors to decrease in the strain in QWs,[14–16] enhanced incorporation of nonradiative defects in InGaN prelayers[17,18] or enhanced formation of V-pits, which are formed around dislocations with a screw component.[19–21] The TEM image of V-pits formed around dislocations in a structure with 10 QWs is shown in Fig. 2.

V-pits help to keep electron–hole pairs in InGaN QW separated from the non-radiative centres around threading dislocations. The reason is a thinner InGaN QW on the V-pit walls, which represents a barrier with respect to the flat region of a thicker InGaN QW between V-pits.[19,22] The evidence that V-pits help to increase luminescence efficiency is demonstrated in Fig. 3. SEM image of a surface with V-pits for the structure with 60 QWs is shown in Fig. 3(a). Panchromatic cathodoluminescence (CL) from the InGaN/GaN MQW region measured for acceleration voltage of 5 kV is shown in Fig. 3(b). To understand the CL image, we have to consider that it gives us information about the location of carrier generation and not about the place of radiative recombination. The lighter spots in Fig. 3(b), which correspond to the dark V-pits in SEM image (see Fig. 3(a) demonstrate that even carriers generated in the vicinity of dislocations do not recombine non-radiatively and are effectively separated from the dislocations. The origin of the lighter contrast's spots is probably due to more efficient carrier generation in the V-pit region. This can be caused by semipolar orientation of QWs with better electron–hole overlap or by excitation of higher number of thinner QWs with thinner barriers in V-pits in the case of incident electrons with energy of 5 keV. Since we did not observe any change in the PL wavelength, we suppose that the carriers generated in V-pits escape rapidly from them and recombine in the thicker flat InGaN/GaN QWs. On the other hand, when the acceleration voltage is increased to 25 keV (Fig. 3(c)), CL originates dominantly from the GaN buffer below InGaN/GaN MQW region; here, without any V-pit protection, the non-radiative recombination of carriers near dislocations can be clearly observed as dark spots.

According to our AFM results, V-pits' diameter and depth increase for higher number of QWs (Fig. 4 and 5). The V-pit density is around $8 \times 10^8$ cm$^{-2}$ for all samples, which corresponds to the density of dislocations with a screw component. The V-pit profiles measured by AFM for our structures

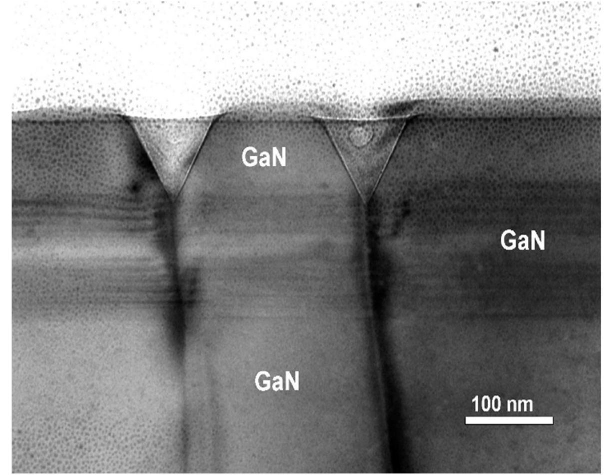


**Fig. 2** Bright field XTEM image ($g$ = 0002) of V-pits formed around dislocations in the structure with 10 QWs.



This journal is © The Royal Society of Chemistry 2019

Published on 26 November 2018. Downloaded by Institute of Physics of the Czech Academy of Sciences on 10/18/2019 6:33:26 AM.

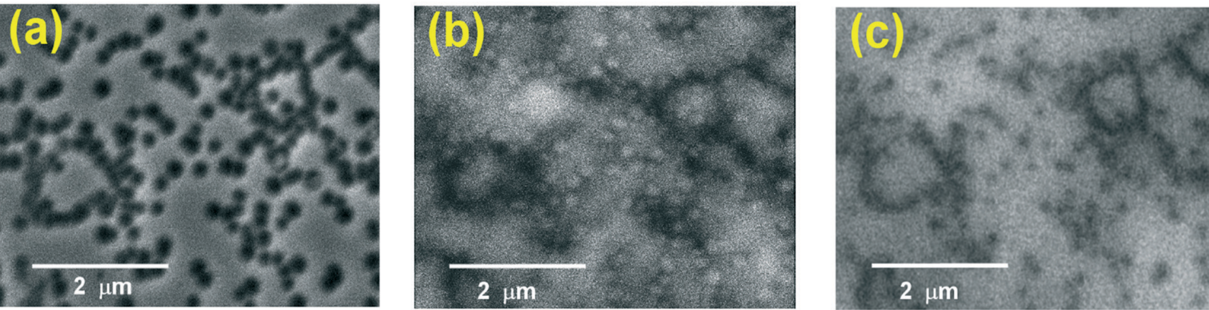


**Fig. 3** Same area of sample with 60 QWs investigated by (a) SEM, (b) CL measured for acceleration voltage of 5 keV and (c) CL measured for acceleration voltage of 25 keV.

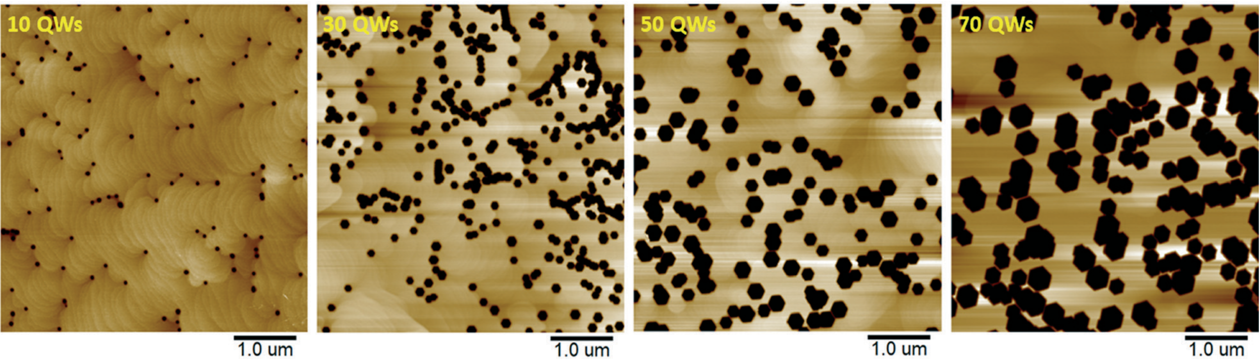


**Fig. 4** AFM images of surface of samples with different QW numbers – the higher the QW number, the larger the size of the V-pits.

are shown in Fig. 5. The most efficient luminescence of upper 10 QWs (Fig. 1(c)) is achieved for structures with 40 and 50 QWs, which have the V-pit surface radius in the range from 200 to 300 nm, as shown in Fig. 5. According to these results, we suppose that the region with increased concentration of non-radiative centres around dislocations with a screw component has a diameter of approximately 250 nm. Our results are in agreement with similar optimal V-pit size with radius of 200–250 nm, which has been already reported.[23–25] However, decrease in the luminescence intensity for structures with 60 QWs (Fig. 1(c)) is observed. The decrease in the luminescence intensity of upper QWs is probably caused by very big V-pits, which can reduce the flat, efficiently luminescent area of QWs between V-pits, as shown in the AFM results in Fig. 4. The area covered by V-pits is 32% of the whole surface for the sample with 70 QWs. Another reason for the decreased PL intensity can be strong V-pit coalescence for structures with 60 and 70 QWs, which is observed to strongly suppress the luminescence, as shown in the CL image in Fig. 3(b). According to these results, very large V-pits can be detrimental for efficient luminescence. This indicates that increasing the active region thickness while preserving the luminescence efficiency requires control of the V-pit size.

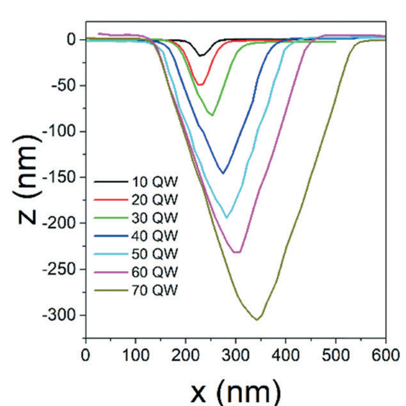


**Fig. 5** Depth profiles of the V-pits measured by AFM.

We measured the excitation–emission maps for samples with different QW numbers to elucidate the mechanism of excitation using different wavelengths. Excitation–emission maps of two samples with 10 and 60 QWs are shown in Fig. 6. Two distinct QW luminescence bands can be observed: the excitonic and defect bands. A yellow defect band originating in GaN buffer beneath the MQW region is also visible in the maps with the most effective excitation at 367 nm. The excitation intensity is very low for this measurement (excitation by xenon lamp); consequently, the QW defect band at 490 nm is much stronger and excitonic QW maximum is weaker when compared to the results shown in Fig. 1. Decreased excitonic/defect band intensity ratio with decreased intensity of excitation is also reported.[1] It can be noted that QW luminescence is strongly enhanced when the photon energy is above the GaN band gap. Direct excitation into

Published on 26 November 2018. Downloaded by Institute of Physics of the Czech Academy of Sciences on 10/18/2019 6:33:26 AM.

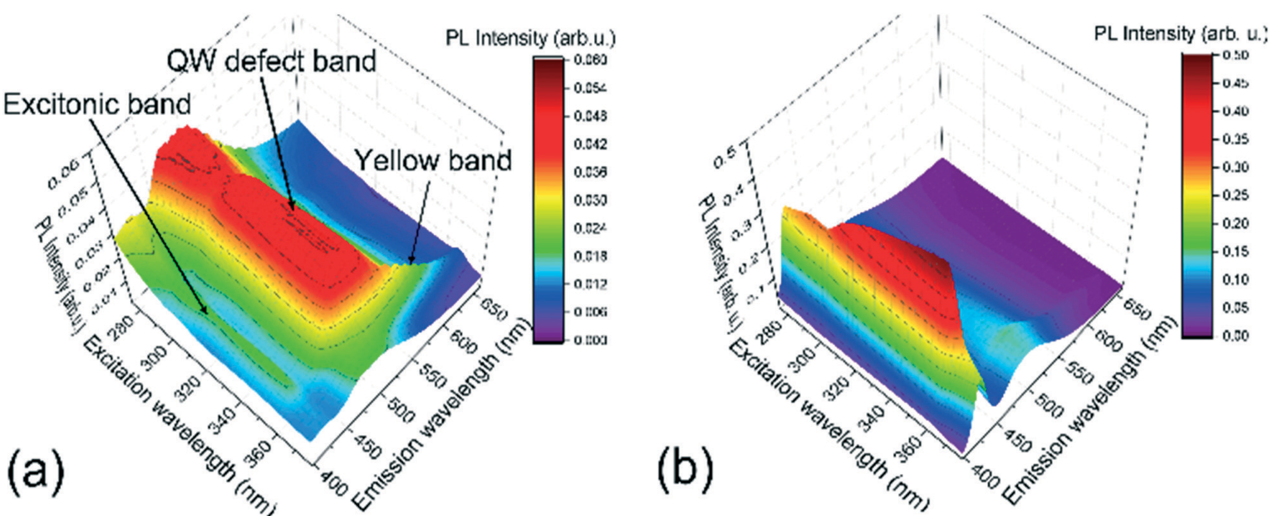


**Fig. 6** Excitation–emission maps of samples with (a) 10 QWs and (b) 60 QWs.

InGaN QWs (below GaN band gap) is much less effective. Excitonic band intensity increases with decreased photon energy and achieves its maximum for excitation by 3.42 eV (362 nm) for 60 QWs. Then, the luminescence intensity slowly decreases probably due to the lower thickness of the excited region. Even this measurement confirms significant increase in the luminescence of upper 10 QWs for samples with higher number of QWs in the active region, whereas the defect band intensity is suppressed.

For fast scintillation applications, the decay time is one of the most important parameters. Therefore, time-resolved soft X-ray excited radioluminescence decays of our structures at room temperature were measured. We observed an increase in the leading decay time value with higher number of QWs (Fig. 7); also, the deepest QWs of the structure exhibited lower quality, which is in accordance with the PL measurement. The structure with 10 QWs had the shortest decay time component of 0.25 ns from all the samples, which is caused by the non-radiative recombination in the deepest QWs (with the worst quality) and by surface states (few topmost QWs). This effect is strongly suppressed for structures with higher QW numbers. Similar phenomenon was observed[26,27] but with lower number of QWs (up to 15). According to these time-resolved results and in agreement with the PL measurement, we conclude that the deepest QWs of the structure have low quality.

We have concluded that the non-radiative recombination on dislocations is already effectively suppressed in upper QWs for the structure with 40 QWs due to sufficient size of the V-pits. Time-resolved measurements suggest that the non-radiative recombination decreases even for structures with higher QW numbers. The decay time of 1.1 ns is obtained for the structure with 60 QWs. In the case of soft X-ray excitation, the whole QW region is excited. In such a case, the number of QWs with suppressed non-radiative recombination increases with increasing QW number, resulting in a longer decay time.

The radiative recombination probability is not influenced only by the non-radiative recombination. Other effects must be considered such as fluctuation of indium concentration and QW width. This QW inhomogeneity influences the radiative recombination process as well.[28] Increased QW

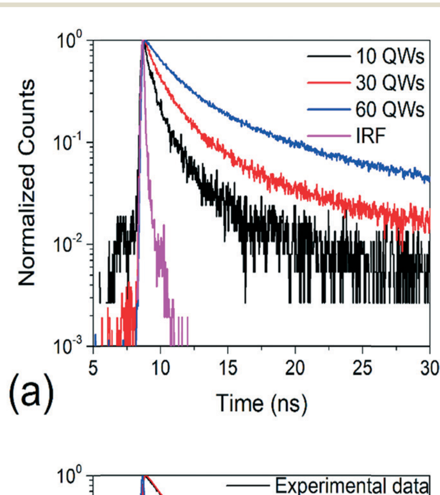


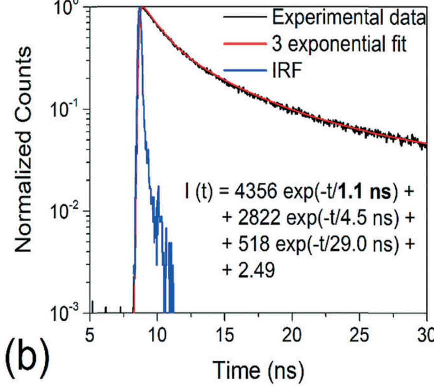


**Fig. 7** Time-resolved soft X-ray radioluminescence data of (a) samples with 10, 30 and 60 QWs and (b) sample with 60 QWs with three-exponential fit of decay time. 10 nm bandpass filters were used to get response only from the excitonic band.

 This journal is © The Royal Society of Chemistry 2019

Published on 26 November 2018. Downloaded by Institute of Physics of the Czech Academy of Sciences on 10/18/2019 6:33:26 AM.

inhomogeneity cannot be excluded for samples with higher QW numbers and may also play a role in the increase in decay time.

## 4. Conclusions

We have prepared InGaN/GaN MQW structures with the highest QW number reported so far in the literature. We have shown that with increased QW number, the luminescence efficiency of the whole structure increases when all QWs are excited. The reason for the increased luminescence efficiency is the sufficient size of the V-pits in structures with higher QW number suppressing non-radiative recombination. It has already been achieved for the growth of 40 QWs in our case (approximately 450 nm-thick active region). Suppression of the non-radiative recombination near dislocations with the help of V-pits was proved by CL measurements at different acceleration voltages.

On the other hand, we have shown that the V-pit size above the optimal value can decrease the PL intensity by strong V-pit coalescence, which was observed for structures with 60 and 70 QWs. According to these results, very big V-pits can also be detrimental for efficient luminescence. To further increase the active region thickness, it is necessary to find a way to control the V-pit size.

From the excitation–emission map measurements, we have shown that 362 nm is the most effective wavelength for InGaN/GaN QW excitation. Additionally, according to these measurements, the defect band originates dominantly in the deepest QWs in the structure. With increasing QW number, the QW excitonic luminescence is considerably enhanced, whereas defect band luminescence is suppressed.

Time-resolved measurements with soft X-ray excitation also support our conclusion as for the suppressed non-radiative luminescence for structures with higher QW numbers. The leading decay time increased from 0.25 ns for the structure with 10 QWs up to 1.1 ns for the structure with 60 QWs.

## Conflicts of interest

There are no conflicts to declare.

## Acknowledgements

The authors acknowledge the support of the GACR project no. 16-11769S and MSMT project no. NPU LO1603 – ASTRANIT, OPPK project LABONIT CZ.2.16/3.1.00/21560. Partial support of EC project H2020-TWINN-2015 no. 690599 (ASCIMAT) and Student Grant Competition of Technical University of Liberec is also gratefully acknowledged. The authors acknowledge Professor Philomela Komninou from Aristotle University of Thessaloniki for HRTEM measurements.

## References

1 A. Hospodková, M. Nikl, O. Pacherová, J. Oswald, P. Brůža, D. Pánek, B. Foltynski, E. Hulicius, A. Beitlerová and M. Heuken, InGaN/GaN multiple quantum well for fast scintillation application: radioluminescence and photoluminescence study, *Nanotechnology*, 2014, **25**, 455501.
2 A. Hospodková, J. Oswald, M. Zíková, J. Pangrác, K. Kuldová, K. Blažek, G. Ledoux, C. Dujardin and M. Nikl, On the correlations between the excitonic luminescence efficiency and the QW numbers in multiple InGaN/GaN QW structure, *J. Appl. Phys.*, 2017, **121**, 214505.
3 P. Lecoq, E. Auffray, S. Brunner, H. Hillemanns, P. Jarron, A. Knapitsch, T. Meyer and F. Powolny, Factors Influencing Time Resolution of Scintillators and Ways to Improve Them, *IEEE Trans. Nucl. Sci.*, 2010, **57**, 2411–2416.
4 P. Lecoq, Development of new scintillators for medical applications, *Nucl. Instrum. Methods Phys. Res., Sect. A*, 2016, **809**, 130–139.
5 C. Dujardin, E. Auffray, E. Bourret-Courchesne, P. Dorenbos, P. Lecoq, M. Nikl, A. N. Vasil'ev, A. Yoshikawa and R.-Y. Zhu, Needs, Trends, and Advances in Inorganic Scintillators, *IEEE Trans. Nucl. Sci.*, 2018, **65**, 1977–1997.
6 A. E. Chernyakov, M. M. Sobolev, V. V. Ratnikov, N. M. Shmidt and E. B. Yakimov, Nonradiative recombination dynamics in InGaN/GaN LED defect system, *Superlattices Microstruct.*, 2009, **45**, 301–307.
7 E. Kioupakis, Q. Yan and Ch. Van de Walle, Interplay of polarization fields and Auger recombination in the efficiency droop of nitride light-emitting diodes, *Appl. Phys. Lett.*, 2012, **101**, 231107.
8 W. Grieshaber, E. F. Schubert, I. D. Goepfert, R. F. Karlicek Jr., M. J. Schurman and C. Tran, Competition between band gap and yellow luminescence in GaN and its relevance for optoelectronic devices, *J. Appl. Phys.*, 1996, **80**, 4615–4620.
9 M. A. Reshchikov and R. Y. Korotkov, Analysis of the temperature and excitation intensity dependencies of photoluminescence in undoped GaN films, *Phys. Rev. B: Condens. Matter Mater. Phys.*, 2001, **64**, 115205.
10 J. Yang, D. G. Zhao, D. S. Jiang, P. Chen, Z. S. Liu, L. C. Le, X. G. He, X. J. Li and H. Yang, Effects of quantum well number on spectral response of InGaN/GaN multiple quantum well solar cells, *Phys. Status Solidi A*, 2014, **211**, 2157–2160.
11 R. M. Farell, C. J. Neufeld, S. C. Cruz, J. R. Lang, M. Iza, S. Keller, S. Nakamura, S. P. DenBaars, U. K. Mishra and J. S. Speck, High quantum efficiency InGaN/GaN multiple quantum well solar cells with spectral response extending out to 520 nm, *Appl. Phys. Lett.*, 2011, **98**, 201107.
12 Z. Chen, X. Zheng, Z. Li, P. Wang, X. Rong, T. Wang, X. Yang, F. Xu, Z. Qin, W. Ge, B. Shen and X. Wang, Positive temperature coefficient of photovoltaic efficiency in solar cells based on InGaN/GaN MQWs, *Appl. Phys. Lett.*, 2016, **109**, 062104.
13 T. Hubáček, A. Hospodková, J. Oswald, K. Kuldová and J. Pangrác, Improvement of luminescence properties of GaN buffer layer for fast nitride scintillator structures, *J. Cryst. Growth*, 2017, **464**, 221–225.
14 N. Nanhui, W. Huaibing, L. Jianping, L. Naixin, X. Yanhui, H. Jun, D. Jun and S. Guangdi, Enhanced luminescence of

Published on 26 November 2018. Downloaded by Institute of Physics of the Czech Academy of Sciences on 10/18/2019 6:33:26 AM.

InGaN/GaN multiple quantum wells by strain reduction, *Solid-State Electron.*, 2007, **51**, 860–864.

15 S. J. Leem, Y. C. Shin, K. C. Kim, E. H. Kim, Y. M. Sung, Y. Moon, S. M. Hwang and T. G. Kim, The effect of the low-mole InGaN structure and InGaN/GaN strained layer super lattices on optical performance of multiple quantum well active layers, *J. Cryst. Growth*, 2008, **311**, 103–106.

16 Q. Mu, M. Xu, X. Wang, Q. Wang, Y. Lv, Z. Feng, X. Xu and Z. Ji, Influence of the InGaN/GaN quasi-superlattice underlying layer on photoluminescence in InGaN/GaN multiple quantum wells, *Phys. E*, 2016, **76**, 1–5.

17 C. Haller, J.-F. Carlin, G. Jacopin, D. Martin, R. Butté and N. Grandjean, Burying non-radiative defects in InGaN underlayer to increase InGaN/GaN quantum well efficiency, *Appl. Phys. Lett.*, 2017, **111**, 262101.

18 C. Haller, J.-F. Carlin, G. Jacopin, W. Liu, D. Martin, R. Butté and N. Grandjean, GaN surface as the source of non-radiative defects in InGaN/GaN quantum wells, *Appl. Phys. Lett.*, 2018, **113**, 111106.

19 A. Hangleiter, F. Hitzel, C. Netzel, D. Fuhrmann, U. Rossow, G. Ade and P. Hinze, Suppression of nonradiative recombination by V-shaped pits in GaInN/GaN quantum wells produces a large increase in the light emission efficiency, *Phys. Rev. Lett.*, 2005, **95**, 127402.

20 K. Sugimoto, Y. Denpo, N. Okada and K. Tadatomo, Effect of superlattices on light output power of InGaN-based light-emitting diodes fabricated on underlying GaN substrates with different dislocation densities, *Phys. Status Solidi C*, 2016, **13**, 207–273.

21 M. J. Davies, F. C.-P. Massabuau, P. Dawson, R. A. Oliver, M. J. Kappers and C. J. Humphreys, Effects of an InGaN prelayer on the properties of InGaN/GaN quantum well structures, *Phys. Status Solidi C*, 2014, **11**, 710–713.

22 Z. L. Fang, Y. X. Lin and J. Y. Kang, InGaN/GaN quantum wells on self-organized faceted GaN islands: Growth and luminescence studies, *Appl. Phys. Lett.*, 2011, **98**, 061911.

23 D. Won, X. Weng and J. M. Redwing, Effect of indium surfactant on stress relaxation by V-defect formation in GaN epilayers grown by metalorganic chemical vapor deposition, *J. Appl. Phys.*, 2010, **108**, 093511.

24 S. L. Rhode, W. Y. Fu, M. A. Moram, F. C.-P. Massabuau, M. J. Kappers, C. McAleese, F. Oehler, C. J. Humphreys, R. O. Dusane and S.-L. Sahonta, Structure and strain relaxation effects of defects in $In_xGa_{1-x}N$ epilayers, *J. Appl. Phys.*, 2014, **116**, 103513.

25 Ch.-Y. Chang, H. Li, Y.-T. Shih and T.-Ch. Lu, Manipulation of nanoscale V-pits to optimize internal quantum efficiency of InGaN multiple quantum wells, *Appl. Phys. Lett.*, 2015, **106**, 091104.

26 M. S. Minsky, S. B. Fleischer, A. C. Abare, J. E. Bowers and E. L. Hu, Characterization of high-quality InGaN/GaN multiquantum wells with time-resolved photoluminescence, *Appl. Phys. Lett.*, 1998, **72**, 1066–1068.

27 G. M. Christian, S. Hammersley, M. J. Davies, P. Dawson, M. J. Kappers, F. C.-P. Massabuau, R. A. Oliver and C. J. Humphreys, Room temperature PL efficiency of InGaN/GaN quantum well structures with prelayers as a function of number of quantum wells, *Phys. Status Solidi C*, 2016, **13**, 248–251.

28 M. Gladysiewicz and R. Kudrawiec, Theoretical studies of the influence of structural inhomogeneities on the radiative recombination time in polar InGaN quantum wells, *Phys. Status Solidi A*, 2012, **209**, 752–760.

 This journal is © The Royal Society of Chemistry 2019

## 4.7 Strong suppression of In desorption from InGaN QW by improved technology of upper InGaN/GaN QW interface [vii]

The growth of upper interface between InGaN QWs and GaN barriers is always a challenge because different growth temperature is needed, which causes many problems, such as indium desorption during the temperature ramp or worse quality of GaN barrier. Many approaches of the growth were published, such as growth interruption or growth of low temperature thin GaN cap layer. We have compared different growth modes in this publication and studied their effect on the luminescence properties. From the PL point of view, we have found that the best technology was when the growth was done without any growth interruption and a small amount of indium was added during the temperature ramp and consequently barrier was pure GaN. Moreover, for the increase of indium in InGaN layers was very sufficient approach of adding indium during the temperature ramp. It increased indium concentration in InGaN in our structures three times, so we were able to grow InGaN QWs at higher temperature then other group with the same indium concentration of InGaN layers and with better quality. Moreover, structure with such increased indium content showed much smaller intensity of defect band. This result is very important for our scintillation applications, where defect band deteriorates our effort. These results confirmed the hypothesis about the source of the defect band from the previous works (recombination between holes confined in QWs and electrons trapped in defect state in the upper InGaN/GaN interface). The growth technique described in this article was successfully patented. The paper was published in Journal of Crystal Growth (IF = 1.57, Q3).

Journal of Crystal Growth 507 (2019) 310–315

Contents lists available at ScienceDirect

Journal of Crystal Growth

journal homepage: www.elsevier.com/locate/jcrysgro

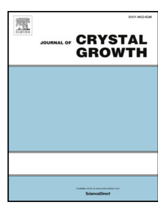

# Strong suppression of In desorption from InGaN QW by improved technology of upper InGaN/GaN QW interface

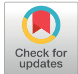

T. Hubáček[a], A. Hospodková[a,*], J. Oswald[a], K. Kuldová[a], J. Pangrác[a], M. Zíková[a], F. Hájek[a], F. Dominec[a], N. Florini[b], Ph. Komninou[b], G. Ledoux[c], C. Dujardin[c]

[a] Institute of Physics CAS, v. v. i., Cukrovarnická 10, 162 00 Prague 6, Czech Republic
[b] Aristotle University of Thessaloniki, GR-54124 Thessaloniki, Greece
[c] Université Lyon, Université Claude Bernard Lyon 1, CNRS, Institut Lumière Matière, UMR 5306, F-69100 Villeurbanne, France

ARTICLE INFO

*Keywords:*
A1. Interfaces
A3. MOVPE
A3. Quantum wells
B1. Nitrides
B2. Scintillators

ABSTRACT

The aim of this work is to elucidate how different growth mode and composition of barriers can influence the QW properties and their PL and to find optimal QW capping process, to suppress the In desorption from QWs and to maintain the QW PL efficiency. It concentrates on the technology procedure for growth of upper quantum well (QW) interfaces in InGaN/GaN QW structure when different temperature for QW and barrier epitaxy is used. We have found that optimal photoluminescence (PL) results were achieved, when the growth after QW formation was not interrupted, but immediately continued during the temperature ramp by the growth of (In)GaN capping layer with small introduction of In precursor into the reactor. Optimal barrier between QW with respect to PL results was found to be pure GaN. We have shown according to SIMS and HRTEM results that by this technological procedure the InGaN desorption was considerably suppressed and three times higher In concentration and two times thicker QWs were achieved for the same QW growth parameters without deterioration of PL intensity in comparison to sample with usually used thin GaN low temperature capping protection. Additionally, for samples covered by the QW capping layer during the temperature ramp the defect band is almost completely missing, thus we can conclude that this defect band is connected with quality of the upper QW interface.

## 1. Introduction

Increasing the In content in MOVPE grown InGaN/GaN multiple quantum well (MQW) structures is a difficult task. It was shown that a possible way to increase the In content is the decrease of the QW growth temperature. However, lower growth temperature is accompanied with weaker decomposition of ammonia which may deteriorate the crystallographic quality and increase the nitrogen vacancies in QWs [1]. In Fig. 1 photoluminescence (PL) spectra of QWs grown at different temperatures are shown, all other growth parameters were kept unchanged. The red shift of PL spectra with decreasing temperature is caused by increased In content in QWs. Increased intensity of excitonic maximum and suppressed defect band maximum of QWs grown at higher temperature is dominantly caused by better quality of InGaN layer, although smaller internal field in QW with lower In content may also enhance the excitonic maximum.

Growth parameters of barrier layers of InGaN quantum wells (QWs) can also considerably influence the properties of InGaN QWs as was discussed in previous reports [2–4]. Important parameters are the temperature and the growth mode, as discussed in [2]. It was shown that to obtain high crystallographic quality of InGaN/GaN MQW structures different temperatures for the growth of InGaN QWs and GaN barriers are required. Lower temperature is used for the growth of InGaN QWs to incorporate sufficient concentration of In atoms, while GaN barriers need higher temperature to keep high crystallographic quality and smooth surface. Technologically the most critical part of InGaN/GaN MQW structure is the upper interface of InGaN QWs. The question is, whether the growth should be interrupted during the temperature increase, since it is generally supposed that In atoms are desorbed from the QW surface during the rise of the temperature from QW to the barrier temperature level [4]. To suppress this desorption is necessary to keep required In content in QWs and their thickness. On the other hand, it was reported that increase of temperature after the InGaN QW growth without any QW protection may be beneficial for obtaining high efficiency luminescence [3]. The aim of this work is to elucidate how different growth procedures of upper QW interface and composition of barriers can influence the QW properties and their PL, suppress the In desorption from QWs and maintain the QW PL

* Corresponding author.
*E-mail address:* hospodko@fzu.cz (A. Hospodková).

https://doi.org/10.1016/j.jcrysgro.2018.11.038

Available online 01 December 2018
0022-0248/ © 2018 Published by Elsevier B.V.

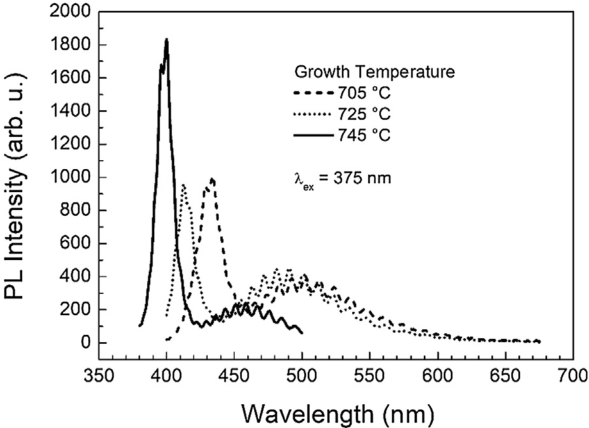


**Fig. 1.** Comparison of PL of structures with ten InGaN/GaN QWs grown at different temperatures, all other growth parameters were kept identical. Thin GaN QW protection layers were grown at the same temperature as QWs. For barrier growth the temperature was increased.

efficiency.

## 2. Experimental

Samples were prepared on Aixtron 3 × 2 CCS MOVPE System equipped by Laytec EpiCurveTT apparatus for in situ measurement of reflectivity and curvature A true wafer temperature was measured in situ by EpiCurveTT. Trimethylgallium (TMGa) and ammonia ($NH_3$) were used as precursors with a hydrogen carrier gas for the growth of buffer layers, triethylgallium (TEGa), trimethylindium (TMIn), ammonia with nitrogen carrier gas were used for the growth of MQW region including barriers. Sapphire substrate with exact c-plane orientation was used. Structures were prepared on buffer layers with optimized technology with respect to PL properties [5]. The upper 1000 nm of the buffer layer was grown at 150 mbar reactor pressure and was n-type doped using $SiH_4$. The whole MQW active region was grown at reactor pressure 400 mbar and $NH_3$ flow rate of 6 l/min.

All MQW structures A-F with 2 × 5 QWs were prepared with graded composition of QWs by temperature profiling during QW growth and with increase temperature for growth of barriers to 820 °C. The schemes of temperature profile during QW and barrier growth can be found in Fig. 2. The set of prepared samples containing structures with different technology of low temperature QW capping or without any QW protection during the growth interruption for the temperature increase are summarized in Table 1. Sample A was prepared with thin (1 monolayer thick) GaN capping of QW at lower temperature (770 °C) followed by growth interruption for the temperature increase. Since the TEGa

**Table 1**
Set of samples with different type of barriers and low temperature QW capping layers.

| Sample | A | B | C | D | E | F |
|---|---|---|---|---|---|---|
| QW cap | thin GaN | GaN | (In)GaN | no | no | (In)GaN |
| Barrier type | GaN | GaN | GaN | GaN | (In)GaN | (In)GaN |

concentration capping layer was kept the same as for the growth of InGaN QW (0.6 µmol/min), long growth time for capping layer formation were used (178 s). Samples B, C and F were grown without growth interruptions for temperature increase. For samples D and E the temperature was increased during growth interruption after QW formation without any protection of QW. For some samples (C, E and F) small amount of In was added to the growth of QW capping layer or barriers with the aim to further suppress the In desorption. The TMIn flow rate was kept constant during the growth of MQW region, but since the TEGa flow was increased from 0.6 µmol/min for QWs to 8.4 µmol/min for the growth of barriers and the temperature was increased for barrier growth, the In content in barriers should be negligible due to the lower incorporation of In at higher temperatures and increased TEGa flow rate. In case of structures with the QW capping layer growth (structures B, C and F) the barrier layer growth time was accordingly shortened with the aim to obtain structures with the same thickness of barriers between successive QWs.

Photoluminescence was used as the main method for the evaluation of the structure quality. A semiconductor laser LD-375 emitting at 375 nm was used for the photoluminescence excitation. The luminescence signal was detected by a GaAs photo-multiplier tube. The resulting photoluminescence was detected using a combination of a double monochromator SDL-1 and a GaAs photo-multiplier tube. Synchronous detection technique was implemented by chopping the laser beam at a modulation frequency of about 35 Hz, and by employing a lock-in amplifier. The excitation intensity 10 W/cm$^2$ and other PL measurement conditions were kept fixed for all presented measurements, so that all presented PL results are mutually comparable, despite arb. u. being indicated in PL results.

To understand better the luminescence properties of our structures and how they depend on excitation wavelength, we have measured also the photoluminescence excitation-emission maps. This measurement was performed on a homemade apparatus. The sample was illuminated by a EQ99X laser driven light source filtered by a Jobin Yvon Gemini 180 monochromator. The exit slit from the monochromator was then reimaged on the sample by two 100 mm focal length, 2 in. diameter $MgF_2$ lenses. The whole apparatus has been calibrated by means of a Newport 918D Low power calibrated photodiode sensor over the range 190–1000 nm. The resolution of the system being 4 nm. The emitted light from the sample is collected by an optical fiber connected to a

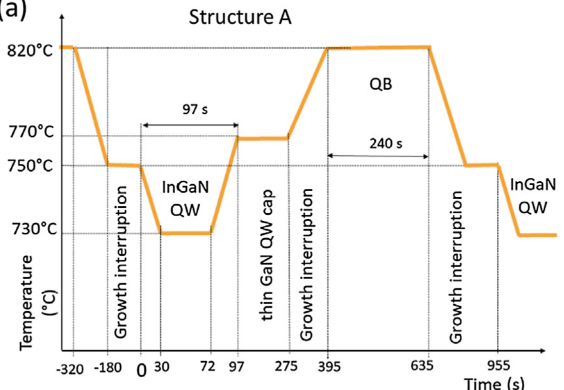


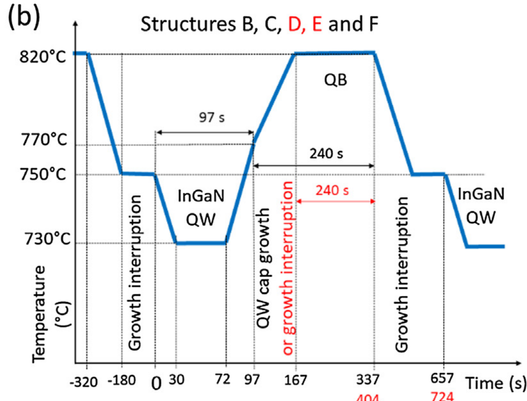


**Fig. 2.** Temperature profile with scheme of growth procedure of prepared structures.

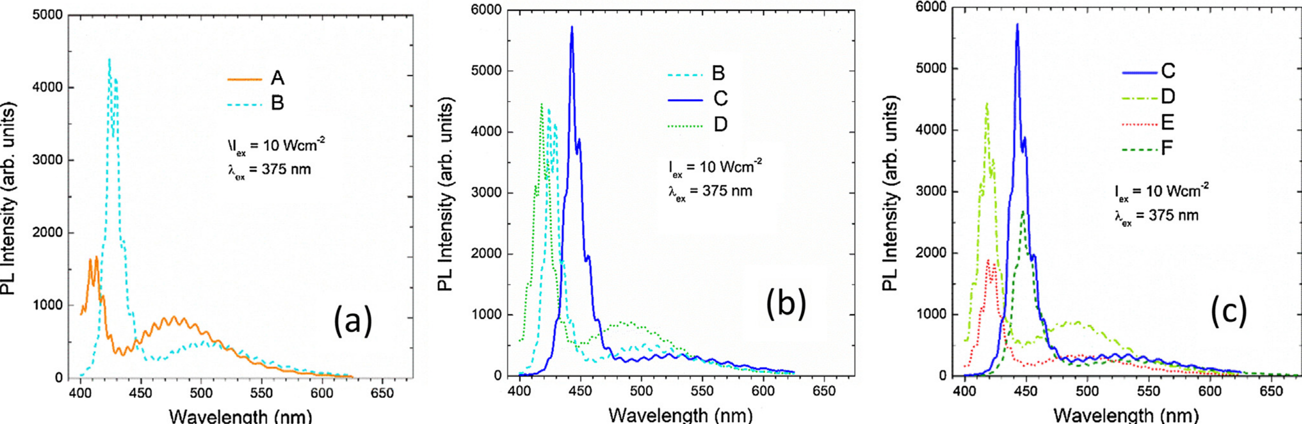


**Fig. 3.** Comparison of PL spectra of samples (a) with different QW capping by GaN and pure GaN barrier, (b) with different QW treatment during the temperature ramp and pure GaN barrier and (c) with (C, F) and without (D, E) QW protection during the temperature ramp with different type of barriers.

Jobin-Yvon TRIAX320 monochromator equipped with a cooled CCD detector. At the entrance of the monochromator different long pass filter can be chosen in order to eliminate the excitation light. The resolution of the detection system is 2 nm.

Cross section TEM specimen preparation was performed by mechanical grinding using the tripod wedge polishing method in the Allied Multiprep, followed by Ar+ ion milling in the Gatan PIPS. Cross sectional TEM (XTEM) and high resolution TEM (HRTEM) observations, along the [11–20] and [1–100] zone axes were performed using a 200 kV JEOL JEM 2011 microscope (point resolution 0.19 nm, Cs = 0.4 mm).

Secondary ion mass spectroscopy (SIMS) were provided by EAG laboratories.

## 3. Results and discussion

### 3.1. Comparison of PL results

A set of A -F samples were prepared, following different technology for the growth of the upper QW interface and characterized in depth. PL spectra of all samples are compared in Fig. 3. To prevent In desorption from QWs during temperature ramp, we have capped the InGaN QW of sample A by thin GaN cap at QW growth temperature prior to the temperature increase for the barrier deposition. This method is often used [1,2]. Sample B was grown with continuous growth of GaN during the whole period of temperature increase. From the shift of PL spectra of sample A with respect to spectrum of sample B (see Fig. 3(a)) can be concluded that under our growth conditions the thin GaN capping is insufficient to protect QW from the In desorption. Additionally, decrease of excitonic PL intensity and increase of the defect band intensity suggest that some kind of defects are probably formed in the low temperature GaN or on the upper QW/barrier interface. The hypothesis of non-sufficient protection of QWs in sample A also confirms similar wavelength of QW excitonic transitions of sample A with thin QW capping and sample D without any QW protection before temperature increase. The difference of QW maximum wavelength of both samples is within the reproducibility range of our reactor (approx. 5 nm). In the Fig. 3(b) the PL spectra of samples B, C and D with GaN barrier and different treatment during the temperature increase are compared. Samples B and C were grown avoiding the growth interruption during the temperature ramp. For sample B GaN was grown immediately after QW during the temperature ramp, for sample C small amount of In into the growth of QW capping layer was introduced to suppress additionally the In desorption. According to our experience on the growth of InGaAs/GaAs structures we know that the massive dissolution of In atoms from InGaAs layers or QDs and In surfacing on the epitaxial surface was observed during the growth of the GaAs capping layer by in situ measurement on reflectance anisotropy spectroscopy [6]. Unfortunately, this measurement method cannot be used for the growth of nitride heterostructures, but from the red shift of PL spectrum of sample C with comparison to sample B we can conclude that this probably occurs also when growing InGaN/GaN heterostructures and introduction of small amount of TMIn into the reactor is very efficient method to suppress In dissolution and desorption. In addition, observed red shift was not accompanied by usual PL efficiency decrease, but PL properties were improved.

We have also checked the influence of small addition of TMIn during the growth of the subsequent part of barrier layer grown at constant temperature after the temperature ramp (samples E and F) and compared them with samples grown similarly but with pure GaN barrier (samples D and C). No further significant shift of PL was observed, see Fig. 3(c). The only effect in both cases was decrease of PL intensity for samples with small In content in barrier layer. Possible explanation of PL intensity decrease may be some crystal imperfections or problems with the lower GaN/InGaN QW interface.

Considering spectra of samples A–F we can conclude that the best results were obtained for sample C grown without any growth interruption after QW with small introduction of TMIn during the growth of QW capping layer and with pure GaN barriers. On the opposite, sample A with thin LT QW capping layer have inferior PL quality with the low excitonic intensity and the strongest defect band.

### 3.2. Structure analyses

To understand better the changes in the structure quality, composition and geometry which can be influenced by different way of QW capping, we have further analyzed structures A and F by SIMS, X-ray diffraction and HRTEM. Structure F was chosen because the same composition of capping and barrier layer containing small amount of In should be more suitable for SIMS as well as XRD measurements.

Strong PL red shift of sample F with respect to the spectrum of samples A is shown in Fig. 4(a). It is evident from SIMS measurement (Fig. 4(b)) that the observed red shift of PL spectra is caused by unexpected strong increase of In content of In in the MQW region. The peak In content in QWs has been three times increased for sample F with respect to sample A. There is also approx. twice increased MQW region thickness of sample F, which cannot be explained by the growth of MQW capping layers, since the time for the barrier layer growth was accordingly shortened to get the same distance between QWs, as described in Section 2.

Unfortunately, the SIMS method does not have sufficient depth resolution to distinguish whether QWs or barriers are more responsible

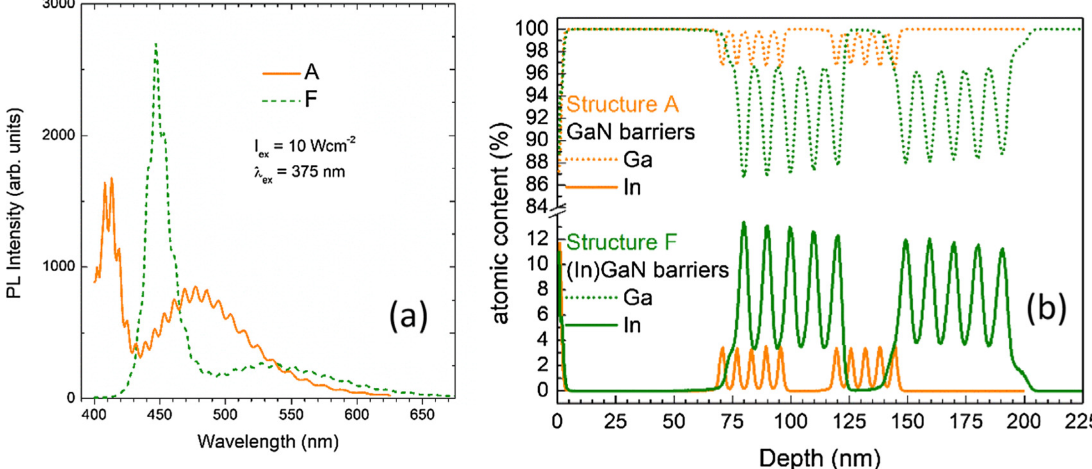


**Fig. 4.** Comparison of results measured on samples with commonly used thin GaN QW cap layer (sample A) and sample with newly designed QW protection (sample F) (a) PL spectra, (b) SIMS results.

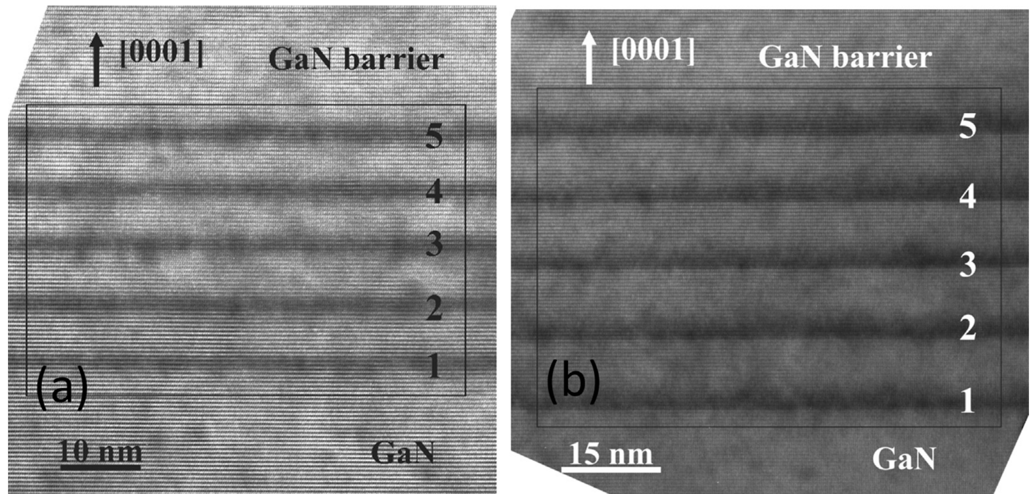


**Fig. 5.** HRTEM images of the first 5× InGaN QW viewed along the [11–20] zone axis. (a) for sample A with thin low temperature GaN protection layer of QWs and GaN barriers, and (b) for sample F capped immediately by (In)GaN layer during temperature increase with (In)GaN barriers.

**Table 2**
Results of structure parameter simulation based on GPA strain analysis from HRTEM images.

| sample | In content % | | Thickness (nm) | |
|---|---|---|---|---|
| | QW | Barrier | QW | Barrier |
| A | 4.0 ± 1.5 | 0 | 1.6 ± 0.1 | 5.6 ± 0.2 |
| F | 15 ± 3 | 4 ± 1 | 2.3 ± 0.1 | 7.9 ± 0.2 |

for the summary thickness increase of MQW region and it cannot be used for precise determination of In content in QW and barrier layers. That is why also HRTEM were done on these samples to see the precise thickness of QW and barriers and to determine their composition, see Fig. 5. According to HRTEM results on samples A and F the thickness of both, QWs and barriers, was increased for sample F. The increase of capping and barrier layer growth rate is caused by addition of TMIn into the reactor atmosphere which was previously reported [7]. Thicker QWs of sample F are caused by suppression of InGaN desorption during temperature increase. Important feature is diffused upper interface of QWs in case of sample F as well as relatively high In content in barrier layers (4%). It may be caused by out diffusion of In atoms during the capping without growth interruption and gradual incorporation into the capping layer during the growth. The In content in barrier layers may also influence the final PL performance of sample F, since in this case the excited light is absorbed also in barrier layers and efficiency of excitation may be several times higher than in the case of sample A, when excited light absorption takes place only in thin QWs. Structure parameters obtained from HRTEM measurement are summarized in Table 2. The In content in the InGaN QWs was calculated, under the biaxial stress approximation, using the strain analysis results obtained by Geometric Phase Analysis (GPA) [8]. Such analysis is not given here.

We have shown that the QW capping without growth interruption is very efficient method to suppress the In desorption from QWs for relatively high QW growth temperatures, when the In desorption is strong and even thin GaN capping does not provide sufficient protection [9]. Although the In content increase obtained only by suggested QW capping procedure is remarkable (compare SIMS and HRTEM results of samples A and F) the final 15% In content of sample F is still not very high. For further increase of In content in QWs their growth temperature would have to be decreased, which could lead to different problems, to be solved, such as In droplets [9] or InGaN quantum dot formation in Stranski-Krastanow growth mode [10]. We believe that suggested QW capping procedure can help to solve even these problems since it will enable to grow QW at higher temperatures to obtain the same In content in QWs as in the case of structure preparation with the

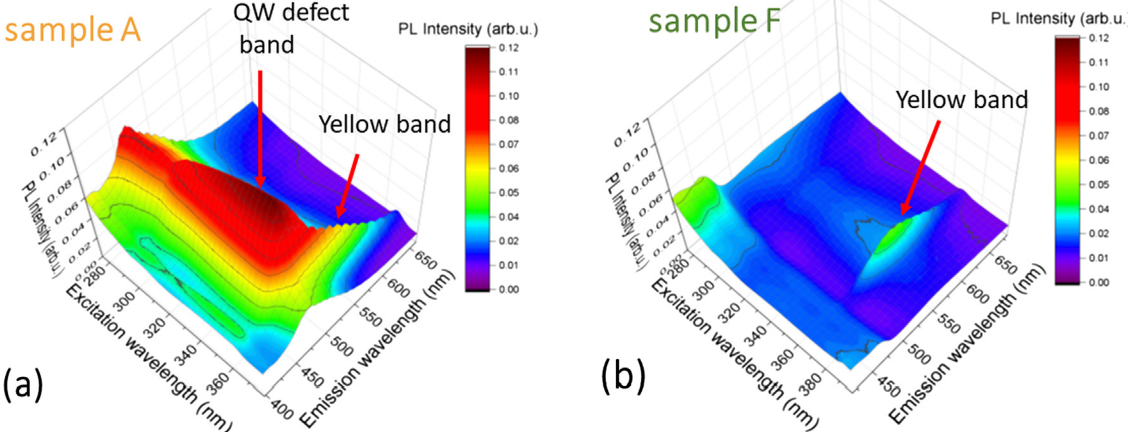


**Fig. 6.** PL excitation-emission maps measured under low excitation intensity for (a) sample A and (b) sample F.

growth interruption. For Stranski-Krastanow growth mode not only strain, but also sufficient time is necessary to form quantum dots [11]. Without the growth interruption after QW growth the system will have less time to switch to the Stranski-Krastanow growth mode and QD formation may be suppressed. Further experiments have to be done to support the hypothesis that this growth procedure could be advantageous also for lower temperature grown InGaN QWs.

### 3.3. Defect band suppression

Very important for some kinds of application is also a suppression of defect band (DB) luminescence of MQW structure [12,13], which was achieved for samples with continual capping of QWs during the temperature ramp. The DB becomes dominant for low excitation intensity [12]. It can be compared in Fig. 6(a) and (b), how different are the PL excitation emission maps for both types of samples, when excited by low excitation intensity. For sample F the defect band is almost completely missing while in case of sample A it becomes dominant.

This defect band is connected with quality of the upper QW interface since its intensity depends on the QW capping process as can be seen on our PL results in Fig. 3. The defect band maximum shifts together with the excitonic luminescence, thus we can ascribe this DB to the recombination of electrons or holes confined in QW with holes or electrons trapped in defects near the upper interface.

We have simulated by NextNano$^{++}$ software [14] the band structure of samples A and F according to the HRTEM and SIMS results, see Fig. 7(a). It can be noticed that due to the increased In content in structure F the tilting of the band structure (polarization field) is considerably increased in comparison to structure A. This tilting will influence the position of electrons and holes confined in QWs and consequently the penetration of electrons and holes to upper and lower interfaces. We know, that the DB is considerably suppressed for sample F with stronger polarization field. Similar behavior was also observed when the band structure tilting was influenced by degree of doping of surrounding layers [15]. We also suppose that DB is connected with the upper QW interface, as mentioned before. At increased tilt the penetration of holes into the upper interface is suppressed. Thus we can ascribe this defect band to the recombination of holes confined in the QW with electrons trapped in GaN near the upper QW interface, see schematic picture in Fig. 7(b). This type of recombination may be even more suppressed for diffused upper QW interface, which was observed by HRTEM.

## 4. Conclusions

We have tried to find optimal technology procedure for growth of upper QW interfaces in InGaN/GaN MQW structure when different temperature for QW and barrier epitaxy is used. Set of samples with different treatment of the upper QW interface were prepared. After evaluation of PL spectra of samples A-F we can conclude that the best PL results and hence optimal upper interface technology was achieved for sample C, when the growth after QW formation was not interrupted, but immediately continued during the temperature ramp by the growth of (In)GaN capping layer with small introduction of TMIn into the reactor. Optimal barrier between QW with respect to PL results was found to be pure GaN. Since the structure C has GaN barriers we can exclude that the PL intensity increase is caused by more efficient absorption of exciting light (375 nm) as in the case of structure F. We have shown that

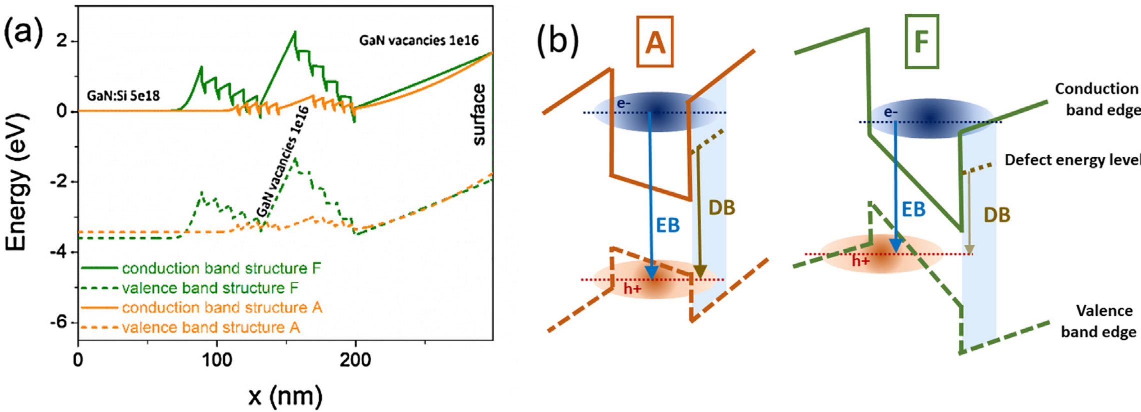


**Fig. 7.** (a) Simulated band structure of samples A and F according to the SIMS and XRD data. (b) suggested mechanism of defect band luminescence.

by this technological procedure the InGaN desorption was considerably suppressed and three times higher In concentration and two times thicker QWs were achieved for the same QW growth parameters without deterioration of PL results. On the opposite, sample A with thin LT buffer layer have inferior PL quality with the low excitonic intensity and strongest defect band. Thin GaN capping layer in sample A did not protect in our case (relatively high growth temperatures) sufficiently InGaN QW from the InGaN material desorption during temperature ramp and, additionally, it caused defects in the upper QW interface. The defect band is almost completely missing for samples covered by the QW capping layer during the temperature ramp, thus we can conclude that this defect band is connected with quality of the upper QW interface. Since we have found that the defect band is also suppressed for samples with stronger polarization field we have ascribed the origin of this defect band to the recombination of holes confined in QWs with electrons trapped in GaN near the upper QW interface.

## Acknowledgements

The authors acknowledge support of the GACR project no. 16-11769S and MSMT project no. NPU LO1603 – ASTRANIT, LNSM infrastructure LM2015087 and by partial support of EC project H2020-TWINN-2015 no. 690599 (ASCIMAT) is also gratefully acknowledged.

## References

[1] F.K. Yam, Z. Hassan, Efficiency enhancement of blue light emitting diodes by eliminating V-defects from InGaN/GaN multiple quantum well structures through GaN capping layer control, Superlatt. Microstr. 43 (2008) 1–23.
[2] M.J. Wallace, et al., Effect of the barrier growth mode on the luminescence and conductivity micron scale uniformity of InGaN light emitting diodes, J. Appl. Phys. 117 (2015) 115705.
[3] R.A. Oliver, et al., The impact of gross well width fluctuations on the efficiency of GaN-based light emitting diodes, Appl. Phys. Lett. 103 (2013) 141114.
[4] N.K. van der Laak, R.A. Oliver, M.J. Kappers, C.J. Humphreys, Role of gross well-width fluctuations in bright, green-emitting single InGaN/GaN quantum well structures, Appl. Phys. Lett. 90 (2007) 121911.
[5] T. Hubáček, A. Hospodková, J. Oswald, K. Kuldová, J. Pangrác, Improvement of luminescence properties of GaN buffer layer for fast nitride scintillator structures, J. Cryst. Growth 464 (2017) 221–225.
[6] A. Hospodková, J. Vyskočil, J. Pangrác, J. Oswald, E. Hulicius, K. Kuldová, Surface processes during growth of InAs/GaAs quantum dot structures monitored by reflectance anisotropy spectroscopy, Surf. Sci. 604 (2010) 318–321.
[7] K. Zhou, M. Ikeda, J. Liu, S. Zhang, Z. Li, M. Feng, A. Tian, P. Wen, D. Li, L. Zhang, H. Yang, Abnormal InGaN growth behavior in indium-desorption regime in metalorganic chemical vapor deposition, J. Cryst. Growth 409 (2015) 51–55.
[8] M.J. Hÿtch, E. Snoeck, R. Kilaas, Ultramicroscopy 74 (1998) 131.
[9] T. Yamamoto, A. Tamura, S. Usami, T. Mitsunari, K. Nagamatsu, S. Nitta, Y. Honda, H. Amano, Jpn. J. Appl. Phys. 55 (5S) (2016) 05FD03.
[10] M. Pristovsek, A. Kadir, C. Meissner, T. Schwaner, M. Leyer, J. Stellmach, M. Kneissl, F. Ivaldi, S. Kret, Growth mode transition and relaxation of thin InGaN layers on GaN(0001), J. Cryst. Growth 372 (2013) 65–72.
[11] E. Hulicius, J. Oswald, J. Pangrác, J. Vyskočil, A. Hospodková, K. Kuldová, K. Melichar, T. Šimeček, Growth and properties of InAs/In(x)Ga(1−x)As/GaAs quantum dot structures, J. Cryst. Growth 310 (2008) 2229–2233.
[12] A. Hospodková, M. Nikl, O. Pacherová, J. Oswald, P. Brůža, D. Pánek, B. Foltynski, E. Hulicius, A. Beitlerová, M, Heuken, InGaN/GaN multiple quantum well for fast scintillation application: radioluminescence and photoluminescence study, Nanotechnology 25 (2014) 455501.
[13] A. Hospodková, J. Oswald, M. Zíková, J. Pangrác, K. Kuldová, K. Blažek, G. Ledoux, C. Dujardin, M. Nikl, On the correlations between the excitonic luminescence efficiency and the QW numbers in multiple InGaN/GaN QW structure, J. Appl. Phys. 121 (2017) 214505.
[14] S. Birner, S. Hackenbuchner, M. Sabathil, G. Zandler, J.A. Majewski, T. Andlauer, T. Zibold, R. Morschl, A. Trellakis, P. Vogl, Modeling of semiconductor nanostructures with nextnano3, Acta Phys. Pol., **A** 110 (2006) 111.
[15] M. Zíková, A. Hospodková, J. Pangrác, T. Hubáček, J. Oswald, K. Kuldová, F. Hájek, G. Ledoux, C. Dujardin, Influence of Si doping of GaN layers surrounding InGaN quantum wells on structure photoluminescence properties, J. Cryst Growth 506 (2019) 8–13.

# 5 Conclusions

This doctoral thesis was devoted to the growth of InGaN/GaN multiple quantum well nanoheterostructures with MOVPE technology. Based on theoretical predictions, these structures should be useful as a very fast and efficient scintillation detector. It should be used especially in fast-timing applications because of its sub-nanosecond excitonic decay time. Therefore, we have modified commonly used blue LED nitride structure to get thick active MQW region as much as possible and obtain very fast excitonic decay time around 1 ns and luminescence spectra without any slow defect bands. Presented results in this thesis showed real possibility of using MOVPE grown InGaN/GaN structures as efficient and fast scintillation structures. The first tests and comparison (made in CERN) of different nanoscintillators (our MQW structures, ZnO:Ga and CdSe/CdS) showed that our structures present the best mechanical and optical properties. From all tested samples only our structures gave light yield comparable to LYSO:Ce [61]. That is a promising result for future work in the field of fast timing applications.

Perfect initial part of GaN growth on sapphire substrate predestines the whole scintillation structure quality for this application. Nucleation and coalescence layer growth on sapphire substrate was investigated at the beginning of our work. Suppression of yellow band and increase of the excitonic band was achieved by proper growth conditions, such as high growth pressure during nucleation or lower $NH_3$ flow during coalescence of islands. The next part of the structure, which is n-type GaN layer, was optimized as well with respect to suppression of YB intensity. Significant suppression of YB was achieved with TEGa precursor which was used instead of usual TMGa precursor. It was found that different growth conditions have to be used, such as $N_2$ carrier gas, higher V/III ratio or slower growth rate.

Luminescence spectra of our InGaN/GaN scintillation structures contain fast excitonic band originating from QWs and defect band which is related to QWs (assumption coming from the observation that it shifts with the position of QWs). We were not able to eliminate this kind of defect band during our work but we have suggested its origin. Influence of n-doped GaN layers surrounded MQW region on PL properties was studied. Different position of n-doped GaN layer changes internal electric field resulting in different tilting of the band structure. Theoretical simulations and PL results suggested that the defect band may originate in recombination between holes confined in QWs and electrons trapped in some defect state in the upper InGaN/GaN interface. Different growth modes of the upper interface were also investigated and results supported our hypothesis about the origin of QW defect band. Special growth of the upper interface, when after InGaN QW is without interruption grown cap layer (during the temperature ramp) and consequently grown barrier, was successfully patented. Unfortunately, the source of the defect state in the upper interface was not established up to now and defect band observed in luminescence spectra was still not fully eliminated.

Finally, we have confirmed the positive role of V-pits on the luminescence properties which was suggested in the literature. On the other hand, their positive influence can be seen when the size of V-pits is not higher than 300 nm in diameter. LED community usually does not reach such big V-pits, but for our scintillation structure, it is the limitation. We found out that bigger V-pits influence negatively the luminescence properties of our structures. Different approach or a way to control the size of V-pits will have to be found to get more than 1 µm thick active region with sufficient luminescence quality.

# References

[1] C. Dujardin, E. Auffray, E. Bourret-Courchesne, P. Dorenbos, P. Lecoq, M. Nikl, A.N. Vasil'ev, A. Yoshikawa and R.-Y. Zhu, Needs, Trends, and Advances in inorganic Scintillators, IEEE Trans. Nucl. Sci. **65** (2018) 1977-1997.

[2] P. Lecoq, Development of new scintillators for medical applications, Nucl. Instrum. Methods Phys. Res., Sect. A **809** (2016) 130-139.

[3] M. Nikl and A. Yoshikawa, Recent R&D Trends in Inorganic Single-Crystal Scintillator Materials for Radiation Detection, Adv. Opt. Mater. **3** (2015) 463-481.

[4] L. Procházková, T. Gbur, V. Čuba, V. Jarý and M. Nikl, Fabrication of highly efficient ZnO nanoscintillators, Opt. Mater. **47** (2015) 67-71.

[5] Z. Wang, C.W. Barnes, J.S. Kapustinsky, C.L. Morris, R.O. Nelson, F. Yang, L. Zhang and R.-Y. Zhu, Thin scintillators for ultrafast hard X-ray imaging, Proc. SPIE, Photon Counting Appl. **9504** (2015) 95040N.

[6] R.M. Turtos, S. Gundacker, A. Polovitsyn, S. Christodoulou, M. Salomoni, E. Auffray, I. Moreels, P. Lecoq and J.Q. Grim, Ultrafast emission from colloidal nanocrystals under pulsed X-ray excitation, J. Instrum. **11** (2016) P10015.

[7] A. Hospodková, M. Nikl, O. Pacherová, J. Oswald, P. Brůža, D. Pánek, B. Foltynski, E. Hulicius, A. Beitlerová and M. Heuken, InGaN/GaN multiple quantum well for fast scintillation application: radioluminescence and photoluminescence study, Nanotechnology **25** (2014) 455501.

[8] J. Grant, W. Cunningham, A. Blue, V. O'Shea, J. Vaitkus, E. Gaubas and M. Rahman, Wide bandgap semiconductors detectors for harsh radiation environments, Nucl. Instrum. Methods Phys. Res., Sect. A **546** (2005) 213-217.

[9] J.-Y. Duboz, M. Laügt, D. Schenk, B. Beaumont, J.-L. Reverchon, A.D. Wieck and T. Zimmerling, GaN for x-ray detection, Appl. Phys. Lett. **92** (2008) 263501.

[10] A.G. Melton, E. Burgett, T. Xu, N. Hertel and I.T. Ferguson, Comparison of neutron conversion layers for GaN based scintillators, Phys. Status Solidi C **9** (2012) 957-959.

[11] P. Pittet, G.-N. Lu, J.-M. Galvan, J.-Y. Loisy, A. Ismail, J.-Y. Giraud and J. Balosso, Implantable real-time dosimetric probe using GaN as scintillation material, Sens. Actuators, A **151** (2009) 29-34.

[12] A. Ismail, P. Pittet, G.N. Lu, J.M. Galvan, J.Y. Giraud and J. Balosso, In vivo dosimetric system based on Gallium Nitride radioluminescence, Radiat. Meas. **46** (2011) 1960-1962.

[13] H.P.D. Schenk, S.I. Borenstain, A. Berezin, A. Schön, E. Cheifetz, A. Dadgar and A. Krost, Cathodoluminescence of epitaxial GaN and ZnO thin films for scintillator applications, J. Cryst. Growth **311** (2009) 3984-3988.

[14] W.C. Johnson, J.B. Parson and M.C. Crew, Nitrogen Compounds of Gallium. III, J. Phys. Chem. **36** (1932) 2651-2654.

[15] R. Juza and H. Hahn, Über die Kristallstrukturen von Cu3N, GaN und InN Metallamide und Metallnitride, Zeitschrift für Anorganische und Allgemeine Chemie **239** (1938) 282-287.

[16] H.P. Maruska and J.J. Tietjen, The preparation and properties of vapor-deposited single-crystal-line GaN, Appl. Phys. Lett. **15** (1969) 327-329.

[17] J.I. Pankove, E.A. Miller and J.E. Berkeyheiser, GaN blue light-emitting diodes, J. Lumin. **5** (1972) 84-86.

[18] H.P. Maruska, W.C. Rhines and D.A. Stevenson, Preparation of Mg-doped GaN diodes exhibiting violet electroluminescence, Mater. Res. Bull. **7** (1972) 777-781.

[19] J. Pastrňák and L. Součková, Herstellung dünner Schichten von Aluminium-, Gallium-, sowie Indiumnitrid unter einer Gasentladung, Phys. Status Solidi B **3** (1963) K71-K74.

[20] J. Pastrňák and L. Roskovcová, Epitaktisches Aufwachsen von AlN-Schichten auf SiC- und Si-Einkristallen in der Gasentladung, Phys. Status Solidi B **9** (1965) K73-K75.

[21] S. Yoshida, S. Misawa and S. Gonda, Improvements on the electrical and luminescent properties of reactive molecular beam epitaxially grown GaN films by using AlN-coated sapphire substrates, Appl. Phys. Lett. **42** (1983) 427-429.

[22] H. Amano, N. Sawaki, I. Akasaki and Y. Toyoda, Metalorganic vapor phase epitaxial growth of a high quality GaN film using an AlN buffer layer, Appl. Phys. Lett. **48** (1986) 353.

[23] H. Amano, M. Kito, K. Hiramatsu and I. Akasaki, P-Type conduction in Mg-Doped GaN Treated with Low-Energy Electron Beam Irradiation (LEEBI), Jpn. J. Appl. Phys. **28** (1989) L2112-L2114.

[24] S. Nakamura, T. Mukai, M. Senoh and N. Iwasa, Thermal Annealing Effects on P-Type Mg-Doped GaN Films, Jpn. J. Appl. Phys. **31** (1992) L139-L142.

[25] S. Nakamura, T. Mukai and M. Senoh, Candela-class high-brightness InGaN/AlGaN double-heterostructure blue-light-emitting diodes, Appl. Phys. Lett. **64** (1994) 1687-1689.

[26] D. Andiwijayakusuma, M. Saito and A. Purqon, Density functional theory study: Electronic structures of RE:GaN in wurtzite $Ga_{15}RE_{1}N_{16}$, J. Phys.: Conf. Ser. **739** (2016) 012027.

[27] H. Morkoc, Nitride Semiconductors and Devices. New York: Springer, 1999. ISBN 978-3-642-63647-9.

[28] P. Perlin, C. Jauberthie-Carillon, J.P. Itie, A. San Miguel, I. Grzegory and A. Polian, Raman scattering and x-ray-absorption spectroscopy in gallium nitride under high pressure, Phys. Rev. B **45** (1992) 83-89.

[29] D.C. Look, D.C. Reynolds, Z.-Q. Fang, J.W. Hemsky, J.R. Sizelove and R.L. Jones, Point defect characterization of GaN and ZnO, Mater. Sci. Eng. B **66** (1999) 30-32.

[30] C. Merz, M. Kunzer, B. Šantić, U. Kaufmann, I. Akasaki and H. Amano, Temperature dependence of excitonic photoluminescence and residual shallow donors in high-purity GaN/$Al_2O_3$, Mater. Sci. Eng. **B43** (1997) 176-180.

[31] D.O. Demchenko and M.A. Reshchikov, Blue luminescence and Zn acceptor in GaN, Phys. Rev. B **88** (2013) 115204.

[32] U. Kaufmann, M. Kunzer, H. Obloh, M. Maier, Ch. Manz, A. Ramakrishnan and B. Santic, Origin of defect-related photoluminescence bands in doped and nominally undoped GaN, Phys. Rev. B **59** (1999) 5561-5567.

[33] D.O. Demchenko, I.C. Diallo and M.A. Reshchikov, Hydrogen-carbon complexes and the blue luminescence band in GaN, J. Appl. Phys. **119** (2016) 035702.

[34] J.L. Lyons, A. Alkauskas, A. Janotti and Ch.G. Van de Walle, First-principles theory of acceptors in nitride semiconductors, Phys. Status Solidi B **252** (2015) 900-908.

[35] Z. Xie, Y. Sui, J. Buckeridge, A.A. Sokol, T.W. Keal and A. Walsh, Prediction of multiband luminescence due to the gallium vacancy-oxygen defect complex in GaN, Appl. Phys. Lett. **112** (2018) 262104.

[36] S.G. Christenson, W. Xie, Y.Y. Sun and S.B. Zhang, Carbon as a source for yellow luminescence in GaN: Isolated $C_N$ defect or its complexes, J. Appl. Phys. **118** (2015) 135708.

[37] M.A. Reshchikov, M. Vorobiov, D.O. Demchenko, Ü. Özgür, H. Morkoç, A. Lesnik, M.P. Hoffmann, F. Hörich, A. Dadgar and A. Strittmatter, Two charge states of the $C_N$ acceptor in GaN: Evidence from photoluminescence, Phys. Rev. B **98** (2018) 125207.

[38] E. F. Schubert, Light-Emitting Diodes. Cambridge University Press, 2006.

[39] I. Vurgaftman and J.R. Meyer, Band parameters for nitrogen-containing semiconductors, J. Appl. Phys. **94** (2003) 3675.

[40] F. Bernardini and V. Fiorentini, Nonlinear macroscopic polarization in III-V nitride alloys, Phys. Rev. B **64** (2001) 085207.

[41] O. Ambacher, J. Majewski, C. Miskys, A. Link, M. Hermann, M. Eickhoff, M. Stutzmann, F. Bernardini, V. Fiorentini, V. Tilak, B. Schaff and L.F. Eastman, Pyroelectric properties of Al(In)GaN/GaN hetero- and quantum well structures, J. Phys.: Condens. Matter **14** (2002) 3399-3434.

[42] D.P. Nguyen, N. Regnault, R. Ferreira and G. Bastars, Alloy effects in GaInN/GaN heterostructures, Solid State Commun. **130** (2004) 751.

[43] Y.-C. Cheng, E.-C. Lin, C.-M. Wu, C.C. Yang, J.-R. Yang, A. Rosenauer, K.-J. Ma, S.-C. Shi, L.C. Chen, C.-C. Pan and J.-I. Chyi, Nanostructures and carrier localization

behaviors of green-luminescence InGaN/GaN quantum-well structures of various silicon-doping conditions, Appl. Phys. Lett. **84** (2004) 2506-2508.

[44] D.M. Graham, A. Soltani-Vala, P. Dawson, M.J. Godfrey, T.M. Smeeton, J.S. Barnard, M.J. Kappers, C.J. Humphreys and E.J. Thrush, Optical and microstructural studies of InGaN/GaN single-quantum-well structures, J. Appl. Phys. **97** (2005) 103508.

[45] T.M. Smeeton, M.J. Kappers, J.S. Barnard, M.E. Vickers and C.J. Humphreys, Electron-beam-induced strain within InGaN quantum wells: False indium “cluster” detection in the transmission electron microscope, Appl. Phys. Lett. **83** (2003) 5419.

[46] A. Hangleiter, F. Hitzel, C. Netzel, D. Fuhrmann, U. Rossow, G. Ade and P. Hinze, Suppression of Nonradiative Recombination by V-Shaped Pits in GaInN/GaN Quantum Wells Produces a Large Increase in the Light Emission Efficiency, Phys. Rev. Lett. **95** (2005) 127402.

[47] M. Hocker, P. Maier, L. Jerg, I. Tischer, G. Neusser, C. Kranz, M. Pristovsek, C.J. Humphreys, R.A.R. Leute, D. Heinz, O. Rettig, F. Scholz and K. Thonke, Determination of axial and lateral exciton diffusion length in GaN by electron energy dependent cathodoluminescence, J. Appl. Phys. **120** (2016) 085703.

[48] G.B. Stringfellow, Epitaxy, Rep. Prog. Phys. **45** (1982) 469-525.

[49] R.M. Biefeld, D.D. Koleske and J.G. Cederberg, 3 - The Science and Practice of Metal-Organic Vapor Phase Epitaxy (MOVPE), Editor(s): Thomas F. Kuech, In Handbook of Crystal Growth, Handbook of Crystal Growth (Second Edition), North-Holland, 2015, Pages 95-160, ISBN 9780444633040.

[50] H. Zhang, R. Zuo and G. Zhang, Effects of reaction-kinetic parameters on modelling reaction pathways in GaN MOVPE growth, J. Cryst. Growth **478** (2017) 193-204.

[51] C. Theodoropoulos, T.J. Mountziaris, H.K. Moffat and J. Han, Design of gas inlets for the growth of gallium nitride by metalorganic vapour phase epitaxy, J. Cryst. Growth **217** (2000) 65-81.

[52] R.P. Parikh and R.A. Adomaitis, An overview of gallium nitride growth chemistry and its effect on reactor design: Application to a planetary radial-flow CVD system, J. Cryst. Growth **286** (2006) 259-278.

[53] P. Capper, S. Irvine and T. Joyce, Epitaxial Crystal Growth: Methods and Materials. In: S. Kasap, P. Capper (eds) Springer Handbook of Electronic and Photonic Materials. Springer Handbooks. Springer, Cham. (2017), Online ISBN 978-3-319-48933-9.

[54] F.K. Yam and Z. Hassan, InGaN: An overview of the growth kinetics, physical properties and emission mechanism, Superlattices Microstruct. **43** (2008) 1-23.

[55] M. Bosi and R. Fornari, A study of Indium incorporation efficiency in InGaN grown by MOVPE, J. Cryst. Growth **265** (2004) 434-439.

[56] R. Czernecki, E. Grzanka, J. Smalc-Koziorowska, S. Grzanka, D. Schiavon, G. Targowski, J. Plesiewicz, P. Prystawko, T. Suski, P. Perlin and M. Leszczynski, Effect of hydrogen during growth of quantum barriers on the properties of InGaN quantum wells, J. Cryst. Growth **414** (2015) 38-41.

[57] R. Czernecki, E. Grzanka, P. Strak, G. Targowski, S. Krukowski, P. Perlin, T. Suski and M. Leszczynski, Influence of hydrogen pre-growth flow on indium incorporation into InGaN layers, J. Cryst. Growth **464** (2017) 123-126.

[58] M.A. Moram and M.E. Vickers, X-ray diffraction of III-nitrides, Rep. Prog. Phys. **72** (2009) 036502.

[59] J.F. Muth, J.D. Brown, M.A. Johnson, Z. Yu, R.M. Kolbas, J.W. Cook and J.F. Schetzina, Absorption coefficient and refractive index of GaN, AlN and AlGaN alloys, MRS Internet J. Nitride Semicond. Res. **4**, S1 (1999) G5.2.

[60] O. Kurniawan and V. K. S. Ong, Investigation of range-energy relationships for Low-energy electron Beams in Silicon and Gallium Nitride, Scanning **29** (2007) 280-286.

[61] R.M. Turtos, S. Gundacker, S. Omelkov, E. Auffray and P. Lecoq, Light yield of scintillating nanocrystals under X-ray and electron excitation, J. Lumin. **215** (2019) 116613.

# List of Publications

## Author's articles related to thesis (in impact journals)

Articles described in this doctoral thesis

[i] T. Hubáček, A. Hospodková, J. Oswald, K. Kuldová, J. Pangrác, Improvement of luminescence of GaN buffer layer for fast nitride scintillator structures, J. Cryst. Growth **464** (2017) 221-225.

Cited in (without self-citations):

[a] A. Hospodková, J. Oswald, M. Zíková, J. Pangrác, K. Kuldová, K. Blažek, G. Ledoux, C. Dujardin, M. Nikl, On the correlations between the excitonic luminescence efficiency and the QW numbers in multiple InGaN/GaN QW structure, J. Appl. Phys. **121** (2017) 214505.

[b] D. Jana, T.K. Sharma, A correlation between the defect states and yellow luminescence in AlGaN/GaN heterostructures, J. Appl. Phys. **122** (2017) 035101.

[ii] T. Hubáček, A. Hospodková, K. Kuldová, M. Slavická Zíková, J. Pangrác, J. Čížek, M.O. Liedke, M. Butterilng, A. Wagner, P. Hubík, E. Hulicius, Improvement of luminescence properties of n-GaN using TEGa precursor, J. Cryst. Growth **531** (2020) 125383.

[iii] M. Zíková, A. Hospodková, J. Pangrác, T. Hubáček, J. Oswald, K. Kuldová, F. Hájek, G. Ledoux, C. Dujardin, Influence of Si doping of GaN layers surrounding InGaN quantum wells on structure photoluminescence properties, J. Cryst. Growth **506** (2019) 8-13.

Cited in:

[a] L. Liu, F. Liu, J. Tian, Study of electronic properties on the n-GaN (0001) surface with points defects, Appl. Phys. A: Mater. Sci. Process. **125** (2019) 840.

[b] R. Kour, S. Arya, S. Verma, A. Singh, P. Mahajan and A. Khosla, Review-Recent Advances and Challenges in Indium Gallium Nitride ($In_xGa_{1-x}N$) Materials for Solid State Lightning, ECS J. Solid. State Sci. Technol. **9** (2020) 015011.

[iv] F. Dominec, A. Hospodková, T. Hubáček, M. Zíková, J. Pangrác, K. Kuldová, A. Vetushka, E. Hulicius, Influence of GaN buffer layer under InGaN/GaN MQWs on luminescent properties, J. Cryst. Growth **507** (2019) 246-250.

Cited in:

[a] Ch. Pan, Ch. Li, Z. Li, D. Peng, D. Zhang, Q. Yang, Y. Sun, S. Wu, Growth of millimeter wave AlN/GaN heterostructures by MOCVD, J. Cryst. Growth **531** (2020) 125265.

[v] A. Hospodková, T. Hubáček, J. Oswald, J. Pangrác, K. Kuldová, M. Hývl, F. Dominec, G. Ledoux, C. Dujardin, InGaN/GaN Structures: Effect of the Quantum Well Number on the Cathodoluminescent Properties, Phys. Status Solidi B **255** (2018) 1700464.

Cited in:

[a] R.M. Turtos, S. Gundacker, S. Omelkov, E. Auffray, P. Lecoq, Light yield of scintillating nanocrystals under X-ray and electron excitation, J. Lumin. **215** (2019) 116613

[b] R.M. Turtos, S. Gundacker, E. Auffray, P. Lecoq, Towards a metamaterial approach for fast timing in PET experimental proof-of-concept, Phys. Med. Biol. **64** (2019) 185018.

[c] R.I.S. Alarcón, M.Á.A. Frutis, S.C. Téllez, C.F. Guajardo, R.B. Urby, N.C. Castro, G.A. Flores, Blue, white, and red tunable light emission from ($Y_2O_3:Sm^{3+}$)-benzoate hybrid nanophosphors, J. Nanophotonics **12** (2018) 046003.

[vi] T. Hubáček, A. Hospodková, K. Kuldová, J. Oswald, J. Pangrác, V. Jarý, F. Dominec, M. Slavická Zíková, F. Hájek, E. Hulicius, A. Vetushka, G. Ledoux, C. Dujardin, M. Nikl, Advancement toward ultra-thick and bright InGaN/GaN structures with a high number of QWs, CrystEngComm **21** (2019) 356-362.

Cited in:

[a] R.M. Turtos, S. Gundacker, S. Omelkov, E. Auffray, P. Lecoq, Light yield of scintillating nanocrystals under X-ray and electron excitation, J. Lumin. **215** (2019) 116613.

[vii] T. Hubáček, A. Hospodková, J. Oswald, K. Kuldová, J. Pangrác, M. Zíková, F. Hájek, F. Dominec, N. Florini, P. Komninou, G. Ledoux, C. Dujardin, Strong suppression of In desorption from InGaN QW by improved technology of upper InGaN/GaN QW interface, J. Cryst. Growth **507** (2019) 310-315.

Articles not described in this doctoral thesis

[viii] A. Hospodková, F. Hájek, J. Pangrác, M. Slavická Zíková, T. Hubáček, K. Kuldová, J. Oswald, T. Vaněk, A. Vetushka, A secret luminescence killer in deepest QWs of InGaN/GaN multiple quantum well structures, J. Cryst. Growth, *in review process.*

[ix] V. Jarý, A. Hospodková, T. Hubáček, F. Hájek, K. Blažek, M. Nikl, Optical Properties of InGaN/GaN Multiple Quantum Wells Structures Grown on Different Substrates, IEEE Trans. Nucl. Sci., *in review process.*

[x] A. Hospodková, M. Slavická Zíková, T. Hubáček, J. Pangrác, K. Kuldová, F. Hájek, F. Dominec, A. Vetushka, S. Hasenöhrl, Improvement of crystalline quality by $SiN_x$ layer grown by MOVPE, Lith. J. Phys. **59** (2019) 179-186.

## Author's articles out of thesis scope (in impact journals)

[xi] O. Rettig, J.-P. Scholz, N. Steiger, S. Bauer, T. Hubáček, M. Zíková, Y. Li, H. Qi, J. Biskupek, U. Kaiser, K. Thonke, F. Scholz, Investigation of Boron Containing AlN and AlGaN Layers Grown by MOVPE, Phys. Status Solidi B **255** (2018) 1700510.

## Patent application related to thesis

[xii] A. Hospodková, T. Hubáček, Preparation method of epitaxial structure with InGaN quantum wells, Patent No.308024 (2019).

## Author's selected conference contributions related to thesis

A. Hospodková, J. Oswald, K. Kuldová, T. Hubáček, J. Pangrác, Yellow Band Luminescence Suppression for Fast Nitride Scintillator Structure, ICMOVPE XVIII, San Diego, USA, 2016, poster presentation.

T. Hubáček, A. Hospodková, J. Oswald, J. Pangrác, E. Hulicius, V. Jarý, T. Parkman, D. Pánek, G. Ledoux, Ch. Dujardin and M. Nikl, Growth and Characterization of InGaN/GaN Multiple Quantum Well Structures used for Scintillation Detectors, SCINT 2017, Chamonix, France, 2017, oral presentation.

T. Hubáček, A. Hospodková, J. Pangrác, M. Zíková, K. Kuldová, J. Oswald and E. Hulicius, Introduction of Different InGaN/(In)GaN Growth Modes on Indium Incorporation and Quality of Layers, ISGN-7, Warsaw, Poland, 2018, poster presentation.

T. Hubáček, V. Jarý, A. Hospodková, J. Oswald, J. Pangrác, K. Kuldová, M. Slavická Zíková, E. Hulicius, A. Vetushka, G. Ledoux, Ch. Dujardin and M. Nikl, Influence of growth parameters on scintillation properties of InGaN/GaN heterostructures, LumDeTr'18, Prague, 2018, Czech Republic, poster presentation.

T. Hubáček, A. Hospodková, K. Kuldová, J. Pangrác, M. Slavická Zíková, R. Novotný, A. Vetushka and E. Hulicius, Photoluminescence and structural properties of n-GaN buffer layers grown from TEGa precursor, EWMOVPE'18, Vilnius, Lithuania, 2019, poster presentation.

T. Hubáček, A. Hospodková, K. Kuldová, J. Pangrác, M. Slavická Zíková, A. Vetushka, J. Oswald, T. Vaněk, F. Hájek, R. Novotný, F. Dominec and E. Hulicius, Improvement of luminescence properties of nGaN using TEGa precursor, ICCGE-19/OMVPE-19, Keystone, USA, 2019, oral presentation.

A. Hospodková, J. Pangrác, K. Kuldová, M. Nikl, O. Pacherová, J. Oswald, T. Hubáček, M. Zíková, P. Brůža, D. Pánek, K. Blažek, G. Ledoux, Ch. Dujardin, M. Heuken, E. Hulicius,

Devices based on InGaN/GaN multiple quantum well for scintillator and detector applications, Proc. SPIE 10036 (2017) UNSP1003617(1).

A. Hospodková, F. Dominec, T. Hubáček, J. Pangrác, J. Oswald, M. Hývl, M. Zíková, E. Hulicius, Role of V-pits in the InGaN/GaN multiple quantum well structures, Nanocon 2017, 9th International Conference on Nanomaterials - Research and Applications, Hotel Voroněž, Brno, Czech Republic, EU. October 18th-20th, 2017. Book of Abstracts, p. 81.

A. Hospodková, T. Hubáček, J. Oswald, J. Pangrác, K. Kuldová, F. Dominec, G. Ledoux, C. Dujardin, Strong suppression of In desorption from InGaN QW by barrier growth, ICMOVPE-XIX, The 19th International Conference on Metalorganic Vapor Phase Epitaxy, June 3-8, 2018, Nara Kasugano International Forum, Nara, Japan. Technical Digest, p.131-132, 2018.

## Author's selected conference contributions out of thesis scope

T. Hubáček, O. Rettig, M. Zíková, J.-P. Scholz, N. Steiger, K. Thonke, Y. Li, U. Kaiser and F. Scholz, Effect of Boron Incorporation into Thin AlGaN Quantum Wells Grown by MOVPE, ICNS 12, Strasbourg, France, 2017, poster presentation.

F. Scholz, O. Rettig, M. Zíková, T. Hubáček, J.-P. Scholz, N. Steiger, S. Bauer, K. Thonke, Y. Li, H. Qi, J. Biskupek, U. Keiser, Investigation of epitaxially grown AlB(Ga)N layers on AlN templates, ICMOVPE-XIX, The 19th International Conference on Metalorganic Vapor Phase Epitaxy, June 3-8, 2018, Nara Kasugano International Forum, Nara, Japan. Invited lecture. Technical Digest, p. 114-115.